FACULTY OF ELECTRICAL ENGINEERING AND INFORMATION TECHNOLOGY

TECHNISCHE UNIVERSITÄT WIEN

Master's Thesis in Smart Grids
Based on the LINK-Paradigm Architecture

Conservation Voltage Reduction in European Grids

A case study over different voltage levels: Customer Plants, Low- and Medium Voltage

Author

Mohamed Magdy Abdelalim

Mt. Nr. 11707696

under supervision of

Ass. Prof. Priv. Doc. Dipl.-Ing. Dr. techn.

Albana ILO

Abstract

Conservation Voltage Reduction (CVR) is the practice of strategically maintaining the voltage of the secondary side of electrical distribution grids in the lower acceptable voltage range to lower the power demand and overall energy consumption. It is an established practice in the USA with proven economic and technical benefits, yet it is still a large potential to be tapped elsewhere, especially in Europe.

This thesis examines this potential in typical designs of the European grids across different voltage levels (Customer Plants, Low- and Medium Voltage) in a holistic view. in order to determine possible savings while avoiding voltage-limit violations.
This research builds on the LINK-Solution, a concept developed by the thesis's supervisor to address a demand for a holistic model of evolving smart grids. The fractal breakdown of the electrical grids applied in this solution, allows for a unified modelling and control strategies across all voltage levels, paving the way for the standardization of smart grids.

CVR itself is still a long way from standardization, such that the reaped benefits of this strategy are normally not straight-forward to calculate, and the applied methodologies vary, with many still under research and development. This thesis discusses examples of real-world applications, factors affecting the savings, as well as existing application methodologies and CVR techniques.

The Simulation-based methodology is chosen to be the basis of researching possible CVR benefits using proven existing techniques and also experimenting with new techniques, in light of the understanding of the LINK-Solution. The research is done using updated modelling parameters, while manipulating several factors to seek the optimal operation point, where a full or partial potential is harvested.

The theoretical grids, where CVR is simulated under various conditions, are explained and illustrated with the different components and their mathematical models and parameters values. The voltage reduction is simulated through the voltage chain (except for the HV Grid-Link), experimenting with new techniques (namely on the LV grid by adding controlled transformers at each customer plant or a Voltage-Reactive power control system on the feeder) as well as the effects of different factors that are relevant in the evolving grid situation, such as the changing load models of customers and the increasing share of distributed generation in grids.

The simulation results are quantified and plotted in comprehensive overview for each simulation case. Indeed, all used techniques achieved full or partial voltage reduction, however, with some proving more economic and practical than others. An open-loop voltage reduction at MV came on the top of the list, proving to be the most economic technique under the simulated methods; it can increase overall system efficiency in a typical European grid,

particularly those with higher power consumption and with underground cable structure. While the experimental techniques simulated on LV have proven to be impractical due to resulting losses that offset the gains of CVR.

The thesis came to the conclusion that CVR is viable for a typical European distribution grid in light of its evolving structure, while there is still more room for further research and development in this field to achieve optimal results.

Kurzfassung

Konservation Spannungsabsenkung (Conservation Voltage Reduction) (CVR) ist die strategische Praxis, die Spannung der Sekundärseite von elektrischen Verteilnetzen im unteren akzeptablen Spannungsbereich zu halten, um den Strombedarf und den Gesamtenergieverbrauch zu senken. Es ist in den USA eine etablierte Praxis mit nachgewiesenen wirtschaftlichen und technischen Vorteilen, aber es gibt noch ein großes Potenzial, das anderswo, insbesondere in Europa, erschlossen werden kann.

Diese Masterarbeit untersucht dieses Potenzial in typischen Auslegungen der europäischen Netze über verschiedene Spannungsebenen (Kundenwerksanlagen, Nieder- und Mittelspannung) in einer ganzheitlichen Betrachtung, um mögliche Einsparungen zu ermitteln und gleichzeitig Spannungsgrenzverletzungen zu vermeiden.

Diese Forschung beruht auf der LINK-Lösung auf, einem Konzept, das vom Betreuer der Masterarbeit entwickelt wurde, um dem Strombedarf nach einem ganzheitlichen Modell der sich entwickelnden Smart Grids gerecht zu werden. Die in dieser Lösung verwendete fraktale Aufteilung der Stromnetze ermöglicht eine einheitliche Modellierung und Regelungsstrategien über alle Spannungsebenen hinweg und ebnet den Weg für die Standardisierung von Smart Grids.

CVR selbst ist noch weit von der Standardisierung entfernt, da die erntete Vorteile dieser Strategie normalerweise nicht einfach zu berechnen ist und die angewandten Methoden variieren, wobei viele noch in Forschung und Entwicklung sind. In dieser Masterarbeit werden Beispiele für reale Anwendungen, Faktoren, die die Einsparungen beeinflussen, sowie bestehende Anwendungsmethoden und CVR-Techniken diskutiert.

Die simulationsbasierte Methodik wird als Grundlage gewählt, um mögliche Vorteile der CVR mit bewährten bestehenden Techniken zu untersuchend und auch mit neuen Techniken im Lichte des Verständnisses der LINK-Lösung zu experimentieren. Die Forschung erfolgt unter Verwendung aktualisierter Modellierungsparameter, während mehrere Faktoren manipuliert werden, um den optimalen Betriebspunkt zu finden, an dem ein volles oder teilweises Potenzial ausgeschöpft wird.

Theoretischen Netze, in denen CVR unter verschiedenen Bedingungen simuliert wird, werden mit den verschiedenen Komponenten und ihren mathematischen Modellen und Parameterwerten erläutert und veranschaulicht.

Die Spannungsreduzierung wird durch die Spannungskette (außer HV Grid-Link) simuliert, mit neuen Techniken experimentiert (nämlich am NS-Netz durch Hinzufügen von geregelten Transformatoren an jeder Kundenwerksanlagen oder einem Blindleistungsregelsystem am Feeder) als sowie die Auswirkungen verschiedener Faktoren, die in der sich entwickelnden Netzsituation relevant sind, wie beispielsweise die sich ändernden Lastmodelle der Kunden und der zunehmende Anteil dezentraler Erzeugung in den Netzen.

Die Simulationsergebnisse werden für jeden Simulationsfall quantifiziert und in einer umfassenden Übersicht dargestellt. Tatsächlich erreichten alle verwendeten Techniken eine vollständige oder partiell Spannungsreduzierung, wobei sich jedoch einige als wirtschaftlicher und praktischer erwiesen als andere.

Eine Open-Loop-Spannungsreduzierung bei Mittelspannung stand ganz oben auf der Liste und erwies sich unter den simulierten Verfahren als die wirtschaftlichste Technik; es kann die Gesamtsystemeffizienz in einem typischen europäischen Netz erhöhen, insbesondere in solchen mit höherem Stromverbrauch und mit Erdkabelstruktur. Während sich die auf Niederspannung simulierten experimentellen Techniken aufgrund der resultierenden Verluste, die die Gewinne von CVR kompensieren, als unpraktisch erwiesen haben.

Die Masterarbeit kam zu dem Schluss, dass CVR angesichts seiner sich entwickelnden Struktur für ein typisches europäisches Verteilnetz praktikabel ist, während es noch mehr Raum für weitere Forschung und Entwicklung auf diesem Gebiet gibt, um optimale Ergebnisse zu erzielen.

Acronyms

AEP American Electric Power.

AMI Advanced Metering Infrastructure.

ANSI American National Standards Institute.

BLiN Boundary Link Node.

BLoN Boundary Load Node.

BPN Boundary Producer Node.

BSN Boundary Storage Node.

CP Customer Plant.

CPUC California Public Utilities Commission.

DG Distributed Generation.

DSO Distribution System Operator.

DSSE Distribution System State Estimator.

DTR Distribution Transformer.

HV High Voltage.

HVR Home Voltage Reduction.

ICT Information and Communication Technology.

LDC Line Drop Compensation.

LTC Load Tap Changer.

LTV Load-to-voltage dependence.

LV Low Voltage.

MV Medium Voltage.

NEEA Northwest Energy Efficiency Alliance.

OH Overhead Line.

OLTC On-Load Tap Changer.

pu Per Unit.

TSO Transmission System Operator.

VHV Very High Voltage.

VVC Voltage/Var Control.

VVWG Volt-Var Working Group.

ZUQDE Zentrale Spannungs (U) – Blindleistungs (Q) Regelung Dezentraler Erzeuge.

Contents

1. Introduction

1.1. Background

The shift towards the decarbonization of energy systems in the European Union gains higher momentum every day to achieve the ambitious target of an 80% reduction in carbon emission by the middle of the century compared to the 1990 levels.

In contrast to the traditional power grids, a decarbonized future will rely -for the most part – on renewable and subsequently decentralized energy sources and will also enable a more democratic frame of work, where the market participants have the right not only to consume but also to produce, store and trade energy among themselves.

This major political and environmental push needs contributions from all sectors of the economy to reshape the energy system. However, the evolution of energy systems has lagged behind that of Information and Communication Technology (ICT)s because power systems are more rigid and require higher initial investments.

Therefore, modern Distribution Systems Operators have been scrambling to find modern solutions for the challenges that appeared with the high penetration of fluctuating renewable energy sources and the redefinition of roles in the grid.

The research interests and budgets have been increasing in all relevant fields of smart grids and renewable energies over the past decade [1], and even though many of the solutions are truly innovative, they, unfortunately, lack widespread applicability due to the economical or social factors, and thus only a fraction of these new ideas come out of the laboratories.

1.2. Motivation

In the traditional grid, utilities make sure to supply the Customer Plant (CP) with the highest voltage possible – within the voltage limits – to minimize losses in the distribution networks, reduce the voltage drop over the same cable diameter and subsequently maximize profits.

However, as the priorities of utilities adapt to the modern challenges, a question is raised if the voltage profile should favor conserving the power and energy consumption at the endpoint rather than minimizing the losses. To answer this question, this voltage reduction strategy has been researched and even applied in real-world applications, coining the term Conservation Voltage Reduction, particularly in the USA grid, where it showed promising returns.

CVR holds much potential in Europe, since the upper voltage range is preferred in most European distribution systems. That is due to the lack of studies on the topic and concerns of possible increases of system losses. Therefore, this thesis is motivated to study this topic and explore some of the possible solutions.

1.3. Scope

The scope of this thesis is on the potential gains of power savings as a result of applying the CVR methods in the European grid. CVR can theoretically be applied at all voltage levels of the grid except for the Transmission (High Voltage) level, as it's counter-productive, therefore this thesis studies the possibilities at the Medium Voltage, Low Voltage, and Customer Plant.

1.4. Objectives

The objective of this thesis is to examine the possible opportunity of CVR application in the European grid structure in light of the holistic view of the LINK-solution, which views the whole power grid as a fractal design.

Furthermore, simulations of established and experimental CVR techniques on theoretical grids with typical European standards to be carried away to determine the effectiveness and drawbacks of CVR, alongside the introduction of distributed renewable generation through the grid. The results are to be comprehensively presented to highlight the power flow, gains of CVR as well as the resulting losses.

A particular focus is given to the study of CVR at the low voltage level and the potential role of voltage transformers connecting LV grids and Customer Plants, a design which would complete the fractal design, coherent with the LINK-Solution.

1.5. Thesis structure

Chapter 2 explains the theoretical background of CVR; the earliest CVR tests carried out in the US and other countries, and their results. It also explains how the European and American power grids have evolved differently and adapted to smart grids. The LINK -Paradigm is introduced along with the different electric devices within the system.

Chapter 3 explains the methodologies used to quantify CVR, technical barriers related to CVR, as well as several CVR techniques. The author includes his considerations and assumptions regarding the research method and approach.

Chapter 4 gives an overview of the simulation grids. With the aid of diagrams, it illustrates the power flow and connections within the Low Voltage and the Medium Voltage Grids. It

also gives a preview whether CVR is applied or not by specifying transformers used, as well as other devices present in the Grid.

Chapter 5 describes the models of the components used in the simulation methodology. Different elements within the grid (i.e., transformer models, lines, buses) are discussed.

Chapter 6 describes the results obtained from simulation load reduction with and without photovoltaic units. It compares the theoretical benefits of CVR to what can be harvested in the grid setup of Low and Medium Voltage.

And finally, chapter 7 concludes the findings of the thesis as seen by the author.

2. General background

This chapter lays the foundation of our understanding of CVR by firstly defining it and then explaining how it influences the behavior in electrical devices (section 2.1). It highlights existing CVR projects across the USA and Europe and explains how they have each evolved differently since the 19th century. Towards the end of this chapter, the LINK-Solution is introduced, and its different components are illustrated by the aid of diagrams.

2.1. CVR definition

> CVR is the practice of intentionally lowering the voltage on the primary distribution circuits to maintain voltages on the secondary side to be in the lower acceptable voltage range.
>
> *American National Standards Institute (ANSI) [2]*

CVR is defined as a cost-efficient solution to reduce power demand and energy consumption. It accomplishes that by reducing the supply voltage to electrical appliances (e.g., air conditioners, home appliances and industrial machinery) to the minimum possible value of the supported voltage spectrum; with the aim of reducing the amount of energy consumption or shaving off the peak demand (according to the applied strategy) with no effect on their daily routines. Furthermore, CVR can be used within consumer premises, both commercial and residential, but does not require their involvement in the installation process nor their feedback in the running state.

It holds the potential of providing high power and energy savings at low costs. This puts it as a focal point for many Distribution Systems Operators as part of their Demand Side Management strategy and Smart grids solutions, aided by the development of Steady State Estimation tools and Volt/var control applications.

The main strategies of using CVR are short-term demand reduction, where voltage reduction is applied in specific time periods (usually peak hours) to reduce demand; and long-term energy reduction, where the voltage is reduced permanently to save energy. A comparison between the two strategies is illustrated in Figure 2.1.

Existing implementations have proven their worthiness in both energy and demand saving, as some systems have achieved an astonishing benefit-cost ratio of over 200 folds [3], although the effects differ from one project to the other. A rule of thumb could be attributed to [4], that a mere 1% of voltage reduction results in a 0.4-1% reduction of energy consumption.

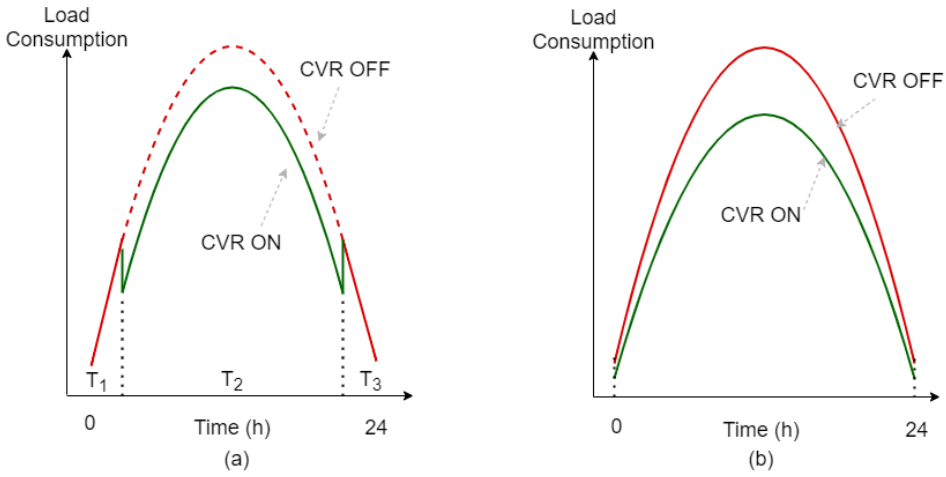

Fig 2.1. (a) Temporary CVR for demand reduction on traditional daily load profile.
(b) CVR for saving energy on traditional daily load profile.

Besides that, many factors put CVR ahead of other solutions:

- First, it can be applied to almost all types of customers – especially at the LV level, which is of most interest to Distribution Systems Operators.
- Secondly, CVR is highly applicable to the entire service territory. Unlike other energy reduction programs (i.e., demand response) that have to attract and enroll customers in order to alter their power and energy, CVR proves to be a better option as it requires no engagement from the end-user, so it cuts out the need for customer education and forms of social resistance to change. An example of that is the movement against smart meters due to a lack of education and privacy concerns on the customers' side [5].
- Thirdly, the strategy can hardly be recognized at work by the customers, since it doesn't put electrical devices out of work or fundamentally reduce their efficiency.
- Fourthly, CVR is not a one-time static solution, but rather an adaptive solution that can be adjusted in response to grid behavioral changes through a classic feedback loop.
- Lastly, costly upgrades and investments to the network are no longer a bother, and even if necessary, are likely to be small. The distribution and sub-transmission systems are also well-equipped with voltage regulation devices that can enable CVR.

Voltage reduction is not a new concept; many electric utilities and their associated grid management authorities have used it for decades to reduce power quickly during a peak load emergency or power supply shortage. In the past, such voltage reduction was referred to as brownout because of its dimming effect on incandescent light bulbs [2]. When voltage reduction is strategically applied either consistently (24/7 operation for energy saving) or temporarily (adaptively for demand reduction), it is referred to as CVR.

Aside from peak shaving and energy conservation, other advantages of CVR include the prospective decrease of greenhouse gases and mitigating the impacts of *DG* integration.

Load-Voltage dependency

The power consumption of most electrical appliances varies with the supply voltage, which is commonly referred to as the term *Load behavior*. This voltage sensitivity, which was traditionally thought of as a burden in the power flow estimations, is the strong point that CVR employs.

The term *electrical appliances behavior* is used here as it is more inclusive and avoids the ambiguity behind the definition of the *Load*, according to *LINK*-Solution concepts.

This relationship is represented as an expression of P and Q as a function of the voltage magnitude and frequency, and the result is placing the appliances into three main categories -forming what will be referred to from here on as the ZIP model as shown in Figure 2.2:

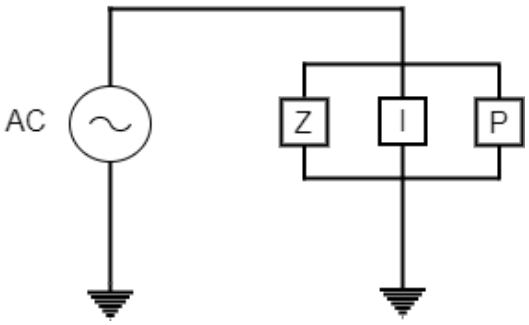

Fig 2.2. The ZIP model.

Firstly, there is the constant impedance (Z), where consumption is $\propto V^2$ (i.e., the load is purely resistive), secondly, there is the constant current (I), where consumption is $\propto V$, and finally the constant power (P), where consumption is constant regardless of V.

Any customer plant is constituted of a mixture of the three types, whereas most of the industrial demand tends to be of constant power due to large motors. In contrast, commercial and residential customers are more diversified.

Figure 2.3 gives an idea of the three categories. Through the allowed voltage range $V_n \pm 10\%$, the actual consumption of a 1 kW rated appliance varies from 0.8kW to 1.2kW for constant Z. That constitutes a 33% savings potential compared to the $1.1V_n$ operating point, or 19% compared to the V_n point. The values range from 0.9kW to 1.1kW for constant I.

Accordingly, industrial demand is not considered a suitable candidate for CVR, while commercial and residential customers can benefit from it as they compromise lighting, heating/cooling applications & electronics.

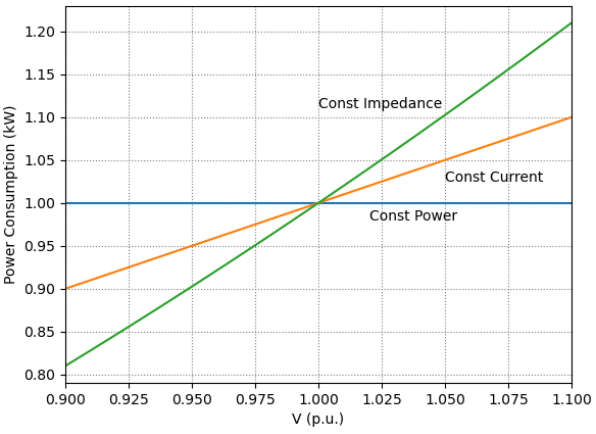

Fig 2.3. Actual Power consumption for 1 kW rated appliance across the three categories.

2.2. Existing CVR projects

2.2.1. The USA

In 1973, the earliest reported CVR test was performed by American Electric Power (AEP) [6], and other utilities in the US soon followed. Key CVR activities date back to the 1980s in the USA, when the California Public Utilities Commission (CPUC) required that utilities lower voltages to conserve energy. Many studies have been conducted ever since to test the applicability and efficiency of various CVR techniques in different utility grids. This section provides an overview of existing solutions and their outcomes.

In 2007, the Northwest Energy Efficiency Alliance (NEEA) of the US concluded a four-year-long major study on CVR effects, known as the NEEA Distribution Efficiency Initiative [7], which conclusively showed that voltage reduction in a utility distribution system saves energy, reduces demand and reactive power requirements without negatively impacting the customer. And in [8], it is found that applying CVR on a wide scale in the North-American grid would yield a 3% saving in the total annual energy consumption.

While PECO, the largest electric and natural gas utility in Pennsylvania, USA, presented a paper titled "Conservation Voltage Reduction: What Are the Savings?" [9] at the 2013 International Energy Program Evaluation Conference, presenting the results of its CVR program. The program involves a static voltage reduction of approximately 1% across PECO's electrical distribution system (also known as voltage fixed reduction), which comprises a physical adjustment in transformer settings to control voltage at the substation.

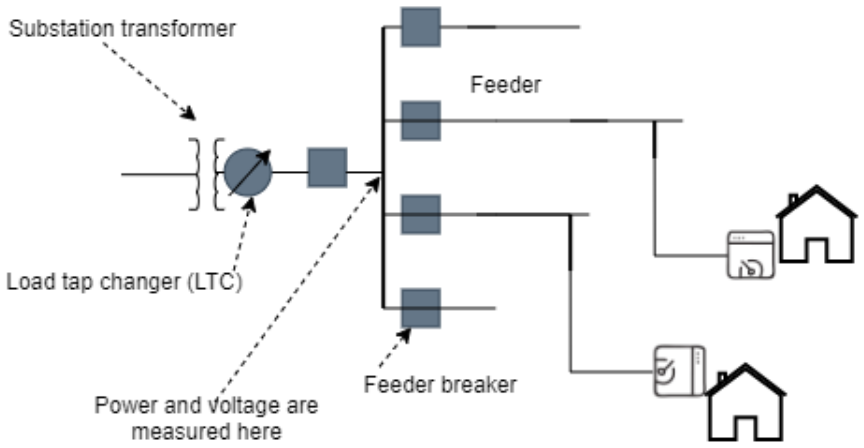

Fig 2.4. Overview of a typical PECO distribution system under CVR [9].

It is essential here to note that PECO's initial attempt to apply a formulaic CVR protocol, used by other utility providers in other regions, did not accurately characterize PECO's distribution system due to the substantial differences in load and weather conditions.

An overview of a typical PECO distribution system under CVR is presented in Figure 2.4, where power and voltage are measured directly on the substation bus bar; however, the real savings cannot be measured directly but were calculated through statistical regression analysis. The study was concluded as a success with a substantial benefit-cost ratio of 262 without affecting customer satisfaction due to large energy savings and minimal implementation costs.

2.2.2. Austria, Europe, and Worldwide

Outside the US., CVR was also tested in Australia [10], where it was found that a 2.5% voltage reduction resulted in 1% energy savings on the residential circuits. It was also reported achieving a 1.7% energy reduction in Ireland [11].

The project Zentrale Spannungs (U) – Blindleistungs (Q) Regelung Dezentraler Erzeuge (ZUQDE) , which translates to "Central voltage (V) – reactive power (Q) control of decentralized generation" [12], is an excellent example of the temporary use of CVR principle to reduce the load, which was concluded in 2014 in the Lungau region (Salzburg, Austria), to accommodate the further integration of Distributed Generation (DG) (of the type hydro-plants) while keeping voltage on the *MV* level within limits. It had a budget of more than half a million Euros, serving around 22000 customers over a connection of more than 40kms, with a maximum load of 23 MW.

The usage of a Distribution System State Estimator (DSSE) and Voltage/Var Control (VVC) applications were the cornerstones, on top of which the project is built on. The real-time optimization process utilized the results of the steady-state calculations to set the target points for V and Q of the *DGs*, *OLTCs* as well as added capacitors.
The project proved to be a success and proved that CVR could be applied on the grid safely to achieve lower-range voltage goals in a real-time control strategy.

In conclusion, the CVR proven benefits for utilities include peak loading relief of distribution network, net loss reduction, potential incentives and requirements from regulatory bodies, less fuel consumption, and emission reduction. CVR can also contribute to achieving optimal Voltage/Var control when combined with other system improvements.

2.3. Quantifying CVR Results

Even with the outstanding positive response from CVR performance and the good results obtained from it, many still remain skeptical [7, 13]; mainly because of the major challenge of quantifying CVR effects.

Therein lies the difficulty of distinguishing the variations in load and energy consumption due to voltage reduction from other causes. It is essential here to note that the energy savings

are not directly bound to the reduction of voltage, as consumption will not remain the same after CVR takes effect.

Electrical appliances treated to CVR require a finite amount of energy delivered either at lower voltage for a longer time, or at higher voltage for a shorter time before CVR effects take place. That explains why appliances used for cooking, heating/cooling typically need to work for a longer time at the lower voltage before their operation objective is met (i.e., raising or lowering the room temperature).

The impact on the savings of energy and peak demand can't be directly measured, as it requires estimating the CVR factor (CVR_f). CVR_f is defined in [14] as a dimensionless value such that:

$$CVR_f = \frac{\Delta E}{\Delta V} \tag{2.1}$$

where: ΔE is the percentage of change in energy consumption, and ΔV is the percentage of change in voltage.

In the long run, electric utilities collect a considerable amount of load and voltage data of each CVR-enabled circuit, then proceeds to estimate this CVR factor. Energy savings gained from the program depend on:

- Data quality
- Data treatment (i.e., collection, cleaning, resolution)
- Methodology applied in CVR factor calculation
  (e.g., comparison-, regression-, simulation-based)

Slight changes in data and methodology may bring about immense differences in the calculated CVR_f and energy savings. That puts the practicality of the approach into question, as well as the validity of the acquired results.

Standardized and comprehensive studies of CVR are essential to ensure the further success of CVR. The Volt-Var Working Group (VVWG) of the IEEE Power and Energy Society is already investigating the need for this industry-accepted standard. It has just recently approved the creation of the CVR Study Group [15] to aid their study. In an effort to gain public support, this study group remains open to industry, academia, and national laboratories to join and support.

2.4. European Grids

The European and American power grids have evolved differently since the first commercial generation and utilization of electricity from the 19th, due to various economic and demographic reasons. Most notable differences include frequency, end customer plant voltage,

voltage level classification, symmetry, balance, type, and the number of transformers and cables.

50 Hz is the standardized system frequency in the European grid (as well as many other parts of the world). This grid is decomposed into transmission, sub-transmission, and distribution, and the voltage levels are Very High Voltage (VHV), High Voltage (HV), Medium Voltage (MV), and Low Voltage (LV), as seen in table 2.1.

Grid	Voltage Levels	Operator	Connection Mostly	R/X Ratio
Transmission	VHV	TSO	Meshed OH	Increases from VHV to LV
Subtransmission	HV	TSO or DSO		
Distribution	MV	DSO	Mostly radial OH	
	LV		Mostly radial CA	

Table 2.1. European grid structure.

As in all *AC* systems, transformers act as the galvanically isolating connection point between different voltage levels. Usually, the HV/MV connection is an on-load tap changer, which provides flexibility in grid control. However, its high cost makes the fixed tap position transformer the usual candidate for MV/LV connection [16].

On the High- and Medium Voltage grids, bidirectional power flow is supported with efficient transmission with low losses depending more on Overhead Lines (OHs) than on underground cables for reasons such as cost, ease of maintenance, and the fact that grid operators are traditionally experienced with overhead lines. However, on the Low Voltage level, it is more underground cables with higher losses as the R/X ratio of the lines increase.

Traditionally, the grid transmits from large scale power plants to the designated sub-transmission grids (which can both be operated by Transmission System Operator (TSO) like in Italy or by Distribution System Operator (DSO) like in Austria and Poland), which distribute it to the medium voltage grids. Medium- and Low- Voltage grids are called the distribution grids, which are operated by DSOs and are usually radial and, unlike the North American grids, symmetrical and balanced [16, 17]. Customers can be connected both on the Medium- and Low-Voltage grids.

The impedance of power network lines in many transmission systems is primarily inductive, i.e., the phase angles of the power line's impedance are usually relatively large and very close to 90 degrees. There is consequently a strong coupling between P and δ, and between Q and parameters, while the coupling between P and $\|\mathbf{V}\|$, and Q and δ is considered weak. That explains why P usually moves from the higher δ bus to the bus with lower one, and Q usually moves from the higher $\|\mathbf{V}\|$ bus to the bus with lower one. However, that does not apply when the phase angle of the power line impedance is relatively small.

2.5. *LINK*-Solution

The building block of this solution, *LINK*-Paradigm, was first introduced in [18] as part of the quest to provide standardized modeling of the emerging smart grids, based on the idea that power systems have fractal structures. This enables the modeling of the entire power system (starting from HV Level down to MV, LV, and CPs) as well as describing its operation processes (such as load-production balance, n-1 security, etc.). As per definition, The *LINK*-Paradigm is composed of an electrical appliance (that could be a part of the grid or production or storage as shown in Figure 2.5), the corresponding controlling schema, and the *LINK*-Interface.

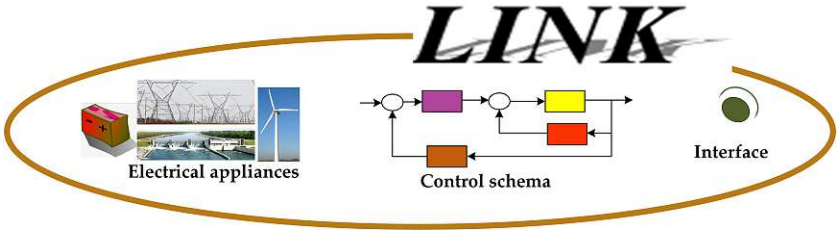

Fig 2.5. Overview of the *LINK*-Paradigm [19].

Subsequently, the *LINK*-Solution was developed according to the fractality principles, providing a holistic model and a unified architecture, so that control strategies of the same architecture can be deployed at all the different levels, to standardize methods for development and implementation. This solution [20] accommodates all necessary components, as shown in fig. 2.6, be it either:

- Power production (independent of technology type and size).
- Power storage (independent of technology type and size).
- Power grid (independent of voltage level and operator).

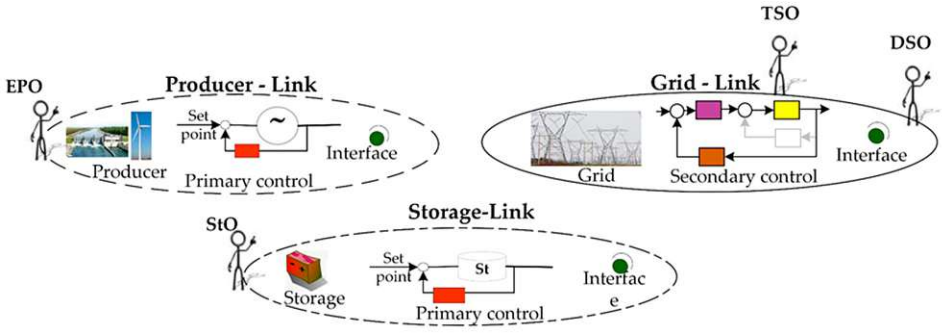

Fig 2.6. Components of the LINK-based holistic architecture: Grid-, Producer- and Storage-Link [19].

Thus, all of these components can be merged into a single structure, that unifies all interactions within the power system itself and between it and market, thereby creating the possibility to harmonize them.

Through this model, a flat business model could be reached across the industry that minimizes the data exchange between the architectural components while taking into account the market rules, cyber-security, and data privacy requirements.

This distributed *LINK*-based architecture is capable of handling the power system operation processes in normal and emergency conditions, allowing the market to evolve with the new smart-grid technologies and encourages further customer participation in the grid in accordance with the privacy regulations.

"The Energy Supply Chain Net" is the basis for the *LINK*-Paradigm. As seen in Figure 2.7, it is a set of automated power grids, intended for "Links", each fitting into the other in order to establish a flexible and reliable electrical connection.

Each Link operates independently and has contractual arrangements with other boundary Links, and communicates with them only through defined communication channels [18].

Within this model, each voltage level has primary control (for the major control factors, i.e., frequency and voltage) as well as the secondary control, which calculates and sends the set-points to the relevant nodes according to dynamic constraints. The end result is that a complete power system can be handled as a set of automated chain links.

The *LINK*-Grid is the main topic of discussion. The electrical appliances in it compromise overhead lines/-cables, transformers, and reactive power devices. Its size is defined according to the area of secondary control set up. The boundary nodes that connect to it are called Boundary Link Node (BLiN), Boundary Producer Node (BPN), Boundary Storage Node (BSN) and Boundary Load Node (BLoN), and only communicate necessary information for operation and safety, abstracting other details that could compromise privacy or other technical details, which the *LINK*-Grid under study needs not know.

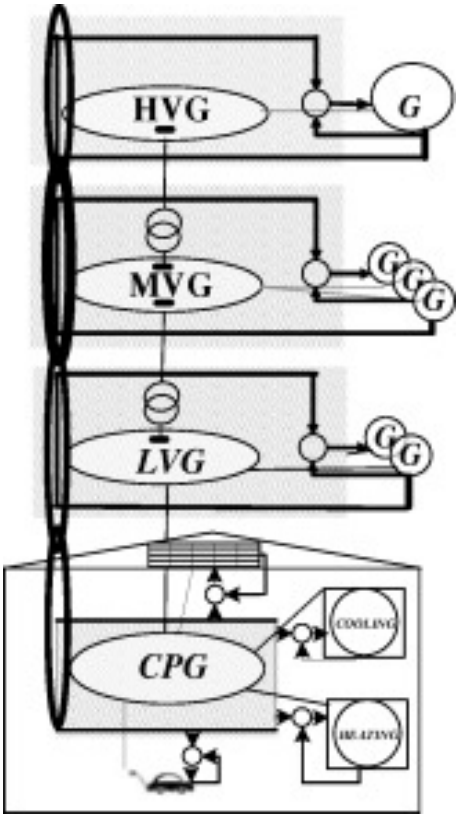

Fig 2.7. Overview of the energy supply chain's power grid [18].

3. Methodology

This chapter details the thesis research methodology, where the author outlines the research method and approach, choice of sample data, considerations and assumptions, as well as the limitations of the project.

3.1. CVR Methods

The methodologies to quantify CVR effects are generally categorized into; comparison-based, regression-based, synthesis-based, and simulation-based methods. The last-mentioned is the chosen method in this thesis.

3.1.1. Comparison-Based

There are two basic methods used here;[21] The first method involves two feeders, one being the control group and the other the treatment group. The feeders must be similar in configuration, topology, load condition, load mix and location. CVR is applied to one feeder (treatment group) while normal voltage is applied to the second feeder (control group) at the same time. The second method involves only one feeder. Voltage reduction is applied onto this feeder (treatment group) as well as the normal voltage (control group) but under different time periods while still maintaining the same weather conditions. CVR effects can then be calculated based on the measurements from the two tests.

This methodology is by far the most straightforward. It does, however, come with challenges. For instance, the time-dependent nature of the CVR factor may easily be compromised. That is due to the fact that after averaging the data, it is not possible to obtain the CVR factor for a specific time on a particular test day. Other shortcomings may include:

- A suitable control group may not exist.
- Noises such as weather impacts are not well-considered, and simple averages may not be sufficient to cancel them.
- Load changes may be caused by other factors and not just voltage reduction (e.g., weather differences).
- Measurement noises included in the calculations sometimes blur the minor CVR effects.

3.1.2. Regression-Based

In regression-based methods, loads are modeled as a function of their impact factors. Linear regression is used to identify the models used in the normal-voltage load process, and the outputs obtained here are compared with the measured reduced-voltage load in order to

calculate the CVR factor. The general process can be summarized into the following points [7]:

1. Model parameters' estimation, depending on a set of training data and factors of temperature and accuracy.
2. Parameter estimation, which can be estimated by minimizing the errors
3. Calculation of load consumption without CVR, taking temperature factors into account
4. CVR factor calculation such that:

$$CVR_f = \frac{\Delta L\%}{\Delta V\%} \tag{3.1}$$

$$\Delta L\% = \frac{L_{normal} - L_{CVR}}{L_{normal}} * 100\% \tag{3.2}$$

The linear regression models used decompose the load, usually, into basic and weather dependent components with some physical interpretations attached to them. This prompts it to be widely used in utilities assessing CVR effects, as it makes it much easier to understand the model behavior. The regression models can also be used to forecast the CVR factors.

It is important to note that this method is heavily reliant on the accuracy of the regression model used. This is nevertheless easily improved by moving from linear to non-linear regression models. Other challenges pertaining to this method would be distinguishing CVR effects from the estimation errors of the regression model used. This mistake is likely made because CVR effects are usually a few percent of energy reduction and may thus fall within the error bound of the regression models.

3.1.3. Synthesis-Based

Synthesis-based methods aggregate Load-to-voltage dependence (LTV) behaviors to estimate the CVR effects of a circuit. There are two ways to perform this[21]: synthesis from load components and synthesis from customer classes. In the component-based synthesis, the energy consumption of major appliance loads is modeled as a function of voltage identified through laboratory tests. The load shares of each appliance are then obtained through surveys. The total energy consumption at the circuit level can be computed as:

$$E_c(V) = \sum_i E_i(V) \cdot S_i \tag{3.3}$$

where $E_i(V)$ represents the energy consumption of appliance i at voltage V; S_i is the load share of appliance i.

Synthesis-based methods can be used to obtain a quick estimation of CVR effects before its implementation. The basic assumptions of synthesis methods are that all the appliances

behave as they did during the lab test, and the load composition information is correct. Note that it is challenging to collect accurate load share information and the LTV response of every existing electric appliance. Results obtained from synthesis methods should therefore be used with caution.

3.1.4. Simulation-Based

The simulation-based methodology used to analyze CVR effects is based on system modeling (see chapter 5) and power flow calculation. The power flow study focuses on the system's capability to supply the connected load. Note that total system losses, as well as individual line losses, are tabulated in this study.

The goal is to obtain information on each bus (voltage, angle, magnitude) in a power system for specified load, power, and voltage conditions [22]. As soon as the information record is provided, analytical determination of P and Q power flow on each branch as well as generator Q output is possible. Due to the non-linear nature of this problem, numerical methods are employed to obtain a solution that is within an acceptable tolerance.

One advantage the simulation method clearly depicts is that it has high precision if the models can accurately represent the load behaviors. However, with the method being largely component-based, it is often challenging to build models for all existing and constantly emerging load components. It would be better to identify the aggregated load models at the circuit level instead, and develop more reliable load models. That is why in this thesis, a new load model was used in the simulation, as clarified in section 3.2

3.2. Load model

Load models are analytical and mathematical representations of a load that can be utilized to analyze and estimate relevant characteristics in studying power systems and their subsequent calculations. They can be developed through [17]:

- Component-based approach, requiring knowledge of modeling parameters and participation percentage of the electrical devices in the total power demand.
- Measurement-based approach, relying on field measurements to develop load models that represent aggregate loads at power system buses.

Either of them has its advantages and disadvantages, but should result in a load model that accurately represents the actual load behavior at the system bus.

- Combined (Hybrid) approach, as its name suggests, combines the previous two in an effort to interpret measurement data in light of electrical devices' composition through techniques like load-signatures and demand pattern identification.

The result of these approaches can be seen in the existing models, which are also categorized to reflect the behavior of different electrical devices and customer types, be it [17]:

- Static, which are popular due to their simplicity as they are independent of the factor of time and frequently used in power flow as well as voltage stability calculations. They represent the relevant characteristics of load in terms of already-known parameters. Examples of static models are exponential, polynomial, and linear models. The general formula for them would be:

$$P = f_P(V, f) \tag{3.4}$$

$$Q = f_Q(V, f) \tag{3.5}$$

  Where P is the active power, Q is the reactive power, while f_P and f_Q are functions of voltage (V) and frequency (f). However, this time-invariant property makes them not well suited to accommodate CVR, and therefore out of this thesis's scope.

- Dynamic, which differ from previous models such that they are time-variant, and thus their equations would include time (t) in the function such as follows:

$$P = f_P(V, f, t) \tag{3.6}$$

$$Q = f_Q(V, f, t) \tag{3.7}$$

  The chosen ZIP model falls under this category as a composite model, encompassing components of both types as an aggregate load. The ZIP model has already been mentioned in section 2.1 and is further explained in section 5.5.

3.3. CVR Techniques

The implementation strategies for voltage reduction are classified into open-loop and closed-loop methods. Both receive input signals (e.g., system setpoints, updated measurements) and accordingly provide an output (e.g., change of system, devices adjustment); however, the closed-loop methods takes the feedback factor into account, as shown in Figure 3.1. Several CVR Techniques are described in this section to evaluate the different strategies.

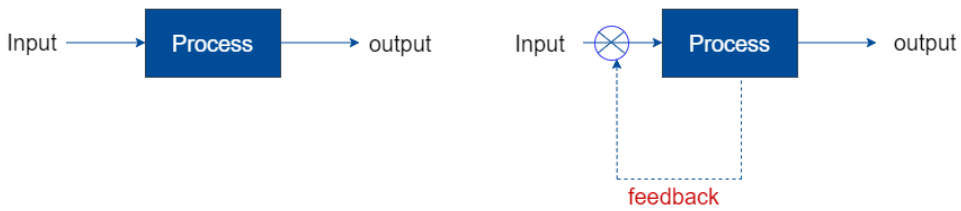

Fig 3.1. Open-loop (left) vs. Closed-loop systems (right).

3.3.1. Open-Loop

Some of the early techniques to reduce voltage include Load Tap Changer (LTC) and Line Drop Compensation (LDC) [two most commonly used], as well as Home Voltage Reduction (HVR). LTC is routinely used to control the secondary voltage of a substation. It is available in almost all substations and considered cost-effective. LTC, however, requires a more careful selection of circuits and may also limit the depth of voltage reduction for a feeder with larger voltage drops.

On the other hand, LDC keeps the most distant portion of the circuit at some minimum acceptable voltage levels. The rest of the circuit voltage is otherwise allowed to vary with load conditions. It can lower the average voltage by 2% to 3% [23]. Despite its ease in controlling voltage, its settings are challenging to determine and cannot adapt to the dynamic nature of distribution loads and changes in network configurations. The voltage reduction potential in LDC is also relatively small, hence decreasing CVR effects.

Capacitors, when coordinated with voltage control methods, can provide Var compensations for CVR. To achieve effective implementation of CVR, a relatively flat voltage profile along the feeder is preferable. Reference [24] proposed a two-step Voltage/Var optimization algorithm for CVR. The first step is to schedule capacitor bank commitment to correct the power factor and flatten the voltage profile. The second is to change the LTC tap ratio to achieve voltage reduction.

Another technique used is HVR, where voltage is regulated at customer meters [25]. One of its disadvantages is that it requires customers to install equipment and also pay the capital costs. It is known to have distribution system losses as well.

In general, open-loop voltage reduction is a convenient and cost-effective way to implement CVR. However, there are three major drawbacks of open-loop voltage reduction:

1. The depth of voltage reduction is limited
2. As control of all devices is based on local data and disjointed from one another, it is not optimized, or at least not systematically optimal
3. It cannot adapt to dynamic changes of distribution networks

3.3.2. Closed-Loop

The installation of SCADA and Advanced Metering Infrastructure (AMI) has led many utilities to implement closed-loop control strategies. CVR would be used as a VVC such as an operation mode in SCADA-based system, which may include other operation modes aimed for loss reduction, power factor correction. An example of that is the advanced real-time control system "AdaptiVolt" which is a closed-loop VVC with CVR function, which is illustrated in Figure 3.2.

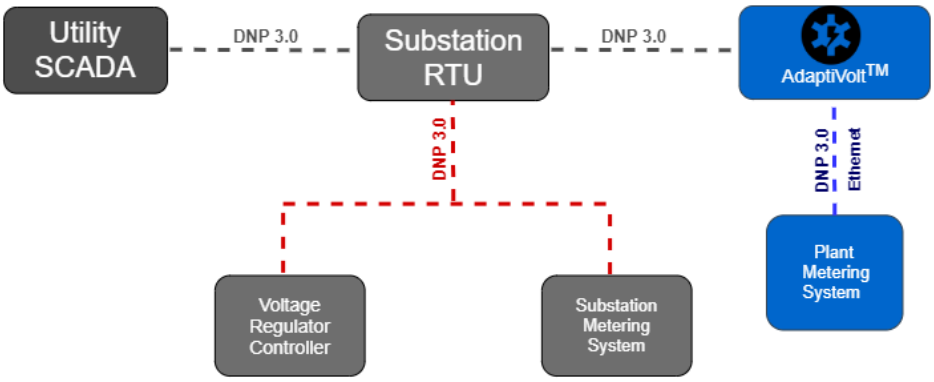

Fig 3.2. Overview of the AdaptiVolt system.

The closed-loop VVC takes advantage of various measurements to determine the best Voltage/Var control actions during specific time periods [26]. Utilities like Inland Power and Clatskanie PUD [27, 28] implemented it to achieve a 3% voltage reduction.

In comparison with LTC and LDC, the advantages of VVC stand out: optimal voltage reduction, greater energy-saving effect, and adaptability to dynamic system changes. Its only shortcoming would have to be its complexity and high cost. However, all control methods achieved a similar range of voltage reduction between 2 and 4% [21].

3.4. Technical Barriers

The technical barriers related to CVR can be summarized into the following aspects:

- Lack of coordination of different Voltage/Var devices to reduce the voltage in a reliable and optimal way
- Lack of standardized assessment and verification of CVR effects
- Lack of coordination between CVR and DG
- Lack of industry standards to quantify results and costs as mentioned in section 2.3

And expanding on that, it is to be mentioned that CVR does not significantly influence PV systems because power inverters can be set to generate constant power [29].

In fact, according to Singh [30], the CVR factor using simulations for a feeder with an added PV system is insignificant due to the failure of the voltage control strategy to keep the voltage levels within the desired range.

Integration of DG makes the feeder voltage profile change more quickly, hence interfering with the control scheme and performance of CVR. Note that the output of DG (PV and wind power) depends on weather and can therefore not be accurately anticipated.

On top of that, the inconsistent output of DG does have impacts on VVC. Traditional VVC is designed for slow and gradual changes of loads on a distribution feeder due to the slow reaction of capacitors and LTC [31, 32]. The random and rapid change of DG output requires a faster controller, such as an inverter [31–33]. The coordination of traditional VVC and inverters is a new challenge when CVR is applied to a feeder with a high penetration of DG.

Moreover, types of customers can be classified into residential (R), commercial (C), and industrial (I). Different classes of customers have different percentages of appliance load composition. CVR effects are closely related to classes of customers on the feeder. Thus, different results will appear based on the type of customers on the feeder.

3.5. Chosen methodology

3.5.1. Chosen method

To the best of the author's knowledge, there are no extensive CVR programs on the EU grid, the simulation method is used to have a proof of concept based on defined typical EU grid parameters, regardless of the differences that may arise from one utility network to the other like the specific topology of the grid. This method simulates what the load consumption would be if there is no CVR and then with CVR.

The simulated grids are detailed in chapter 4, and the modeling is detailed in chapter 5.

3.5.2. Chosen technique

The author utilizes both open and closed-loop techniques according to the voltage level and the goals of simulations.

As detailed in chapter 4, load reduction in the LV link-grid is realized through controlled OLTCs connecting LV feeders and CPs or coil at the end of the feeder. Both are closed-loop systems aimed at achieving the best result to find if a proof of concept is possible. However, other techniques have been proven in the reviewed literature and mentioned above.

On the other hand, at the MV, CVR is realized by a simple open-loop voltage drop at the high – medium voltage transformer TR_{MV}^{Hv}. This technique, however, is not always suitable if the same transformer feeds more than one MV line, in which case they would have different voltage profiles according to their length and the type of customers connected to them. Additional *Q-V* control strategies could be of help in that case, as done in section 2.2.2.

3.5.3. Chosen data and results handling

Data handling

New load models have been a matter of research not only to counter the cons of traditional models but also to adapt to dynamic customer and load behaviors in an effort to accommodate new applications such as CVR.

A good example is seen in [34], which is the data model used in this thesis's simulations, where it takes into account updated measurements, load composition, and the trend of switching from incandescent lamps to LED lighting in residential customers. The resultant ZIP-coefficients are made available to the public in [35] and used to define the load in simulation.

Results handling

The resulting database of each test case (from the simulation suite Sincal) is further processed through an object-oriented python, plotting the significant data in order to give a comprehensive overview of the relevant system state.

In order to represent the possible changes of active power and reactive power when using CVR, they are represented across the allowed voltage range ($V_n \pm 10\%$) as a percentage change compared to the optimal case at the minimum voltage $0.9V_n$. Such that for the voltage range $V_i \in \{0.9V_n, \ldots, 1.1V_n\}$:

$$\Delta\%(P_{V_i}) = \frac{P_{V_i} - P_{0.9V_n}}{P_{0.9V_n}} * 100 \tag{3.8}$$

And similarly for Reactive power:

$$\Delta\%(Q_{V_i}) = \frac{Q_{V_i} - Q_{0.9V_n}}{Q_{0.9V_n}} * 100 \tag{3.9}$$

3.5.4. Considerations and assumptions

Considering the previous technical barriers section 3.4 and other factors mentioned before, the author took the following consideration and assumptions into consideration:

- The grids used in simulation are theoretical with typical values of EU grids to avoid the variations from one utility provider to the other. They are simulated in both forms of cable and overhead lines.
- The type of customer plants considered in simulations is rural residential.
- Since the scope of this thesis covers the power reduction (not the energy savings) of CVR, the simulation type is discrete, not continuous. This also bodes well with avoiding the problem of time-sensitive of devices that might not keep up with PV output variations.
- Adopting the new data model solves the problem of not-accurate and time-insensitive customer models.
- Other specific considerations of simulations are mentioned in chapter 4.

4. Investigation schemes in the vertical chain

This chapter focuses on the simulated theoretical grids with diagrammatic illustrations. It briefly explains them and shows the *CVR* principle applied through the voltage chain as adopted from the *LINK* structure of the grid, building on the energy supply chain net [36].

The investigation of CVR takes place at the MV Grid-Link (investigation level 3), LV Grid-Link (investigation level 2), and the CP level (investigation level 1). This structure is depicted in fig. 4.1, which theoretical background is discussed in section 2.5.

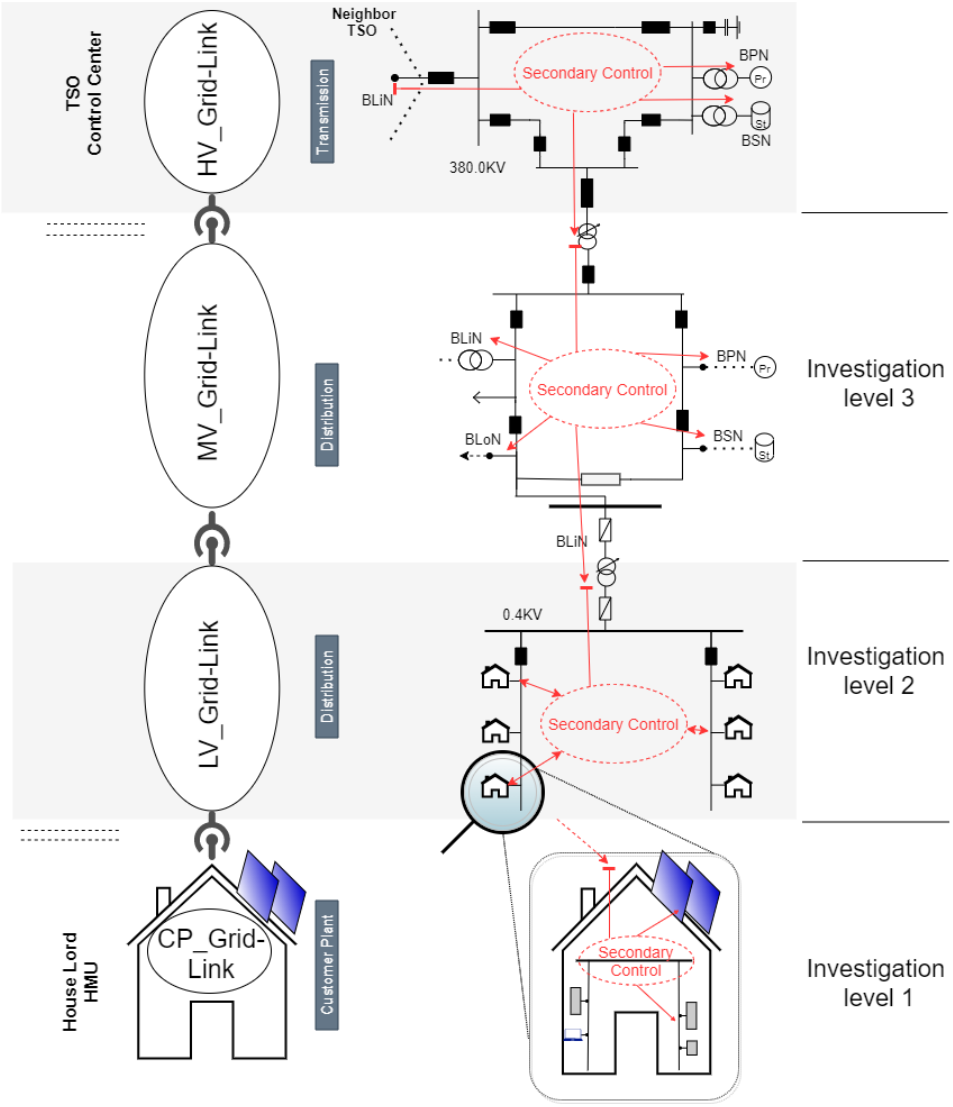

Fig 4.1. Link Structure of the Grid - Secondary Control in the Vertical Chain.

The link-structure spreads across all voltage levels from HV down to customer plants, each

with its own primary control (keeping the system within boundaries of major factors such as voltage and frequency) and secondary control (determining the set points of the primary controls and sharing them to neighbor nodes). This view of the grid allows for the same design of the secondary control scheme in all Grid-Links, with clearly defined link interfaces as points of communication between each Grid-Link and its neighbors. This allows for a flat business structure and enhancing privacy, as only the aggregated data that are relevant for the neighbor nodes are shared to them.

4.1. Customer plant level

The customer plant is modeled generically with normalized consumption/injection. That represents the demanded active and reactive power as a ratio to its peak active power demand in winter, so that the results are independent of the actual consumption values; as well as their active power generation resulting from *PV* units.

Customer plants can be without a photovoltaic system (i.e., purely consumers) or with PV. The latter are able to inject power efficiently and safely into the grid thanks to the grid-tie inverters. The consumption is modeled mathematically into a ZIP model adapted as the base simulation model. All customer plants used are identical in terms of maximum winter load ($P_{peak} = 1.368kW$) and a *PV* installation ($PV_{Rated} = 5kW$), which are typical values for a rural house.

However, in practice, the *CVR* results differ according to the location of the customer plant on the feeder. The customer plant located at the beginning of the distribution feeder is affected most. This is because the voltage is at its highest level before it starts to decrease along the feeder gradually.

CVR implications on customer plants are further elaborated in section 6.1. The type of customer discussed is residential, where customer satisfaction is not affected by CVR in any way, whereas other types of customers (industrial and commercial) could be affected and could need additional measures of protection if CVR is applied.

4.2. Low voltage level

In this grid, 20 houses are placed uniformly over ten connection points on a 1 km aluminum-based feeder with 150 mm^2 cross-section in both cable and overhead form. Furthermore, since all customer plants are identical, only one customer plant of the two at each connection point is presented on the diagrams.

This basic grid, which would be the reference for *CVR* results, is presented in Figure 4.2a for zero percent *PV* penetration and in Figure 4.2b for a hundred percent *PV* penetration. In the former, active power passes in one direction, from MV to LV grid, while in the latter, power is bidirectional, as indicated in the figure.

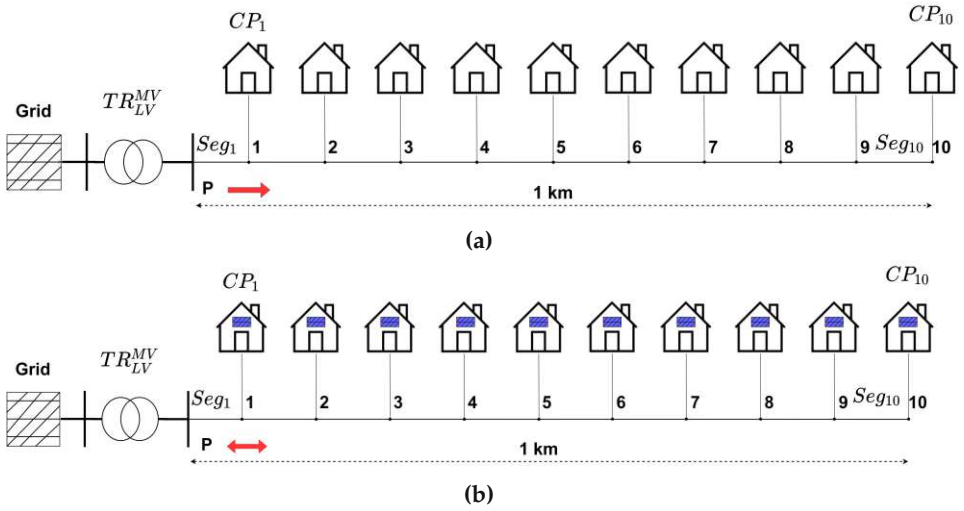

Fig 4.2. Theoretical *LV* grid model with directly connected *CPs* (a) Without *PV* (b) with *PV*.

The line specifications can be determined from the parameters in table A.1 where the parameters of the simulated lines are compared with other typically used ones. It is to be noted that the main difference between the cable and overhead feeder is that the former has a higher *R/X* ratio as well as much higher capacitance.

This shall show some differences in the simulation results, as shown in chapter 6. Assumptions for these simulations include that the active power losses or reactive power resulting from the feeder are assumed to be distributed equally along the feeder segments, to emphasize the load results and also for simplicity since their values are minimal at the LV level. The no-load losses of Distribution Transformers (DTRs) are ignored in this simulation; this is because they vary according to many factors (such as manufacturer and quality).

The first technique used to apply *CVR* on LV, is introduced by connecting each customer plant to the grid through a LV On-load tap changer transformer at as illustrated in Figure 4.3a with no *PV* presence and in Figure 4.3b with *PV* at each customer plant.

Such a specialized *LV-CP* transformer is not a common product on the market, however there are other *LV-LV* transformers that can be used. The specifications of them differ according to the size and manufacturer. However, the one used in simulation is a two-winding *LV-LV* transformer with the lowest power the author could find, and the details of it are found in table A.3.

And since there are no controller devices available for such a case, the author used trial and error till reaching the controller values that reach the best accuracy - regardless of its applicability in a real product, since this would be a whole different study on its own.

The specifications are adopted from the smallest commercially available LV-LV transformer, as there are no existing solutions specialized for this type of connection. However, the

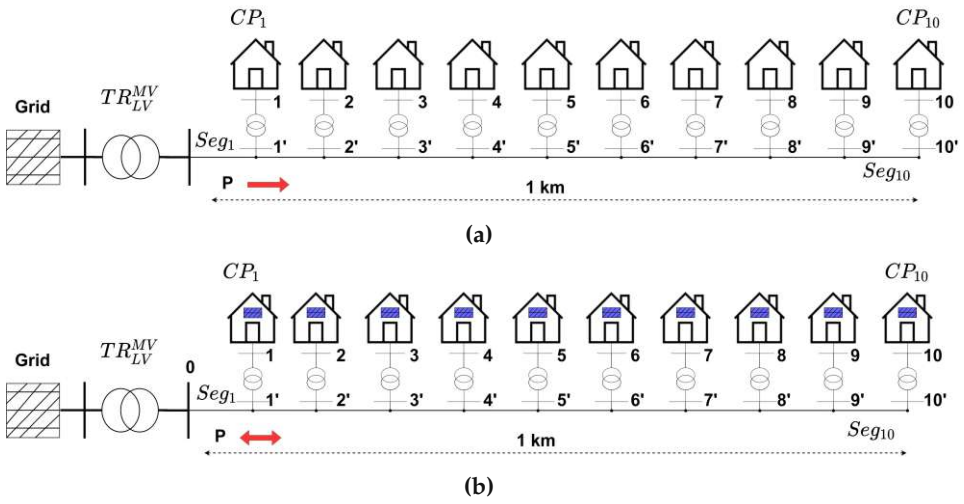

Fig 4.3. First technique: *LV* grid with *CPs* connected through transformers (a) Without *PV* (b) with *PV*.

smallest option is still rated much higher (10 kVA) than the peak consumption and double the maximum injection of *PV* back into the grid (5kW at a power factor of 1.0).

This already implies that the percentage of no-load losses suffered will be higher than needed; this resulted in a 40 step, with each step adding/subtracting one percent of the voltage. However, in reality, most control systems have 6 or 9 steps, but the goal here is a proof of concept.

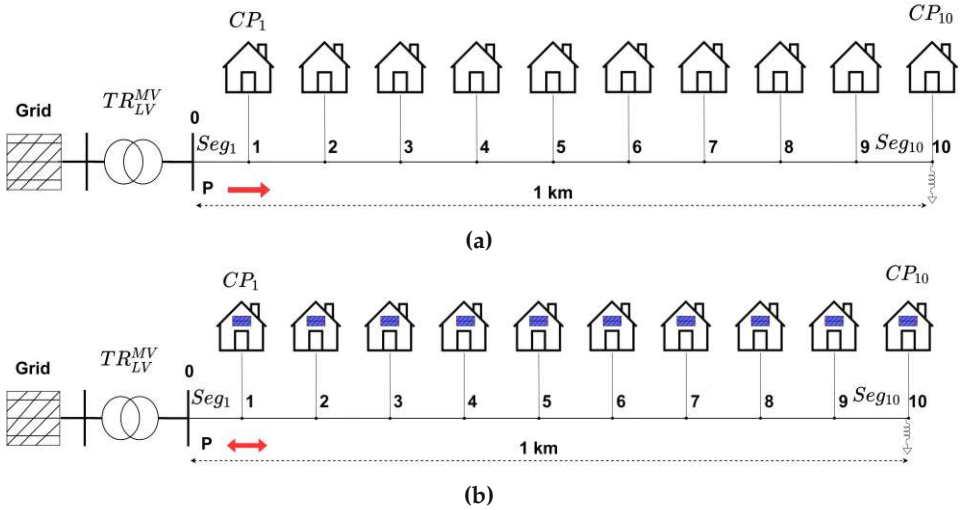

Fig 4.4. Second technique: *LV* grid with controllable coil and directly connected *CPs* (a) Without *PV* (b) with *PV*.

The second technique applied is to use a controllable coil with a voltage-based control strategy at the end of the feeder, as illustrated in Figure 4.4a with no PV presence and in Figure 4.4b with PV at each customer plant. The basic idea is that the coil will be partially/fully connected to the grid as needed to consume reactive power and, subsequently, drop the voltage.

The controllable coil has a rated reactive power Q_n of 1 Mvar and its controller has 2000 positions with 1 kvar increase with each position. The target voltage at the last node of the feeder is the ideal $0.9V_n$. The problems with this technique are that, it only keeps the ideal voltage at the last node not all of them (as in the first technique), and the increased consumption of reactive power. This shall be estimated in chapter 6.

The MV grid is provided here as an abstract infeeder with a voltage of 20 kV and a load flow based on terminal voltage $\|\mathbf{V}_{term}\|$ and voltage angle δ; where $\|\mathbf{V}_{term}\|$= 106%, $\delta = 0$ and a rated apparent power S= 100 MVA.

4.3. Medium voltage level

Simulated medium voltage grids have both cable and overhead lines. The figure displays an MV theoretical grid divided into 32 segments, feeding 32 LV grids placed uniformly along the 24 km long aluminum-based feeder with 150 mm^2 cross-section in both cable and overhead form. The lines depicted are modeled according to the equivalent circuit section 5.2.

The LV grids used are the exact ones used in the previous simulations, such that an MV overhead grid is connected with 32 LV overhead grids, and similarly, the MV cable grid is connected to 32 LV cable grids. The specifications of the MV feeders are seen in table A.2.

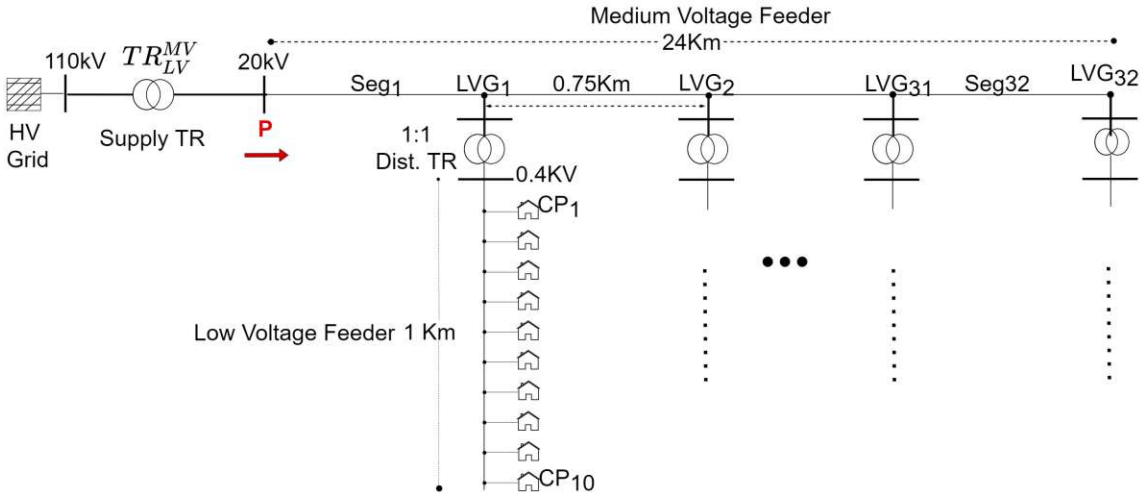

Fig 4.5. Overview of simulated theoretical MV Grid without PV.

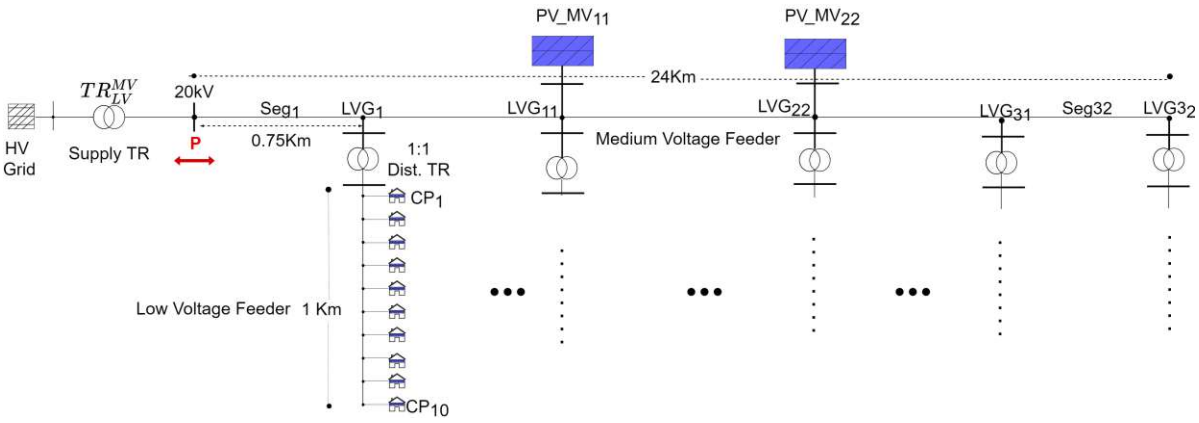

Fig 4.6. Overview of simulated theoretical MV Grid with *PV*.

The basic (reference) grid without *PV* (i.e., customer plants are purely consumer) is shown in fig. 4.5, where the LV grids are connected to the MV grid through fixed-tap transformers at a 1:1 ratio with a typical voltage profile.

The HV grid is provided here as an abstract infeeder with voltage 110kV and load flow type of terminal voltage $|\text{vterm}|$ and voltage angle δ; where $|\text{vterm}| = 106\%$, d = 0 a rated apparent power S= 100 MVA.

The distance between the LV feeders is 0.75 km each, and the MV feeder occupies 24 km (32 feeders). Active power passes along the MV feeder to supply each of the 32 segments and decreases uniformly upon distribution. In the case of *PV*, note that power is bidirectional, as indicated in the figure.

While fig. 4.6 gives an overview of the grid with the case of *PV* integration, such that the grid accepts *PV* injection from all LV customer plants as well as PV power plants at the MV level at Node 11 and 22.

The CVR technique is realized here by a simple open-loop voltage drop at the supply transformer TR_{MV}^{Hv} by 2%. This means that no other changes are introduced to the grid structure, which would be a very cost-effective measure, making it a popular CVR technique. For this grid simulation, no-load losses of DTR are ignored as in the case of LV grids simulation and for the same reason.

5. Modeling

The models of the components used in the simulation grid are detailed in this chapter. In order to find a solution to the power flow problem, it is best to begin by understanding the system itself. The chapter, therefore, briefly introduces the slack bus, lines, transformers, customer plants, and LV Grids used in the simulation grid. The photovoltaic models used in PV generation are also explained, as well as the Load zip model.

5.1. Slack Bus

A slack bus is generally defined as a bus with generating units that balances the system P and Q while analyzing the load flow. It is also known as a "Reference Bus" because its voltage and phase angle are known and assumed quantities, so there can be no more than one of it in a load flow analysis.

Its absence would result in a not adequately constrained system and non-matching number of unknown variables and corresponding equations. This would cause complexity in the solution, or will sometimes be deemed unsolvable. The primary purposes of it are:

- It provides a reference for $\|\mathbf{v}\|$ and δ in the system, coining its name.
- It is used to provide the system losses, both real and reactive, which are not known until the final solution is reached.

5.2. Lines

The lines are modeled according to standard the equivalent circuit in Figure 5.1 and the relevant eqs. (5.1) to (5.3).

$$R_{seg} = R^{'} \cdot l \tag{5.1}$$

$$L_{seg} = X_L^{'} \cdot l \tag{5.2}$$

$$B_{seg} = 2\pi f \cdot C^{'} \cdot l \tag{5.3}$$

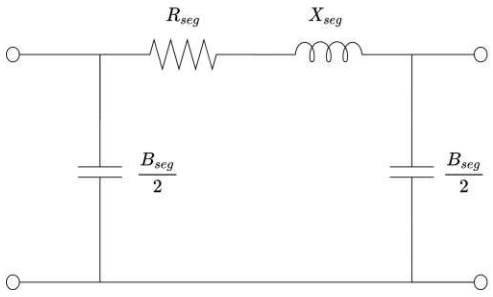

Fig 5.1. Lines equivalent circuit.

where l is the length of the line in km; $R^{'}$ is the specific resistance; $X_L^{'}$ is the specific reactance; $C^{'}$ is the specific capacitance; f is the system frequency. See table A.1 for values of R_{seg}, $Xseg$ and $Bseg$.

5.3. Transformers

Transformers are modeled according to the standard equivalent circuit in Figure 5.2 and the eqs. (5.4) to (5.6). The relevant parameters of the distribution transformers used in this thesis can be found in table A.3.

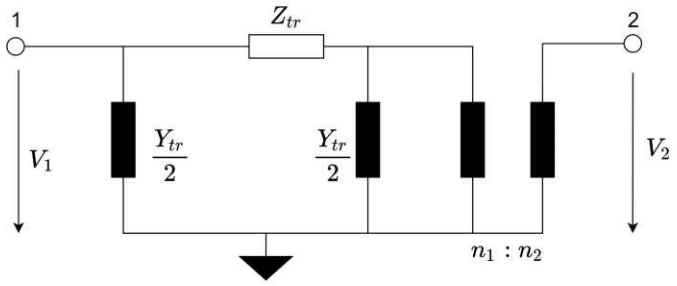

Fig 5.2. Transformers equivalent circuit.

$$Z_{tr} = R_{tr} + jX_{tr} = \frac{V^2(v_r + j\sqrt{v_{sc}^2 - v_r^2} \times 10^{-2})}{S_n} \tag{5.4}$$

$$Y_{tr} = \frac{V_{fe} \times 10^{-3} - j\sqrt{(i_0 \times 10^{-2} \times S_n)^2 - (V_{fe} \times 10^{-3})^2}}{V_{n2}^2} \tag{5.5}$$

$$\frac{n_1}{n_2} = \frac{V_{n1}}{V_{n2}} \tag{5.6}$$

where Z_{tr} is the short circuit impedance in the rated transformation ratio [Ω]; Y_{tr} is the no-load admittance [S] and $n_1 : n_2$ is the rated transformation ratio.

It is worth noting that the no-load losses of the distribution transformers (MV-LV) are ignored in the used simulations since they vary according to many factors (such as manufacturer and quality) and they do not affect the comparison between different cases as they are constant. However, the no-load losses of the LV-LV transformers used in CVR application are taken into consideration due to their significance in estimating the losses of this CVR technique.

5.4. PV generation

Photovoltaic systems are built of PV panels, inverters, and over-voltage protection. In order to maintain a generic model away from uncontrolled and unexpected factors, the *PV* system must have some assumption:

- The installed rated capacity is at 2.5x the P_Peak, which is the average ratio of installation which varies among rural, small urban, and large urban customer plants.
- The weather conditions are optimal such that the system can produce the optimal power curve (shaped as a positive-half a Sine-Wave power over the day-time), achieving the rated capacity at midday.

- The inverters are assumed to be uncontrolled and modeled as a PQ-producer injecting P at a power factor ($cos(\phi)$) of 1.0.
- The PV system losses are neglected (i.e., 100% efficiency)

And relating to section 5.5, a mathematical approach is identified in eq. (5.7).

$$F_{PV} = \frac{PV_t}{PV_{Rated}} \tag{5.7}$$

where F_{PV} is normalized dimensionless values that describe PV_t in terms of PV_{Rated}, PV_t is the production of the local PV unit at time-point t and PV_{Rated} is the installed rated capacity of the PV system.

5.5. Load-ZIP model

The mathematical model of the ZIP model mentioned in section 2.1 is described in detail in [17] and formed the basis for the load model [34], which is adopted here as the base simulation model. According to the ZIP model, explained in section 5.6, the following eqs. (5.8) and (5.9) are used to build the daily profile as follows:

$$F_P = \frac{P_t}{P_{Peak}} = \frac{P_{nom,t}}{P_{Peak}} \cdot (C^Z_{P,t} \cdot V^2_{pu,t} + C^I_{P,t} \cdot V_{pu,t} + C^P_{P,t}) \tag{5.8}$$

$$F_Q = \frac{Q_t}{P_{Peak}} = \frac{Q_{nom,t}}{P_{Peak}} \cdot (C^Z_{Q,t} \cdot V^2_{pu,t} + C^I_{Q,t} \cdot V_{pu,t} + C^P_{Q,t}) \tag{5.9}$$

$$V_{pu,t} = \frac{V_t}{V_{nom,t}} \tag{5.10}$$

where the factors F_P, F_Q are normalized dimensionless values that describe P_t, Q_t in terms of P_{Peak}; P_t, Q_t are the actual active and reactive power consumption of the customer at the time-point t respectively; $P_{nom,t}, Q_{nom,t}$ are the active and reactive power consumption of the customer at time-point t at nominal grid voltage $U_{nom,t}$ respectively; P_{Peak} is the peak active power demand in winter; $V_{pu,t}$ is the per-unit voltage at t; $C^Z_{P,t}, C^I_{P,t}, C^P_{P,t}$ are the active power ZIP coefficients and $C^Z_{Q,t}, C^I_{Q,t}, C^P_{Q,t}$ are the reactive power ZIP coefficients at the time-point t.

CVR can reduce the core losses of transformers [7, 37, 38]. Transmission line losses may still occur, since line current increases when voltage is reduced for constant-power loads. This, however, does not hold for constant-impedance and constant-current loads. As per studies in [7], CVR can still reduce the net system losses when all losses are taken into account.

5.6. Customer plants

The customer plants connected to the *Link*-Grids are an aggregation of their active and reactive power consumption in the ZIP format, as well as their active power generation resulting from PV units. In the simulation itself, they are only represented as a node to which its subsequent components are connected.

5.7. LV and MV grids

Within the system are known and unknown variables dependent on the bus type. There are three bus types, as shown in Figure 5.3 which are:

- The load bus with no generators connected to it.
- The generator bus with at least one generator connected to it.
- The slack bus, a previously selected bus with an infeeder/generator.

And as mentioned in chapter 2, it is usually the case that P moves from the bus with higher δ to the bus with lower δ, while Q moves from the bus with $|V|$ to the bus with lower $|V|$.

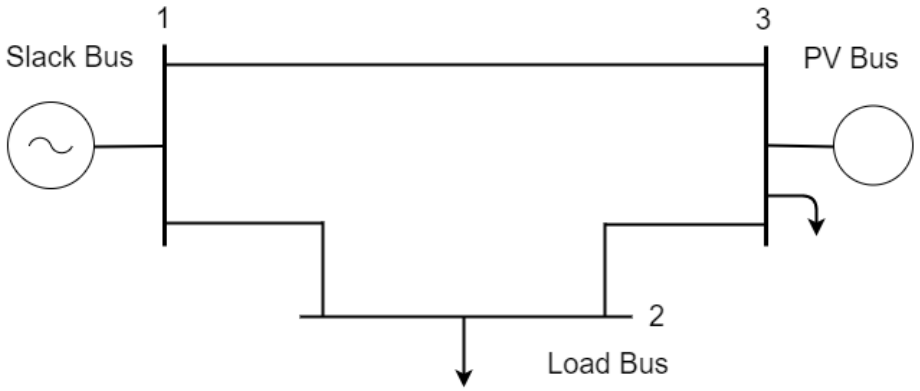

Fig 5.3. Grid model including the three bus types

The simulation program analyzes the power flow, solving a nonlinear equation system that describes the power flow in each line. There are different solving methods of this system of equations. The method used here (and the most-popular) is the *Newton–Raphson* method, which is illustrated in [39].

Finally, losses are a crucial factor to be taken into consideration, where it should be assessed if the losses resulting from the CVR techniques applied are indeed beneficial. The detailed modeling of each grid component is found in chapter 5, and only the equations of the net losses of the grids are presented.

Losses are estimated on the investigation level 2 and 3 (MV Grid-Link and LV Grid-Link, respectively), and in order to determine the losses of the LV grid in the standard connection case as well as the Voltage-Reactive power control case, eq. (5.11) is used.

$$Net\ P_l^{LV} = P_l(\ TR_{LV}^{MV}\ ) + P_l(Line^{LV})\ \ (kW) \tag{5.11}$$

Where the net losses ($Net\ P_l^{LV}$) is the sum of the MV-LV distribution transformer losses and the line losses of the distribution feeder.

And to calculate the LV losses in the case of OLTC connections between customer plants and the feeder, eq. (5.12) is used.

$$Net\ P_l^{LV} = P_l(\ TR_{LV}^{MV}\ ) + \sum_{i=1}^{n} P_l(\ TR_{CP_n}^{LV}\ ) + P_l(Line^{LV})\ \ (kW) \tag{5.12}$$

where the net losses ($Net\ P_l^{LV}$) are the sum of the distribution transformer *MV-LV* losses, all *LV-CP* transformers losses, and finally, the line losses in kW. From the previous, it is concluded that the transformers' losses are primarily no-load (iron) losses.

While in the case of the MV grid, losses are calculated as a sum of all connected LV grids losses as well as other elements of the MV grid (i.e, supply transformer and MV feeder), as seen in eq. (5.13).

$$Net\ P_l^{MV} = \sum_{i=1}^{n} Net\ P_l^{LV} + P_l(\ TR_{MV}^{HV}\ ) + P_l(Line^{MV})\ \ (kW) \tag{5.13}$$

Where $Net\ P_l^{MV}$ are the net losses of the MV grid, $\sum_{i=1}^{n} Net\ P_l^{LV}$ is the sum of the definite number (n) of LV grid losses, $P_l(\ TR_{MV}^{HV}\ )$ is the losses of the supply transformer, and $P_l(Line^{MV})$ is the line losses of the MV feeder.

6. CVR behavior

This chapter discusses the simulation results of CVR techniques seeking to achieve load reduction by applying the minimum possible voltage at the relevant points across the voltage chain. In section 6.1, the simulation is applied to a theoretical customer plant setup, examining the difference a photo-voltaic unit makes in the result. While in sections 6.2 and 6.3, it is examined just how much of these theoretical benefits can be harvested in the grid setup of Low- and Medium Voltage, respectively.

6.1. Customer plant Grid-Link

This section examines the potential of applying consistent load reduction at the customer plant on the Link-Grid scheme independently of other links specifications, both in the case of PV absence section 6.1.1 and presence section 6.1.2. Each subsection contains a brief schematic of the system under focus, its daily power profile, and accordingly determines the system behavior before and after CVR at selected simulation points throughout the day.

6.1.1. Without PV

This subsection discusses the case of customer plants without a photo-voltaic system, i.e., pure consumers link as depicted in fig. 6.1. The CP has normalized power values (i.e., power in terms of the peak active power demand in winter, to maintain a generic model) throughout the day to build the daily profile seen in fig. 6.2. The key simulation points throughout the day are selected based on the resulting graph at dawn, noon, and twice in the evening, as summarized in table 6.1.

Simulation Point	Time of Day	Consumption	
		P	Q
t1	04:00	Average	Average
t2	12:00	Relatively Low	Relatively High
t3	20:00	High	Low
t4	22:00	Relatively High	Slightly capacitive (-ve)

Table 6.1. Simulation points in time for customer plants without PV and their characteristics.

The active and reactive power consumption against the voltage differs according to the corresponding ZIP coefficients seen in table A.4, which reflect the characteristics at the simulation times $t \in \{t1, t2, t3, t4\}$, and the eqs. (5.8) and (5.9).

The result is depicted in figs. 6.3 and 6.4 for active and reactive power, respectively. In the active power case, the normalized P consumption exhibit an almost linear association with the voltage at all four times, with just the magnitude differing.

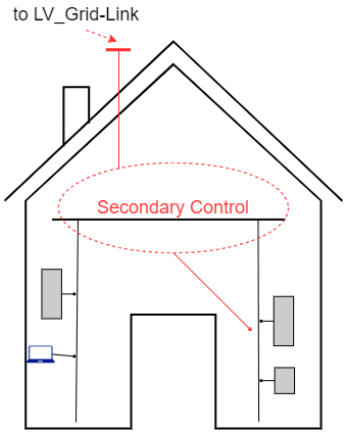

Fig 6.1. CP Grid-Link without PV.

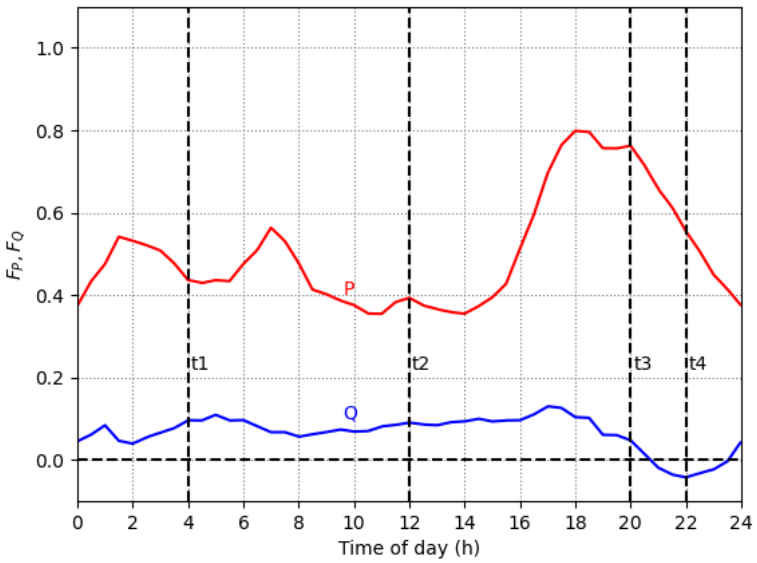

Fig 6.2. Normalized daily profile of CP at V_{nom} based on [35]

However, with reactive power, the almost-linear relationship is only present at $t1, t2$ where the demand is average or more. However, at $t3$ the reactive power demand is very low, that means that its relationship with the voltage is almost constant. The ($t4$) relationship is even more interesting, where the customer plant has a capacitive behavior (i.e., injecting Q into the grid), the amount of Q differs significantly with V. The amount of Q injected is steeply lowered when constant voltage reduction is applied, resulting in the customer plant being less capacitive at the time.

To further describe the potential for power savings, an illustrated result in fig. 6.5 depicts the possible percentage change of active power across the allowed voltage range ($V_n \pm 10\%$).

The possible power savings at the four time-points increase steeply as the original operating voltage (before CVR) increases. That fact suggests that CVR would affect a customer plant located at the beginning of a distribution feeder the most, where normally the voltage is at its highest level before it starts to decrease along the feeder gradually.

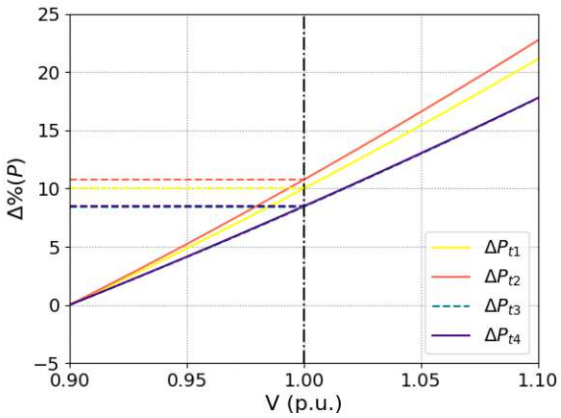

Fig 6.5. Possible P reduction at CP without PV at defined time-points.

It is notable that power savings at ($t3$ and $t4$) are almost identical as their slope in fig. 6.3, while ($t1$ and $t2$) are higher as they are characterized by lower active power demand.

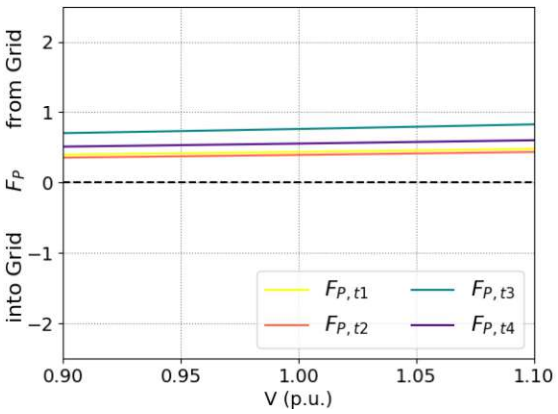

Fig 6.3. Normalized P behavior with V at defined time-points.

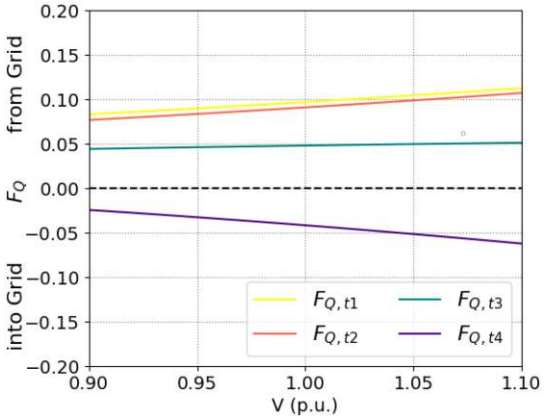

Fig 6.4. Normalized Q behavior with V at defined time-points.

6.1.2. With PV

This subsection discusses the case of customer plants with a photo-voltaic system as schemed in fig. 6.6. Figure 6.7 represents the normalized daily profile of the customer plant. Load behavior at the selected simulation time-points are also discussed here, as well as possible savings and changes due to a theoretical optimal CVR by keeping the voltage at $0.9V_{nom}$. However, since this subsection is an extension of section 6.1.1, it will only mention the differences and additions. Therefore, the table pf simulation points characteristics is updated as follows:

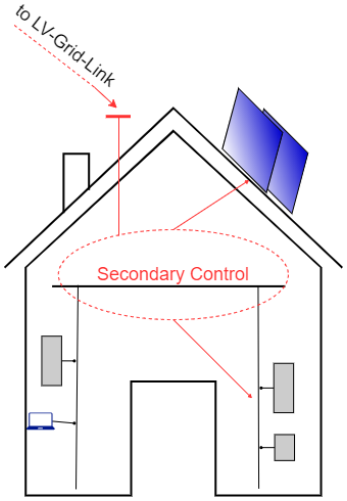

Fig 6.6. CP Grid-Link with PV.

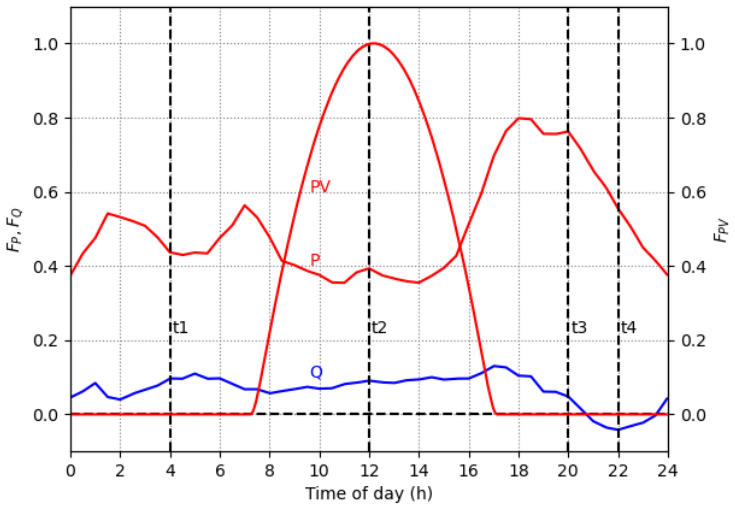

Fig 6.7. Normalized CP daily profile with PV at V_{nom} based on [35].

It is essential to mention that the reactive power behavior and changes, in this case, are

Simulation Point	Time of Day	Consumption		Production
		P	*Q*	*PV*
t1	04:00	Average	Average	Zero
t2	12:00	Relatively Low	Relatively High	High
t3	20:00	High	Low	Zero
t4	22:00	Relatively High	Slightly Capacitive (-ve)	Zero

Table 6.2. Simulation points in time for customer plants with PV and their characteristics.

identical since the presence of PV only affects the net active power. The difference then lies in the possible active power changes and the amount of energy injected into the grid. The notable difference is at the second time-point of the day (*t2*), where the CP is injecting *P* into the grid, which increases as CVR is applied since the consumption is lowered while the production stays the same.

In the case of (*t2*), the customer plant active power demand (increasing with voltage) will first be consumed from the PV production, and the remaining extra power is then fed into the grid. This explains the negative slope of ΔP_{t2} in fig. 6.9. It is not as steep as the other points because the change in customer plant power consumption is relatively small compared to the amount of active power fed into the grid.

Customer plants are able to inject power efficiently and safely into the grid thanks to the grid-tie inverters, which manage to match the voltage amplitude and phase of the grid sine wave. In the case of *CVR* application, this means that the customer plant will consume less and thus will inject the amount of saved power into the grid (assuming that there is a control strategy to regulate the voltage so that it does not go out of range at some point in the feeder). A summary of results is found in table A.5.

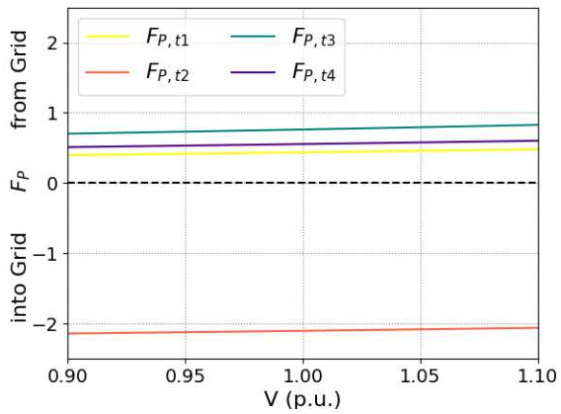

Fig 6.8. Normalized *P* behavior with *V* at a *CP* with *PV* at defined time-points.

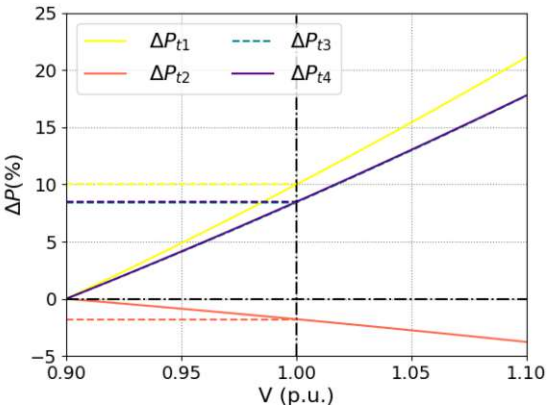

Fig 6.9. Percentage change of *P* along *V* at *CP* with *PV* at defined time-points.

6.2. LV Grid-Link

In this section, load reduction is examined in a theatrical model of an EU *LV* Grid-Link (detailed in section 4.2 and graphically depicted in fig. 6.10), while manipulating the following simulation factors:

- Connection type between customer plants and the *LV* feeder:
  - Direct (standard method without load reduction).
  - Through On-Load Tap Changer (OLTC).
- Reactive power control: Either present or not (as a voltage-controlled coil at the end of the feeder).
- Type of feeder: Overhead or cable.
- PV presence: Either present at all customer plants or at none.

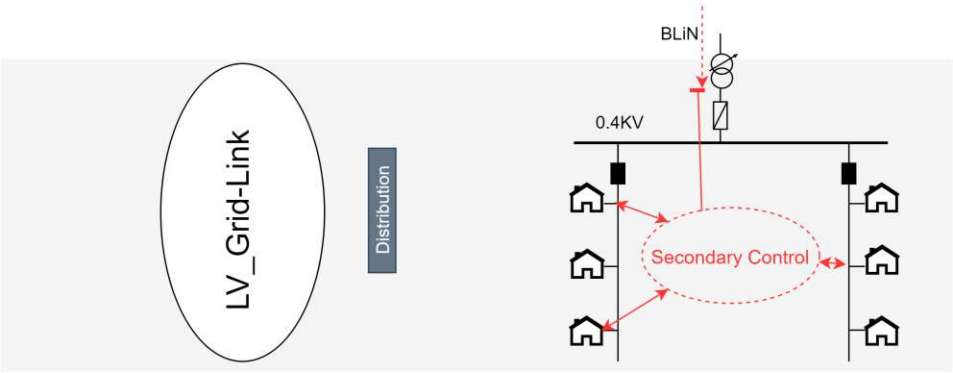

Fig 6.10. LV Grid-Link.

6.2.1. Overhead lines structure

This subsection examines the implication of CVR on load reduction in the LV grid with overhead lines structure. It depicts the results for each simulation case with the help of graphs, focusing on the parameters of interest, i.e., voltage profile, active power flow, and losses.

6.2.1.1. CP connected directly to LV grid

6.2.1.1.a. Without PV (pure consumer) This is the basic simulation case without CVR implementation to be used as a reference for the case without any PV presence. Figure 4.2a gives an overview of the grid under simulation; in this case, the customer plants are directly connected to the LV overhead feeder without any PV presence.

A typical voltage profile is seen in fig. 6.11 , where the voltage drops with the distance of the feeder. An observation here is that V_{t3} slope is the steepest, since this is the time-point of the highest power consumption, fitting to the load model in section 6.1.

And as seen in fig. 6.12, the total P losses increase proportionally with the total consumption. The losses are almost solely due to conductor losses and have minimal effect from 0.9% to 1.7%.

Figure 6.11 depicts the voltage profile of a pure consumer Customer Plant case in the LV grid with overhead lines. The curves present the voltage for different time-points, labeled $V_{t1} \dots V_{t4}$ as it covers the distance from the first node at the beginning of the feeder to the last one.

All the four curves begin at a voltage of 1.06 pu and drop with distance. The curve slope of the third time-point of the day V_{t3} is the steepest. The Y-axis is the voltage in Per Unit (pu) and the X-axis is the feeder's length starting from the secondary side of the distribution transformer, represented as nodes of customer connections.

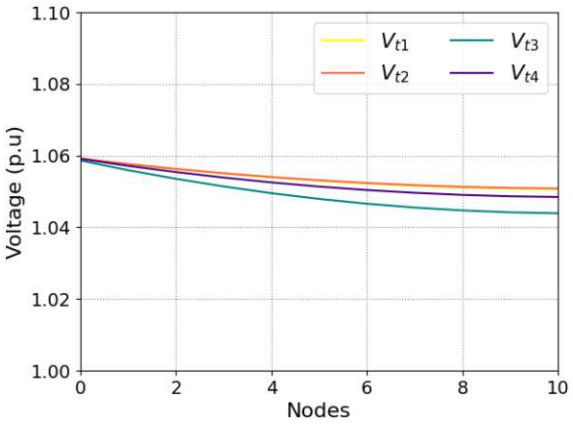

Fig 6.11. Voltage profile of LV OH grid without CVR or PV.

Figure 6.12 depicts the power flow and losses of the feeder. The left Y-axis is the total power consumed from MV Grid-Link in kW, while the right Y-axis is a vertical color bar representing the losses in kW. The X-axis is the simulated time-points of the day.

At the first and second time-points of the day (*t1* and *t2*), the system incurs the minimum loss of around 0.1 kW (pale yellow), while the third time-point of the day (*t3* - dark orange color) incurs the most significant loss which is slightly over 0.20 kW; it also has the highest amount of power flow. In between, slightly over 0.15 kW, comes the loss at the fourth time-point of the day (*t4* - bright yellow color).

While fig. 6.13 depicts the active and reactive power flow at four different time-points, labeled $P_t1 \dots P_t4$ in the case of active power and $Q_t1 \dots Q_t4$ in the case of reactive power.

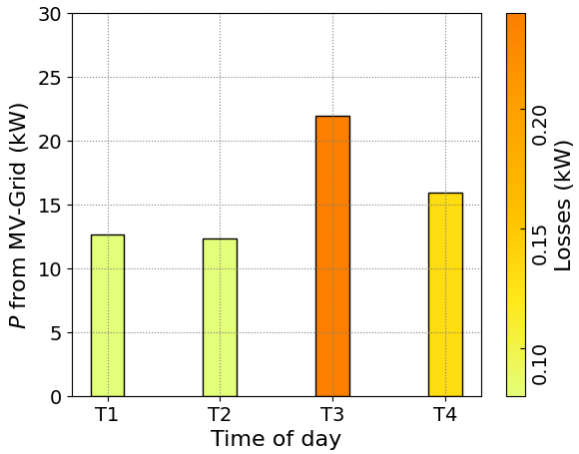

Fig 6.12. Feeder P flow and losses of LV OH grid without CVR or PV.

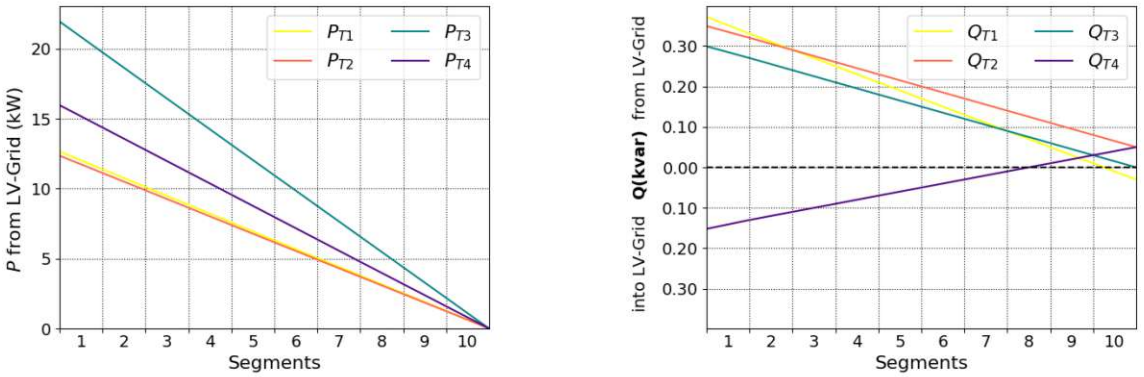

Fig 6.13. Net P (left) and Q (right) at each segment of LV OH grid without CVR or PV.

The Y-axis of the left subfigure is the active power *(P)* from the LV grid in kW, and that of the right subfigure is the reactive power *(Q)* in kvar, while the X-axis is the length of the feeder as segments where power flow is under observation. Different colors for the different time-points help distinguish and read the data more efficiently.

The active power starts above 10 kW at the first and second time-points of the day (yellow and orange lines, respectively). Moreover, at the third time-point of the day, green line, the power starts slightly above 20 kW, while it starts at the fourth time-point of the day, purple line, slightly above 15 kW.

There is a distinction in the uniformity of the slopes between the two figures. The active power passing at each segment decreases uniformly with slightly lower power consumption along the length of the feeder as the voltage drops; this is translated into a strong but slightly decreasing potential for load reduction for all four time-points.

On the other hand, reactive power has small values and does not have a similar slope since its losses are a non-linear function of the voltage, while at (*t4*) the slope is reversed due to the capacitive behavior of the load at the time.

While fig. 6.14 depicts the percentage change of active power for respective customer plants as calculated in eq. (3.8) such that the Y-axis is the active power percentage change ΔP, and the X-axis represents the customer plants along the feeder, with different colors representing each time-point of the day, labeled $dP_T1 \ldots dP_T4$.

The plotted values indicate the difference in power compared to the estimated theoretical values for each of the time-points at the

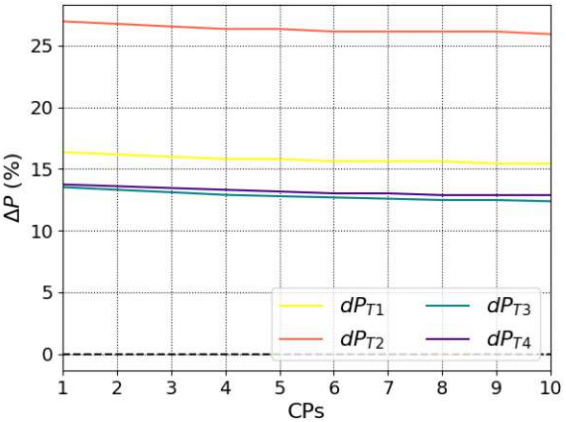

Fig 6.14. Percentage change of active power compared to optimal values of LV OH grid without CVR or PV.

minimum voltage $0.9V_n$. This graph makes it easy to determine how beneficial CVR would be, as potential for CVR increases as the percentage change does. The highest potential is thus at the second time-point of the day in red, lying above 25%, followed by *t1* (yellow) slightly above 15%, and then by *t4* (dark blue) and *t3* (light blue), both around 13%.

6.2.1.1.b. With PV Expanding on the previous simulation case, PV installation is added to each customer plant in this typical LV grid (without the addition of CVR), as illustrated in fig. 4.2b. It is to be noted that the voltage exceeds the upper limit, since there are no counter measures such as reactive power – voltage (*Q-V*) control applied in this simulation.

Figure 6.15 depicts the voltage profile of the case customer plants after a PV installation. The Y-axis is the voltage per-unit *(pu)* and the X-axis is the length of the feeder as nodes. The upper limit at $1.1V_{nom}$ is indicated by a dashed line.

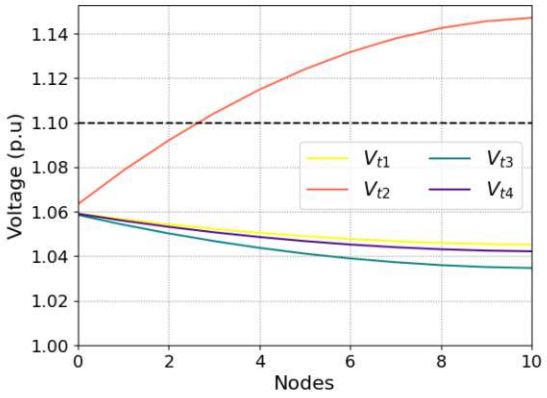

Fig 6.15. Voltage profile of LV OH grid with PV, without CVR.

In comparison to the previous simulation case (without PV), the only change occurs at V_{t2} (red line), where voltage increases significantly, as the customer plants are now injecting back power into the grid after covering their local consumption. After the third connection point (0.3 km), the upper limit is already exceeded.

While fig. 6.16 depicts the total active power flow and losses of the LV Link-Grid as obtained after PV installation. The left Y-axis is the power injected into the MV Grid-Link or consumed from the MV Grid-Link in kW, while the right Y-axis is a vertical color bar representing the Losses in kW as a color range, while the X-axis represents the time-points of the day.

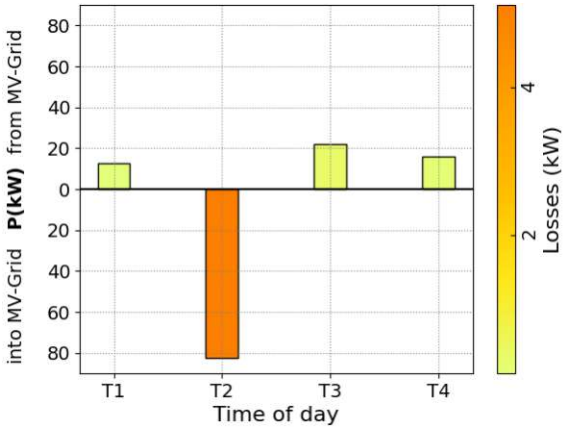

Fig 6.16. Feeder *P* flow and losses of LV OH grid with PV, without CVR.

The most significant loss, above 4 kW, is incurred at the second time-point of the day (*t2*) (dark orange color) where the highest amount of power (around 80kW) is injected. while the rest exhibit the same losses' behavior as in the case without PV, around 1 kW, (pale yellow) as in the case of pure consumers.

Moreover, fig. 6.17 depicts the active and reactive power flow obtained after PV installation. The Y-axis of the left subfigure is the active power *(P)* from the LV grid in kW, while the one of the right subfigure is the reactive power *(Q)* in kvar. The X-axis is the length of the feeder as segments where power flow is under observation.

The only change occurs at the second time-point of the day (*t2*), where there is a substantial active power injection and reactive power consumption (red line). The latter diminishes the values occurring at the other time-points.

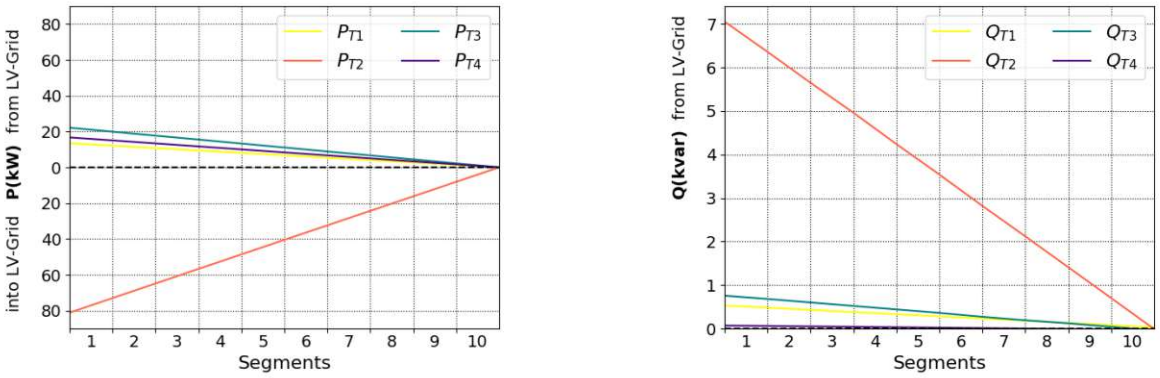

Fig 6.17. Net P (left) and Q (right) at each segment of LV OH grid with PV, without CVR.

While fig. 6.18 depicts the percentage change of active power for respective customer plants after PV installation. The Y-axis is the active power percentage change ΔP, and the X-axis represents the customer plants.

The plotted values indicate the difference in power compared to the estimated theoretical values for each of the time-points. The lines are therefore labeled $dP_T1 \ldots dP_T4$.

The difference from the previous simulation case (without PV installations), is noticed at the second time-point of the day, where dP_{T2} (red line) deviates only slightly from the optimal result now, but in the negative direction due to the power direction (injection into the grid).

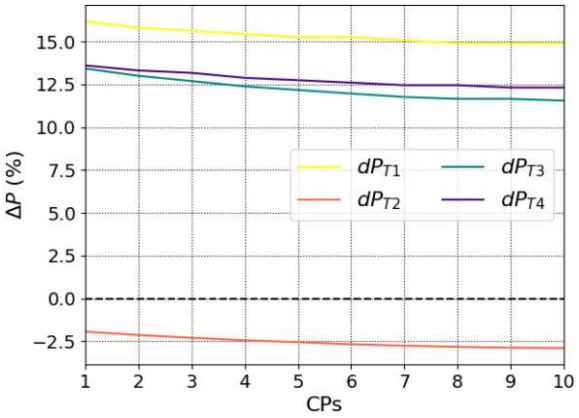

Fig 6.18. Percentage change of active power compared to optimal values of LV OH grid with PV, without CVR.

6.2.1.2. CP connected through OLTC transformers

6.2.1.2.a. Without PV (pure consumer) This simulation case examines the effects of connecting customer plants to the LV Grid-Link through On-load tap changer transformers, without

PV penetration. Thus, in this case, the two voltage profiles are presented such that fig. 6.19a on the left presents the voltage on the LV side of the transformers, and fig. 6.19b on the right represents the voltage on the customer plants' side.

The Y-axis is the voltage in per-unit *(pu)* the X-axis represents the length of the feeder as nodes of customer plants connection, for the left subfigure on the LV side of the OLTCs, and on the customer plants side for the right subfigure.

On the LV side, voltage decreases starting from a voltage of 1.06(pu) at the secondary side of the distribution transformer, with a similar slope for all time-points. On the customer plants' side; however, the ideal voltage is implemented at the customer plants and kept constant at $0.9V_{nom}$.

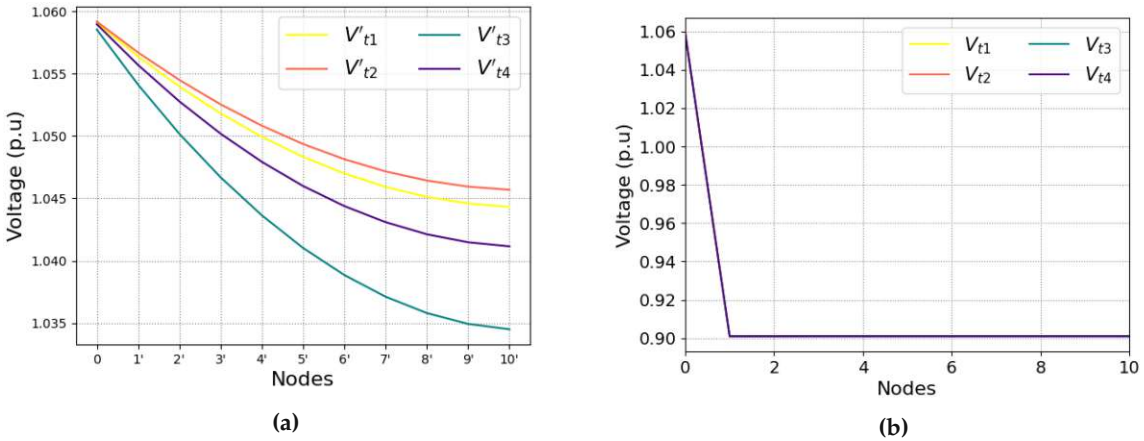

(a) (b)

Fig 6.19. Voltage profile of LV OH grid without PV, with OLTC CVR on (a) *LV* side (b) *CP* side.

While fig. 6.20 depicts the transformer losses in comparison to the line losses at all time-points. The Y-axis is the losses obtained in kW, while the X-axis is the time of the day.

The color green represents line losses, orange is for transformer losses, and blue sums all transformer losses (including the ones of the distribution transformer) as in eq. (5.12).

The result exhibits that the overwhelming part of losses is due to transformers, particularly the *LV-CP* ones, with very minimal effects of the $MV-LV$ transformer. The increase of line losses at *t3* is due to a higher active power consumption, while transformer losses only increase slightly.

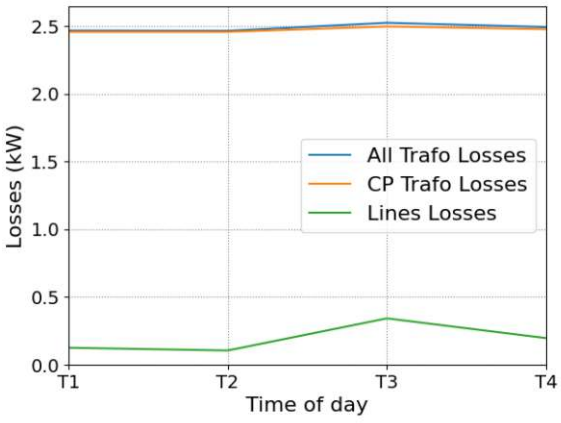

Fig 6.20. Transformers vs. lines losses of LV OH grid without PV, with OLTC CVR.

While fig. 6.21 depicts the total active power flow and losses of the LV Link-Grid. The left Y-axis is Power injected from the MV Grid-Link in kW, while the right Y-axis is a vertical color bar representing the Losses in kW. The X-axis represents the time-points of the day.

At the first and second time-points of the day (*t1* and *t2*), the system incurs the minimum loss of around 2.6 kW (pale yellow), while the third time-point of the day *t3* (dark orange color) incurs the most significant loss which is slightly over 2.8 kW; it also has the highest amount of power flow. In between, slightly under 2.7 kW, comes the loss at the fourth time-point of the day (*t4*) (bright yellow color).

Note that the percentage of losses decreases as the power flow increases, cohering to the same observation in the previous simulation cases.

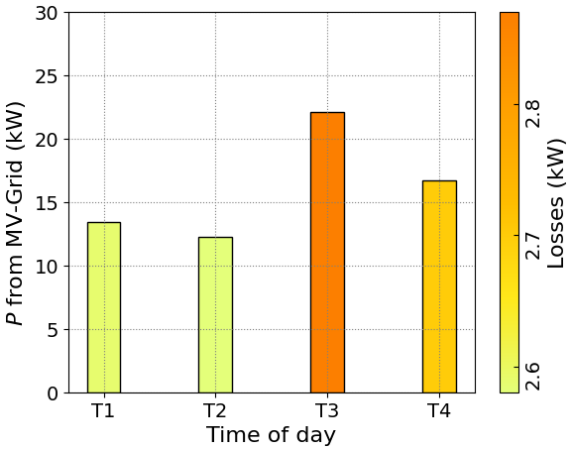

Fig 6.21. Feeder *P* flow and losses of LV OH grid without PV, with OLTC CVR.

While fig. 6.22 depicts the Net *P* (left) and *Q* (right) at each segment. The Y-axis of the left subfigure is the active power *(P)* from the LV grid in kW, and the Y-axis of the right subfigure is the reactive power *(Q)* consumed from the LV grid in kvar. The X-axis is the length of the feeder as segments where power flow is under observation.

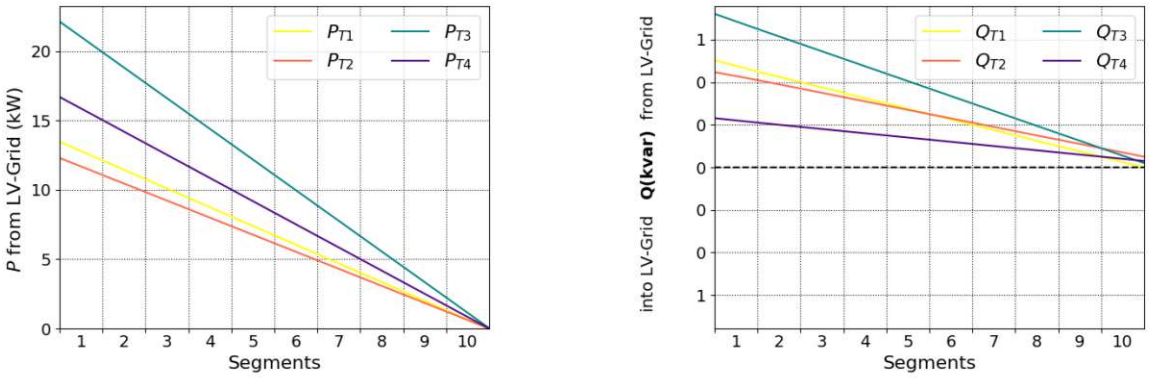

Fig 6.22. Net *P* (left) and *Q* (right) at each segment of LV OH grid without PV, with OLTC CVR.

The active power starts above 10 kW at the first and second time-points of the day (yellow and orange lines). Moreover, at the third time-point of the day (green line), it starts slightly above 20 kW, and at the fourth time-point of the day (purple line) slightly above 16 kW. There is a uniform decrease in P and an almost uniform decrease in Q along the feeder's length for all the time-points observed.

Figure 6.23 depicts the percentage change of active power for respective customer plants compared to values at $0.9V_{nom}$. The Y-axis is the active power percentage change ΔP, and the X-axis represents customer plants.

This is the ideal case, since the percentage change nears 0% along the whole line, meaning there is no difference between the theoretical and obtained results and the full potential of CVR is applied on each and every customer plant that is connected to the feeder.

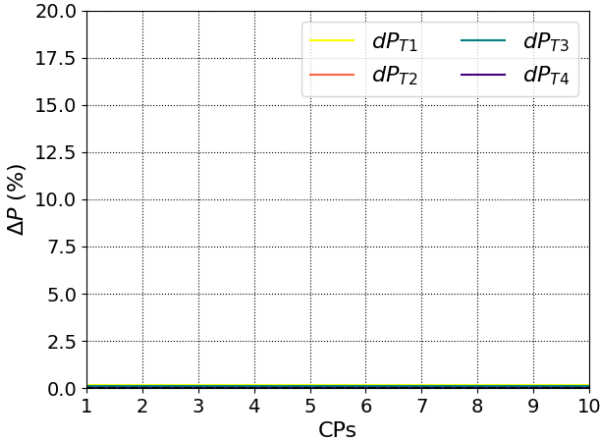

Fig 6.23. Percentage change of active power compared to optimal values of LV OH grid without PV, with OLTC CVR.

6.2.1.2.b. With PV In this case, PV is introduced along with load reduction as illustrated in fig. 4.3b and therefore the two voltage profiles only change again at V_{t2}. Figure 6.24b indicates the value on the LV side of the transformer, and fig. 6.24a on the customer plants' side. The Y-axis is the voltage in per-unit *(pu)*, and the X-axis represents the length of the feeder as nodes of customer plants connection, for the left subfigure on the LV side of the OLTCs, and on the customer plants side for the right subfigure.

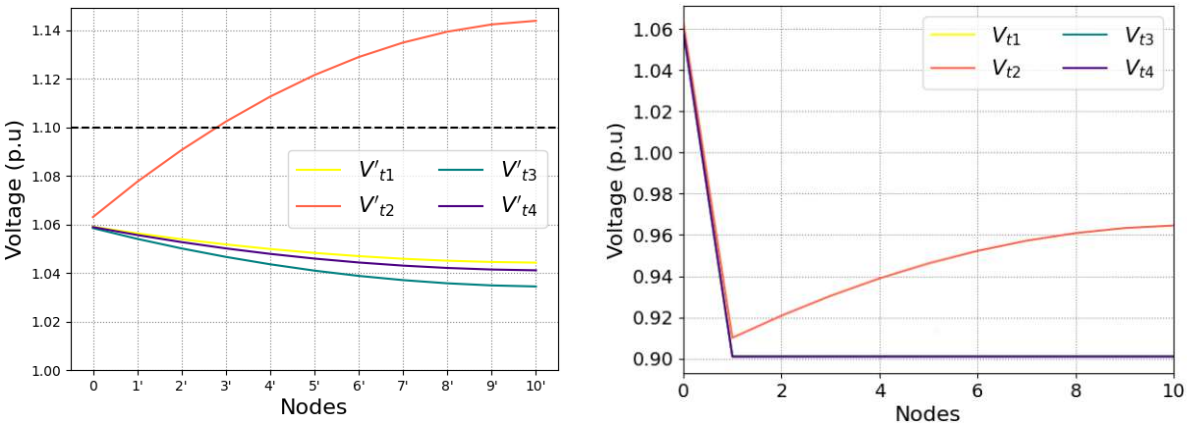

(a) **(b)**

Fig 6.24. Voltage profile of LV OH grid with PV and OLTC CVR on (a) *LV* side (b) *CP* side.

The voltage profile changes at V_{t2} exceeding the upper limit (1.10V) on the LV side and also on the customer plants' side. This means that the On-load tap changer fails to keep the voltage at the ideal level due to the significant increase of injected energy into the grid, which increases along the feeder.

However, there is a positive side effect here, that there would be no need for a control strategy to keep the voltage within limits because the voltage reaching the customers is within

limits in any case, even if it increases above the $1.1V_{nom}$ threshold on the LV side.

Figure 6.25 depicts transformer losses in comparison to lines losses at the different time-points after PV installation. The Y-axis represents the losses obtained in kW, while the X-axis represents the time-points of the day. All transformer losses are represented by the green line and customer plant transformer losses is represented by the orange line, while the lines losses is represented by the blue line.

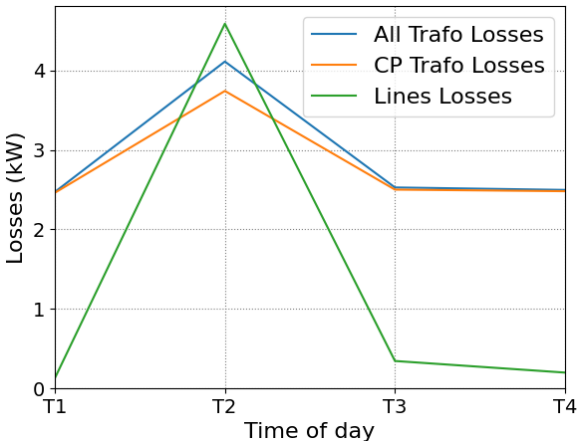

Fig 6.25. Transformers vs. Lines Losses of LV OH grid with PV and OLTC CVR.

Losses show a significant change only at the second time-point of the day (*t2*) with the most increase in line losses due to higher *P* injected back into the grid. And since the transformers losses are split into no-load- and load-losses, *P* losses increase at the second time-point of the day (*t2*) mainly due to an increase in lines and transformer load losses.

While fig. 6.26 depicts the total active power flow and losses of the LV Link-Grid. The left Y-axis is the power injected into the MV Grid-Link or consumed from the MV Grid-Link in kW, while the right Y-axis is a vertical color bar representing the Losses in kW. The X-axis represents the time-points of the day.

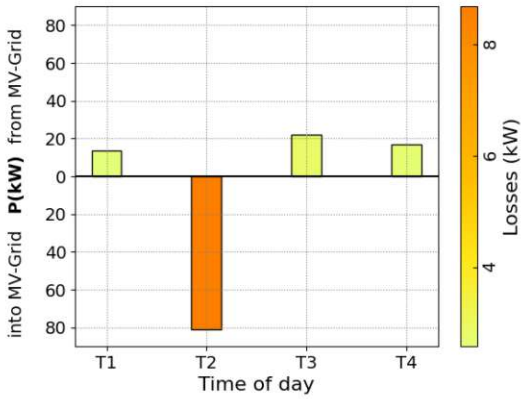

Fig 6.26. *P* flow and losses of LV OH grid with PV and OLTC CVR.

The most significant loss, above 8 kW, is incurred at the second time-point of the day (*t2*) (dark orange color) where the highest amount of power (around 80kW) is injected, while the rest exhibit the same losses' behavior, under 4 kW, (pale yellow) as in the case of pure consumers (around 20kW). As seen before, the losses as a percentage of *P* are lowest at the highest power flow (*t2*), although it has the highest magnitude of losses, and highest, as a percentage of *P*, at the lowest flow (*t1*).

While in fig. 6.27, it is seen that active power injection flow and its losses. The Y-axis of the left subfigure is the active power *(P)* from the LV grid in kW, and the Y-axis of the right subfigure is the reactive power *(Q)* consumed from the LV grid in kvar. The X-axis is the length of the feeder as segments where power flow is under observation.

The difference is found at the second time-point of the day *t2* (red line), where there is a much higher reactive power flow (both consumption and losses), due to the high increase of voltage.

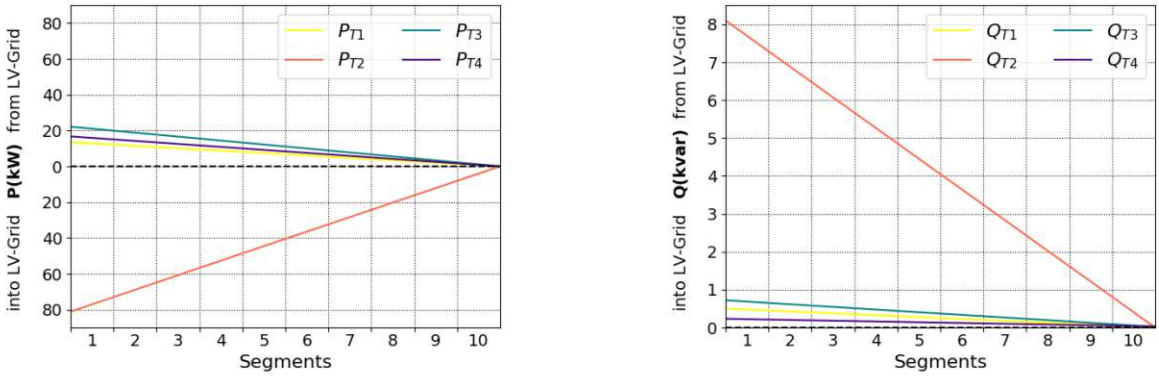

Fig 6.27. Net P and Q across feeder of LV OH grid with PV and OLTC CVR.

While fig. 6.28 depicts the percentage change of active power for respective customer plants compared to values at $0.9V_{nom}$. The Y-axis is the active power percentage change ΔP, and the X-axis represents the customer plants.

The resulting curve approaches zero at all time-points, meaning that CVR has almost reached its full potential. However, a slight difference is noticed at the second time-point of the day (*t2*), as the dP_{t2} deviates slightly in the negative direction as a result of the OLTCs not keeping the ideal voltage on the CPs' side in the case of injecting into the grid.

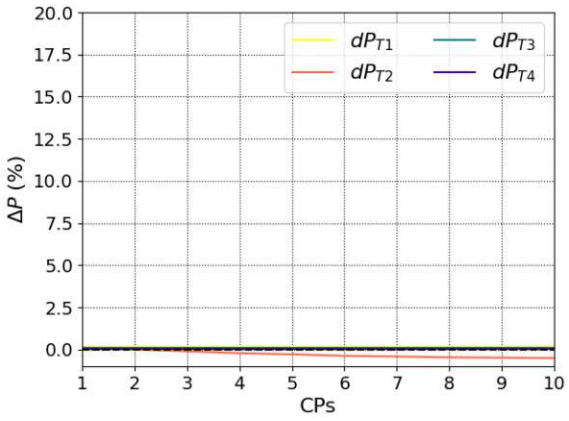

Fig 6.28. Percentage change of active power compared to optimal values of LV OH grid with PV and OLTC CVR.

6.2.1.3. Feeder with controllable coil

6.2.1.3.a. Without PV (pure consumer) In this simulation case, a coil is added at the end of the distribution feeder with a closed-loop control to achieve the ideal CVR voltage at the feeder's end, of which fig. 4.4a gives an overview.

Figure 6.29 depicts the voltage profile of a pure consumer customer plant case in a LV grid with overhead lines. The Y-axis is the voltage in per-unit *(pu)* and the X-axis is the feeder's length starting from the secondary side of the distribution transformer, represented as nodes of customer connections.

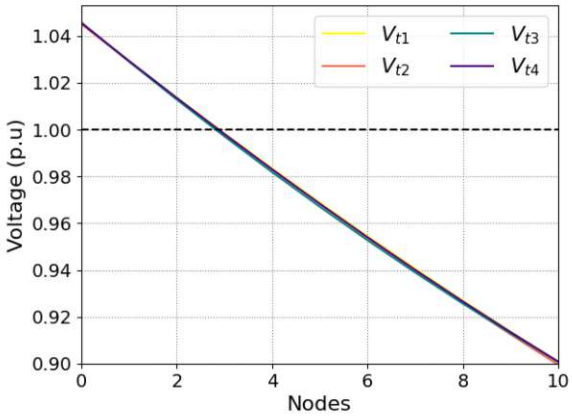

Fig 6.29. Voltage profile of LV OH grid without PV, with controllable coil CVR.

As seen in the figure, the voltage at all time-points start at slightly over 1.04 pu, and then drops with the distance of the feeder. The four lines nearly have an identical slope since they are controlled by the same control strategy and target value, controlled by the coil at the end of the feeder, where it reaches 0.9 pu.

While fig. 6.30 depicts the power flow and losses of the feeder. The right Y-axis indicates different magnitudes of loss for the different time-points. The left Y-axis is the total power consumed from MV Grid-Link in kW, while the right Y-axis is a vertical color bar representing the Losses in kW. The X-axis represents the time-points of the day.

At the third time-point of the day, the system incurs the minimum loss of below 6.4 kW (pale yellow); it also has the highest amount of power flow, while the second time-points of the day (*t2*) (dark orange color) incurs the most significant loss, which is slightly over 7 kW. In between, around 6.7 kW, comes the loss at the first and fourth time-point of the day *t1* and (*t4*) (pale orange color).

There is a significant increase of active power losses in the four points of simulation compared to the base case with no CVR. Also, the total P losses increase with the decrease of total consumption.

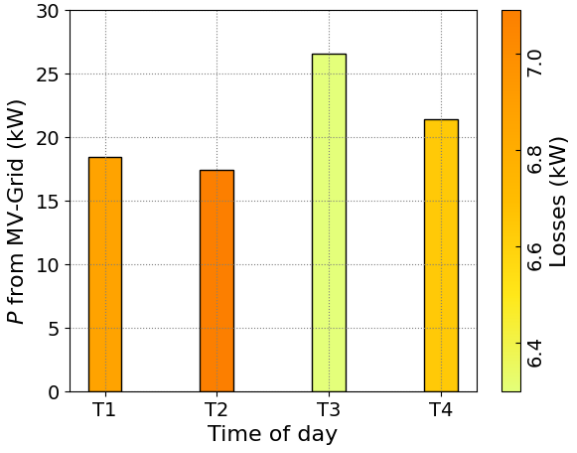

Fig 6.30. Feeder *P* flow and losses of LV OH grid without PV, with controllable coil CVR.

While fig. 6.31 depicts the net active and reactive power at each segment (1 to 10) with losses included. The Y-axis of the left subfigure is the active power from the LV grid in kW,

and the Y-axis of the right subfigure is the reactive power *(Q)* in kvar. The X-axis is the length of the feeder as segments where power flow is under observation.

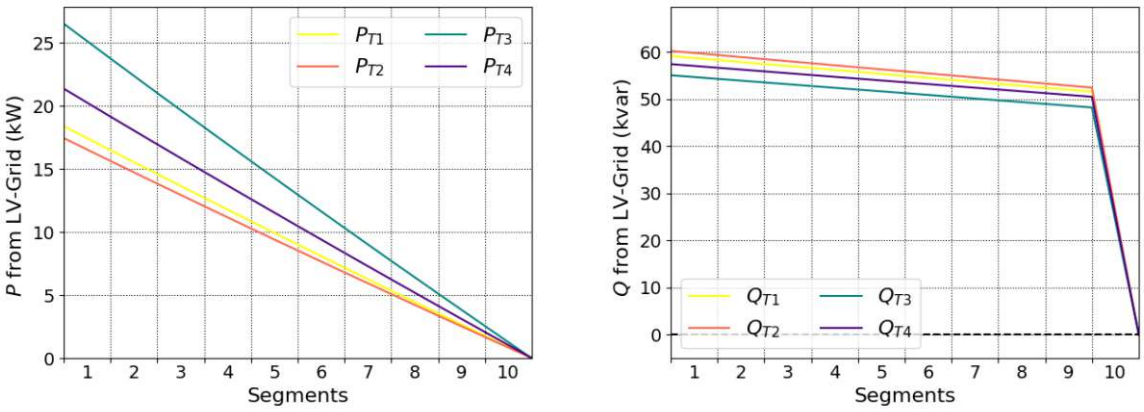

Fig 6.31. Net *P* (left) and *Q* (right) at each segment of LV OH grid without PV, with controllable coil CVR.

The active power starts above fifteen kW at the first and second time-points of the day, yellow and orange lines respectively. At the third time-point of the day, green line, the power starts slightly above twenty-five kW, and it starts at the fourth time-point of the day, purple line, slightly above fifteen kW.

The active power passing at each segment decreases uniformly, with a similar slope for the four time-points, with slightly lower power consumption along the length of the feeder as the voltage drops. While the reactive power, on the other hand, has a distinct inductive behavior compared and is lightly consumed along the feeder's length and then the most part of it is consumed at segment 10 (where the controlled coil is located).

While fig. 6.32 depicts the percentage change of active power for respective customer plants compared to values at $0.9V_{nom}$. The Y-axis is the active power percentage change ΔP, and the X-axis represents the customer plants along the feeder's length. The percentage change of active power for respective customer plants is calculated just as in eq. (3.8).

The graph depicts that the maximum potential of CVR is only achieved at the customer plants connected to the last node of the feeder, where the value reaches zero for

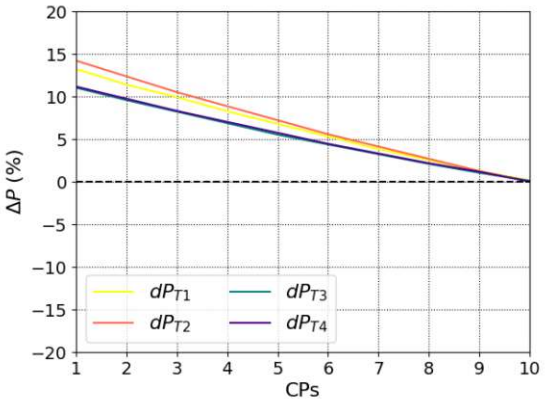

Fig 6.32. Percentage change of active power compared to optimal values of LV OH grid without PV, with controllable coil CVR.

all time-points. This potential decreases towards the beginning of the feeder, where the $0.9V_{nom}$ was not achieved, and therefore, the percentage increases till it reaches just under 15% in the case of the second time-point of the day (red) and over 10% for the third and fourth time-point, with the first time-point(yellow) in between.

6.2.1.3.b. With PV In this simulation case, a PV production unit is added to each customer plant, with the CVR still implemented through a controlled coil at the end of the distribution feeder. An overview of the grid under study fig. 4.4b gives an overview.

Figure 6.33 depicts the voltage profile of the case customer plants after a PV installation with overhead lines. The Y-axis is the voltage in per-unit *(pu)* and the X-axis is the feeder's length starting from the secondary side of the distribution transformer, represented as nodes of customer connection.

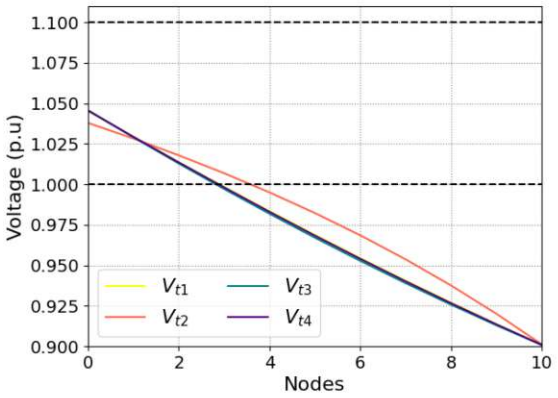

Fig 6.33. Voltage profile of LV OH grid with PV and controllable coil CVR.

The difference here in comparison to the previous simulation case lies at the slope of the second time-point of the day, with a relatively small increase across most of the feeder length, due to power injection. For the remaining time-points, voltage decreases with an almost similar slope along the feeder's length.

While fig. 6.34 depicts the total active power flow and losses of the LV Link-Grid as obtained after PV installation with overhead lines. The left Y-axis is the power injected into the MV Grid-Link or consumed from the MV Grid-Link in kW, while the right Y-axis is a vertical color bar representing the Losses in kW. The X-axis represents the times of the day.

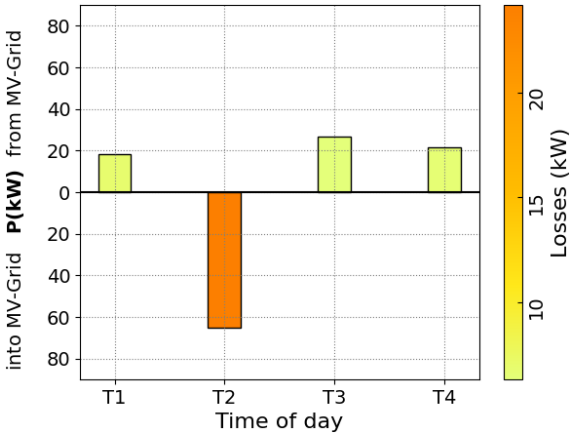

Fig 6.34. Feeder P flow and losses of LV OH grid with PV and controllable coil CVR.

The most significant loss, almost 25 kW (orange-red color), is incurred at the second time-point of the day ($t2$) where the highest amount of power (around 80kW) is injected, that makes the loss values that were already high at the other 3 points look insignificant,

as they are under 10 kW, (pale yellow). It is observed that *t2* is the only different value than the case of no PV.

And fig. 6.35 depicts the net active and reactive power at each segment (1 to 10) with losses included after PV installation. The Y-axis of the left subfigure is the active power *(P)* from the LV grid in kW, and the Y-axis of the right subfigure is the reactive power *(Q)* in kvar. The X-axis of the two subfigures is the length of the feeder as segments where power flow is under observation.

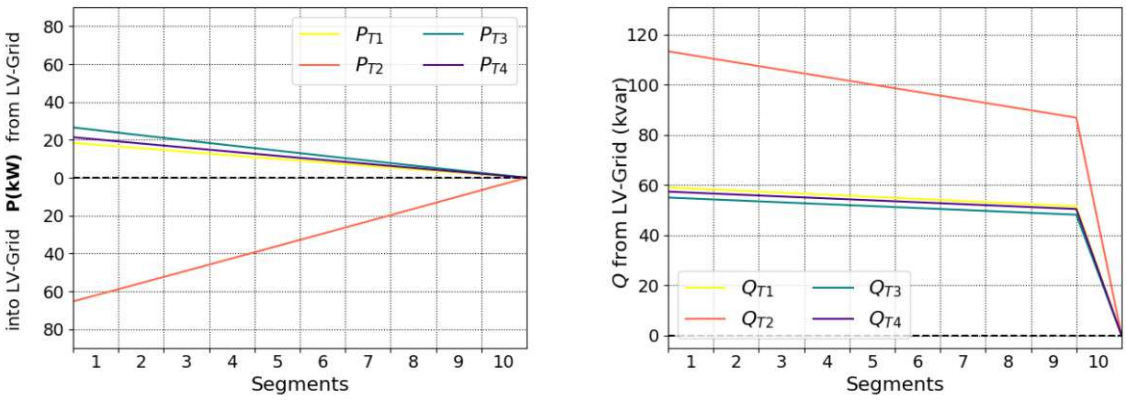

Fig 6.35. Net *P* and *Q* for each segment of LV OH grid with PV and controllable coil CVR.

The only change occurs at the second time-point of the day, when there is a substantial active power injection and reactive power consumption (red line). At *t2*, the active power *P* is injected uniformly into the grid to eventually reach more than 60 kW at the beginning of the feeder. The reactive power consumption *Q* also increases, most notably at segment 10 as a result of the controlled coil trying to bring down the extra voltage.

And fig. 6.36 depicts the percentage change of active power for respective customer plants after PV installation. The Y-axis is the active power percentage change ΔP, and the X-axis represents the customer plants.

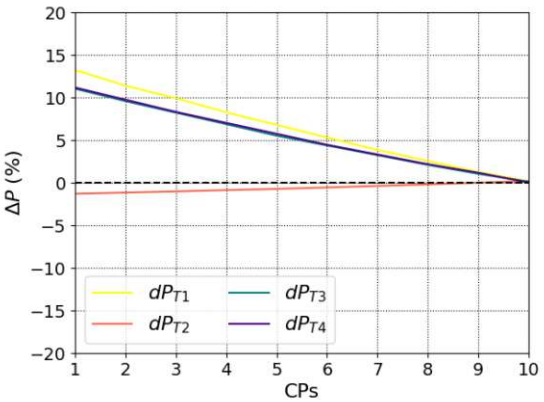

Fig 6.36. Percentage change of active power compared to optimal values of LV OH grid with PV and controllable coil CVR.

The plotted values indicate the difference in power compared to the estimated theoretical values for each of the time-points and are calculated as in eq. (3.8). The difference is also seen at the second time-point of the day (red line), as it deviates from the optimal value slightly in the negative direction (due to the power injection), while the other time-points remain above 10%.

6.2.1.3.c. With PV, targeting upper voltage limit According to the previous results, the controllable coil solution to achieve optimal CVR at the operating voltage of $0.9V_{nom}$ (both in the case of PV presence or absence) can already be excluded from further comparison due to its extremely high losses and not achieving the optimal results for all customer plants on the feeder.

However, and building on the previous test case (paragraph 6.2.1.3.b), there might be potential in this method, only to limit the voltage at the second time-point of the day (*t2*) to the upper limit of $1.1V_{nom}$. This simulation case is presented here, and its results shall be presented in the upcoming comparison of CVR methods.

Figure 6.37 depicts the voltage profile of this simulation case, where the target voltage of the controlled coil is the upper voltage limit and PV systems are producing their rated power at all customer plants, which are connected to an overhead line feeder. The Y-axis of the graph is the voltage in per-unit *(pu)* and the X-axis is the feeder's length starting from the secondary side of the distribution transformer, represented as nodes of customer connection.

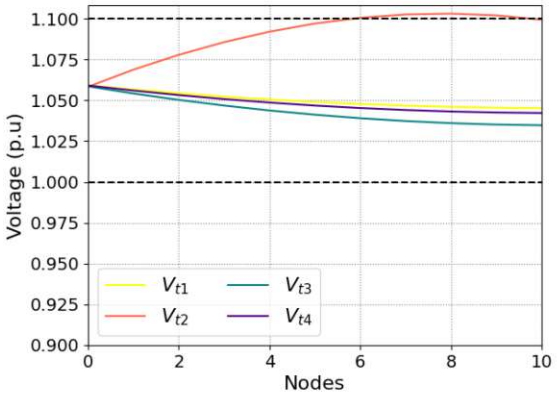

Fig 6.37. Voltage profile of LV OH grid with PV and controllable coil-based CVR targeting $1.1V_{nom}$.

It's clear from the results that the target of this method is achieved, such that the voltage at the second time-point of the day (red line) does not significantly cross the upper voltage limit of $1.1V_{nom}$, although with some inaccuracy in the second half of the feeder's length. There are no changes to the other time-points, with their results remaining as before CVR.

While fig. 6.38 depicts the total active power flow and losses of the LV Link-Grid as obtained after PV installation with overhead lines. The left Y-axis is the power injected into the MV Grid-Link or consumed from the MV Grid-Link in kW, while the right Y-axis is a vertical color bar representing the Losses in kW. The X-axis represents the time-points of the day.

The most significant loss, about 6 kW, is incurred at the second time-point of the day (*t2*) (dark orange color) where the highest amount of power (around 80kW) is injected,

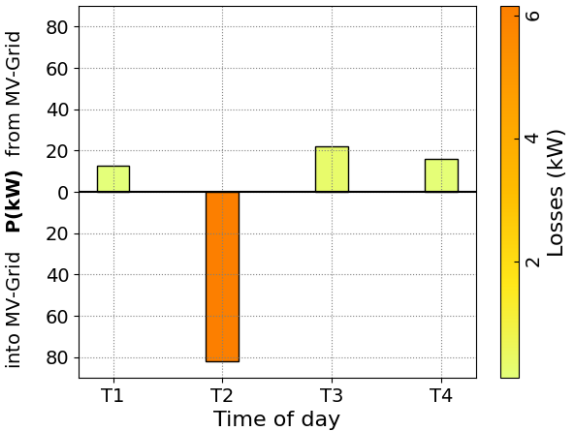

Fig 6.38. Feeder *P* flow and losses of LV OH grid with PV and controllable coil-based CVR targeting $1.1V_{nom}$.

while the rest exhibit the same losses' behavior, around 1 kW, (pale yellow) as in the case of pure consumers (around 20kW). It is noticeable that the losses are significantly less than the previous simulation case (see fig. 6.34).

And fig. 6.39 depicts the net active and reactive power at each segment. The Y-axis of the left subfigure is the active power *(P)* from the LV grid in kW, and the Y-axis of the right subfigure is the reactive power *(Q)* in kvar. The X-axis is the length of the feeder as segments where power flow is under observation.

The difference is seen at the second time-point of the day (red line), as a significant boost to the active power injected into the grid is recorded (red line), reaching a sum of more than 80 kW, accompanied by a significant decrease in reactive power consumed compared to the previous simulation case (see fig. 6.35).

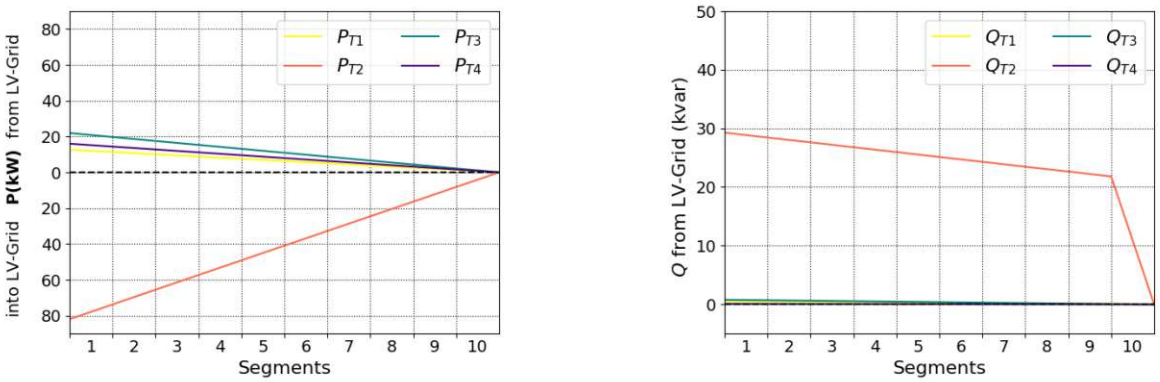

Fig 6.39. Net P and Q for each segment of LV OH grid with PV and controllable coil-based CVR targeting $1.1V_{nom}$.

This depicts a better potential for using a controllable coil to suppress voltage in case of PV injection with lower losses than the previous simulation case.

And fig. 6.40 depicts the percentage change of active power for respective customer plants after PV installation. The Y-axis is the active power percentage change ΔP, and the X-axis represents the customer plants. The plotted values indicate the difference in power compared to the estimated theoretical values for each of the time-points and are calculated just as in eq. (3.8).

In comparison to the previous simulation case, a difference is seen at the second time-point of the day (red line), such that it stays

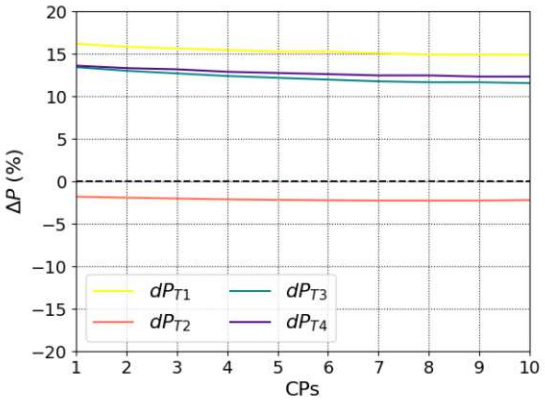

Fig 6.40. Percentage change of active power compared to optimal values of LV OH grid with PV and controllable coil-based CVR targeting $1.1V_{nom}$.

relatively close to the optimal value (around -2.5%) along the length of the feeder. The other time-points remain at the values before CVR application.

6.2.1.4. Comparison of simulation cases in LV grid with overhead lines

Comparing the CVR methods applied on this theoretical LV grid with overhead line feeder and typical values of a European grid, it is clear that the targeted voltage profile is achieved best with the first technique of using On-load tap changer connections to connect customer plants with the LV Grid-Link; however, the no-load losses of the transformers still propose a challenge as they overshadow the savings. While the second technique of using a controllable coil in a *Q-V* control strategy proved impractical due to the resulting losses, except to keep the voltage within acceptable boundaries in the case of PV injection.

The effects of the employed CVR techniques on power flow and losses (from the perspective of the DTR) are compared and presented in fig. 6.41. In the left subfigure (a), the Y-axis represent the magnitude and direction of the total active power flow in kW, and the X-axis is the time-points of the day. While in the right subfigure (b), the Y-axis is the and the magnitude of the total active power losses (kW) in kW, and the X-axis is also the time-points of the day.

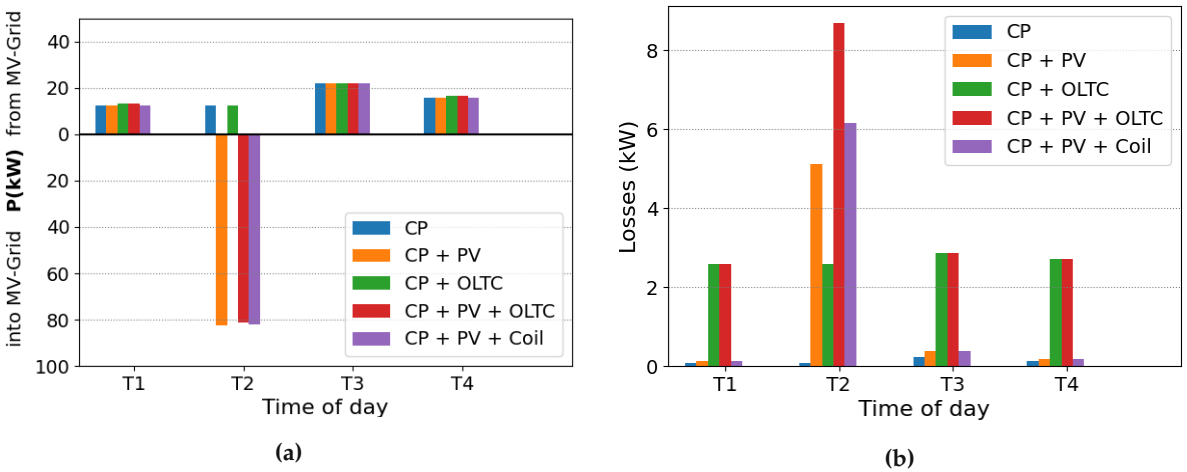

Fig 6.41. Comparison of CVR on overhead lines LV-grid (a) total power flow, (b) total losses.

The color blue represents the base case of normal customer plants without PV or CVR, the orange is the case of customer plants with PV installation, the green is the case of customer plants with OLTC-based CVR and without PV, the red is the case of customer plants with OLTC-based CVR and PV, and finally the violet is the case of customer plants with PV and a controlled coil-CVR targeting only the upper voltage limit of $1.1V_{nom}$.

At the second time-point of the day and as shown in the left subfigure (a), using On-load tap changer connections with PV, the total active power injected into the MV Grid-Link is slightly more than 80 kW at the second time-point of the day (*t2*), but the right subfigure (b) depicts that the same case has active power losses of about 10% (more than 8 kW).

While with using the controllable coil with PV, it injects about the same amount of power into the grid but with fewer losses (about 6 kW). In both cases the losses are still higher compared to the case of customer plant with PV and without CVR (about 5kW); however, they offer the advantage of keeping the voltage within acceptable limits.

At the base case, the total consumption at the distribution transformer's point of view is seen in the left subfigure (a) at about 11kW from the MV Grid-Link but with only 0.1 kW of losses (seen in the right subfigure (b)). Meanwhile, the first CVR technique applied using OLTCs (without PV), has about the same total power consumption, but with more losses of 2.6 kW.

The other 3 time-points of the day do not feed any power into the MV Grid-Link. At the first time-point of the day *t1* the power consumption, in cases of using of PV, On-load tap changer connections, coil or without using them, is around 13kW, but the losses are increased by around 19% in the case of using On-load tap changer connections with and without PV, in red and green column respectively.

In the case of using On-load tap changer connections with and without PV, in red and green column respectively, the power consumption at the third time-point of the day *t3* is about 22kW, but the losses are about 13%. And about 16kW are consumed at the fourth time-point of the day (*t4*), but in the case of using On-load tap changer connections with and without PV, in red and green column respectively, the losses are about 16%.

CVR	PV	Factor	Unit	t1	t2	t3	t4	Remark
No	No	P Flow (MV to LV)	kW	12.65	11.44	21.96	15.98	Losses are primarily
		P Losses		0.12	0.099	0.37	0.19	due to line losses
	Yes	P Flow (MV to LV)		12.66	-82.68	21.96	15.98	Losses spike with significant
		P Losses		0.12	5.12	0.37	0.19	injection at *t2* (line losses)
OLTC	No	P Flow (MV to LV)		13.47	12.3	22.13	16.69	Significant stable increase of losses due to
		P Losses		2.59	2.58	2.87	2.70	no-load losses offsetting CVR savings
	Yes	P Flow (MV to LV)		13.47	-81.63	22.13	16.70	More losses in lines at *t2* due to
		P Losses		2.59	8.65	2.87	2.70	the inefficiency of CVR transformers
Coil for $1.1V_{nom}$	Yes	P Flow (MV to LV)		12.65	-81.99	21.96	15.98	Acceptable losses at *t2* compared
		P Losses		0.12	6.16	0.37	0.19	to case of coil to achieve ideal voltage

Table 6.3. Comparison of CVR on overhead lines LV-grid by power flow at distribution transformer.

It is clear that power savings due to CVR are replaced or even exceeded by the increased losses in both methods of CVR applied. With the On-load tap changer connections, the main losses come from the no-Load losses, while in the case of feeder with controllable coil strategy the losses are mainly due to a lowered power factor.

A summary of results is found in table 6.3, where the exact numbers are presented, for the net active power flow (i.e., power flow after subtracting the losses) and the corresponding losses for all the simulation cases, along with the most important remark on each simulation case.

In conclusion, CVR potential is not worth pursuing with the mentioned techniques in the LV Overhead grid unless the customer plants' power consumption is much higher such that it makes the On-load tap changer no-load losses negligible or has much higher PV output that voltage boundaries need the controllable coil method to be kept, and both cases are not realistic according to the available data models. Other proven LV CVR methods such as reducing the secondary voltage of the DTR_{LV}^{MV} by a mere 1 or 2% would provide a better cost-to-performance ratio.

6.2.2. Cable lines structure

This subsection examines the implication of CVR on load reduction in the LV grid with cable lines structure, explained in section 4.2, and depicts the results for each simulation case with the help of graphs, focusing on the parameters of interest like voltage profile, active power flow, and losses.

6.2.2.1. CP connected directly to LV grid

6.2.2.1.a. Without PV (pure consumer) The LV grid depicted in fig. 4.2a applies to this case too, as the only change from the Overhead section is the nature of the feeder (cable lines structure). In this case, the customer plants are directly connected to the LV via cable lines without any PV presence.

The voltage profile in fig. 6.42 depicts a pure consumer customer plant case in a LV grid with cable lines connections instead of overhead lines. The Y-axis is the voltage in per-unit (pu) and the X-axis is the feeder's length starting from the secondary side of the distribution transformer, represented as nodes of customer connections.

Similar to the same case in overhead LV grid, and due to the high active power consumption at *t3*, the V_{t3} slope is the steepest and voltage drops with distance in all time-points, according to the load model in section 6.1.

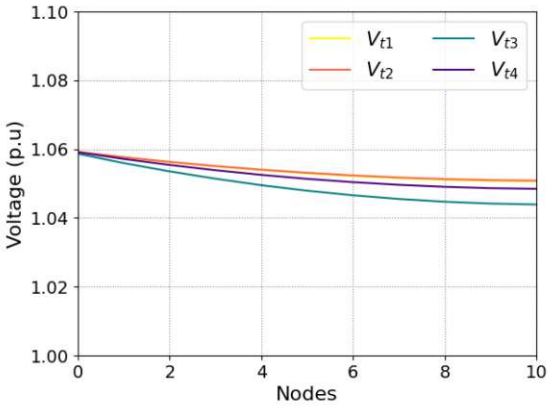

Fig 6.42. Voltage profile of LV CA grid without CVR or PV.

And fig. 6.43, like fig. 6.12 in the overhead case, depicts the power flow and losses of the feeder but using cables instead. The right Y-axis is a vertical color bar representing the Losses in kW. The left Y-axis is the total power consumed from MV Grid-Link in kW, while the Right Y-axis is a vertical color bar representing the losses for the different time-points. The X-axis is simulation time-points of the day.

At the first and second time-points of the day (*t1* and *t2*), the system incurs the minimum loss of around 0.08 kW (pale yellow), while the third time-point of the day *t3* (dark orange color) incurs the most significant loss which is slightly over 0.24 kW; it also has the highest amount of power flow. In between, around 0.12 kW, comes the loss at the fourth time-point of the day (*t4*) (bright yellow color). Feeder power flow and total losses are most significant at *t3*, as the total *P* losses increase with the increase of total consumption. The losses are almost solely from conductor losses and have minimal effects.

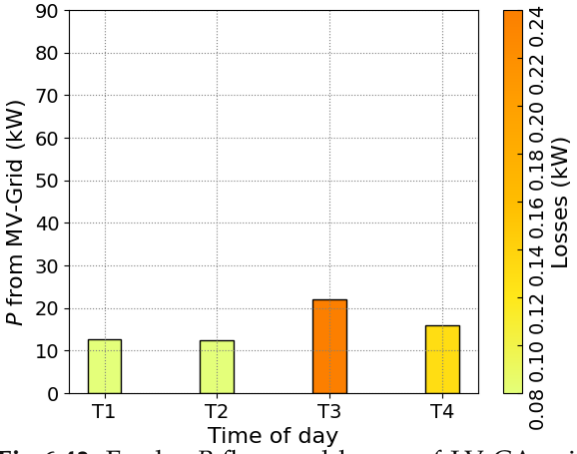

Fig 6.43. Feeder *P* flow and losses of LV CA grid without CVR or PV.

While fig. 6.44, like fig. 6.13 depicts the amount of power consumption at four different time-points but with cable lines instead. The Y-axis of the left subfigure is the active power *(P)* from the LV grid in kW, and the Y-axis of the right subfigure is the reactive power *(Q)* in kvar. The X-axis is the length of the feeder as segments where power flow is under observation. The active power starts above ten kW at *t1* and *t2*, yellow and orange lines respectively. At *t3*, green line, the power starts slightly above twenty kW, and it starts at the fourth time-point of the day, purple line, slightly above 15 kW.

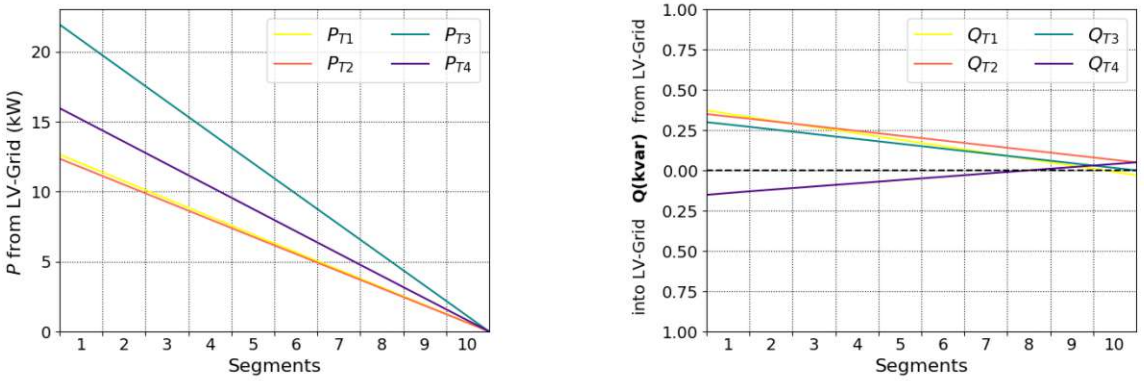

Fig 6.44. Net *P* (left) and *Q* (right) at each segment of LV CA grid without CVR or PV.

Active power decreases uniformly for the four time-points. But for the reactive power, the behavior changes from the case of overhead lines, due to the capacitive characteristics of cable lines, the slope of the curves are more linear and more minor values for Q (less consumption), while at (*t4*) it is more capacitive.

While fig. 6.45 depicts the percentage change of active power for respective customer plants. The Y-axis is the active power percentage change ΔP, while the X-axis represents the customer plants along the feeder. The plotted values indicate the percentage change of power compared

to the estimated theoretical values for each of the time-points. There are no major differences from the overhead case, as the percentage at *t2* lies above 25% and at the other time-points around 15%.

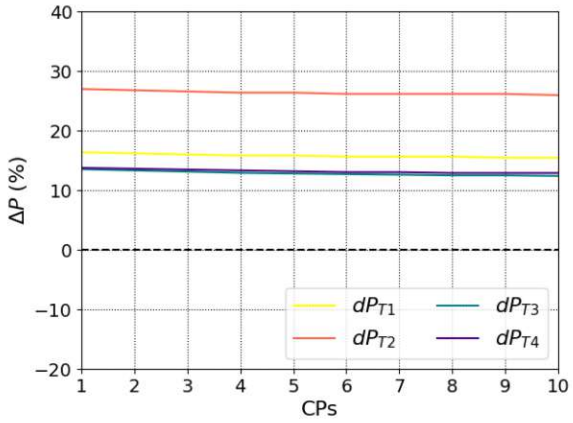

Fig 6.45. Percentage change of active power compared to optimal values of LV CA grid without PV or CVR.

6.2.2.1.b. With PV In this case, PV installation is added to each customer plant, as illustrated in fig. 4.2b and the customer plants directly connected to the LV grid via cable lines.

The voltage profile of this case is presented in fig. 6.46, such that PV installations are added to customer plants with LV cable feeder. The Y-axis is the voltage per-unit *(pu)* and the X-axis is the length of the feeder as nodes of customer plants connection.

In comparison to the case without PV, the voltage profile only changes at V_{t2} where it exceeds the upper limit of $1.1V_{nom}$ after the fourth connection point, since there are no countermeasures such as the reactive power-voltage Q-V control applied in this simulation. However, the results for the remaining time-points remain unchanged as they decrease along the feeder's length.

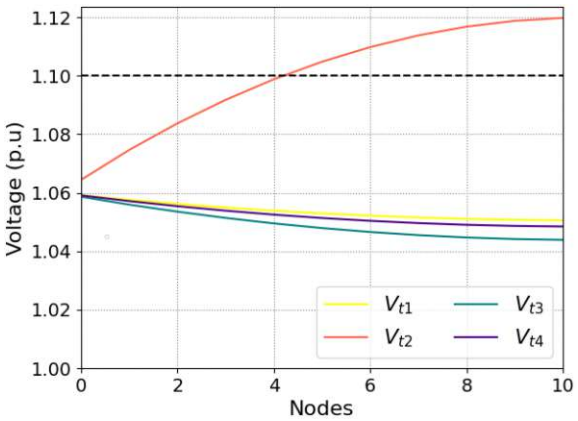

Fig 6.46. Voltage profile of LV CA grid with PV, without CVR.

While fig. 6.47, like fig. 6.16, depicts the total active power flow and losses of the LV Link-Grid as obtained after PV installation but with cable connection. The left Y-axis is the active power injected into the MV Grid-Link or consumed from the MV Grid-Link in kW, while the right Y-axis is a vertical color bar representing the Losses in kW. The X-axis represents the time-points of the day.

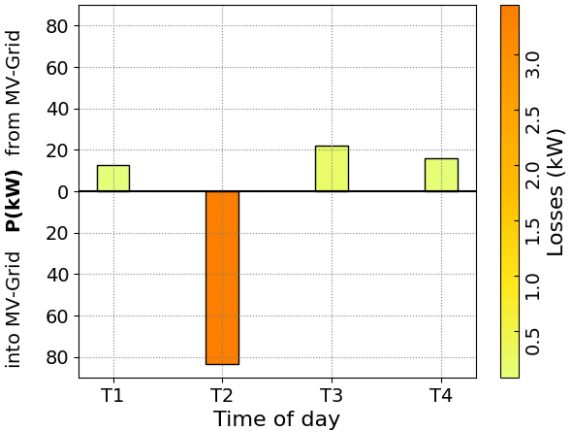

Fig 6.47. Feeder *P* flow and losses of LV CA grid with PV, without CVR.

The most significant loss, above 3 kW, is incurred at the second time-point of the day (*t2*) (dark orange color) where the highest amount of power (around 80kW) is injected, while the rest exhibit the same losses' behavior, below 0.5 kW, (pale yellow) as in the case of pure consumers (around 20kW).

The figure depicts that a significant amount of power injected into the grid at the second time-point of the day (*t2*) is accompanied by a jump in the losses that diminish losses at the other simulation times, as calculated with eq. (5.11).

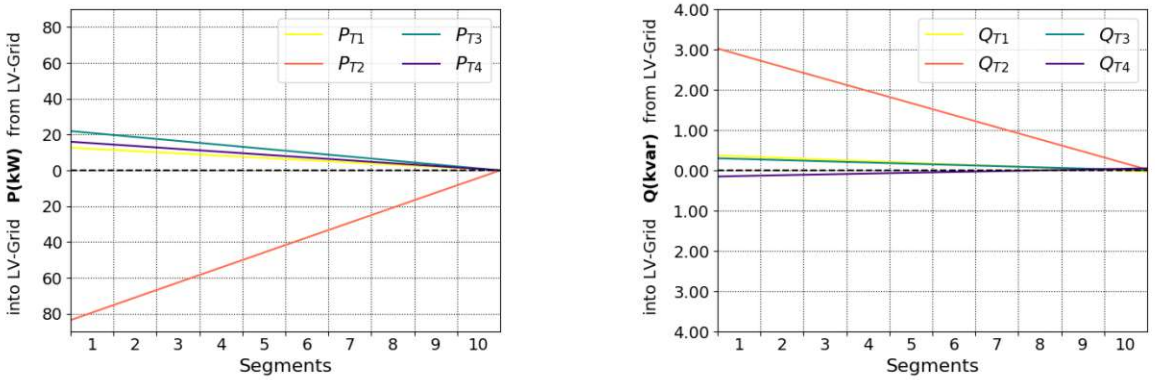

Fig 6.48. Net *P* (left) and *Q* (right) at each segment of LV CA grid without PV or CVR.

And fig. 6.48 depicts the active and reactive power flow obtained after PV installation, but with cable connections. The Y-axis of the left subfigure is the active power *(P)* from the LV grid in kW, while the Y-axis of the right subfigure is the reactive power *(Q)* in kvar. The X-axis is the length of the feeder as segments where power flow is under observation.

There are few differences in comparison to the same case but with the overhead line feeders. The amount of active power injected in each segment at (*t2*) (red line) is slightly higher, and there is substantially less overall reactive power flowing into the first segment (about 3 kvar in comparison to 7 kvar). The other time-points exhibit a more capacitive behavior as well along the feeder's length.

While fig. 6.49, depicts the percentage change of active power for respective customer plants after PV installation with cable connection. The Y-axis is the active power percentage change ΔP, while the X-axis represents the customer plants along the feeder.

The plotted values indicate the difference in power compared to the estimated theoretical values for each of the time-points.

As in the same case with overhead lines, there are no major differences and the dP_{T2} deviates from the optimal result in the negative axis due to power direction (injection into grid).

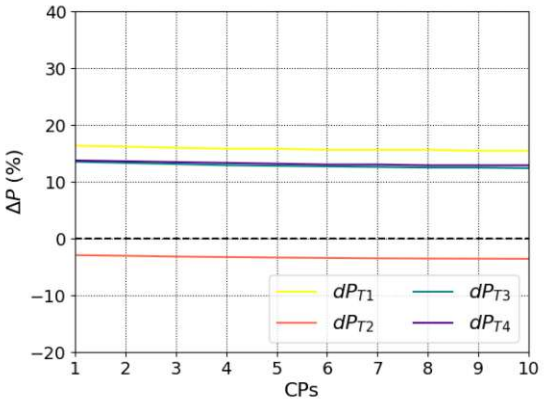

Fig 6.49. Percentage change of active power compared to optimal values of LV CA grid with PV but without CVR.

6.2.2.2. CP connected through OLTCs

6.2.2.2.a. Without PV (pure consumer) In this case, CVR is introduced through connecting an *LV OLTC* at each customer plant, as illustrated in fig. 4.3a without PV penetration.

For the voltage profile, fig. 6.50a presents the value on the LV side of the transformer, and fig. 6.50b on the customer plants' side. The Y-axis is the voltage in per-unit *(pu)* and the X-axis represents the length of the feeder as nodes of customer plants connection, for the left subfigure on the LV side of the OLTCs, and on the customer plants side for the right subfigure.

As in the case of the overhead lines, it is observed that the voltage drops on the LV side along the feeder's length; however, for the customer plants' side, the voltage is kept constant at $0.9V_{nom}$.

While fig. 6.51 depicts the transformers losses in comparison to the lines losses at the different time-points, but with cable connection. The Y-axis is losses obtained in kW, while the X-axis is the time of the day. Green represents line losses; orange is for transformer losses, and blue sums all transformer losses.

As in the case of overhead lines, the figure exhibits that the overwhelming part of losses is due to the TR^{LV}_{CP} , with very minimal effects of the TR^{MV}_{LV}. The increase of line losses, specifically at $t3$ due to higher P consumption, are significant while transformer losses

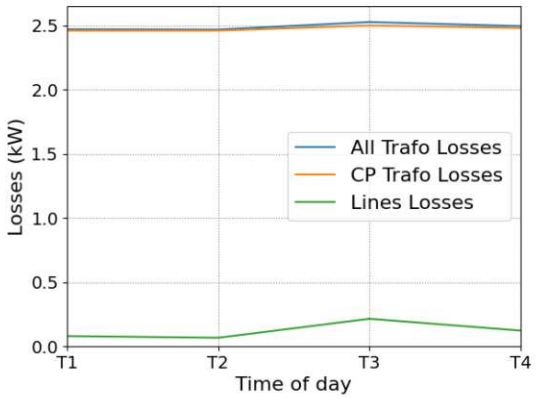

Fig 6.51. Transformers vs. Lines Losses of LV CA grid without PV, with OLTC CVR.

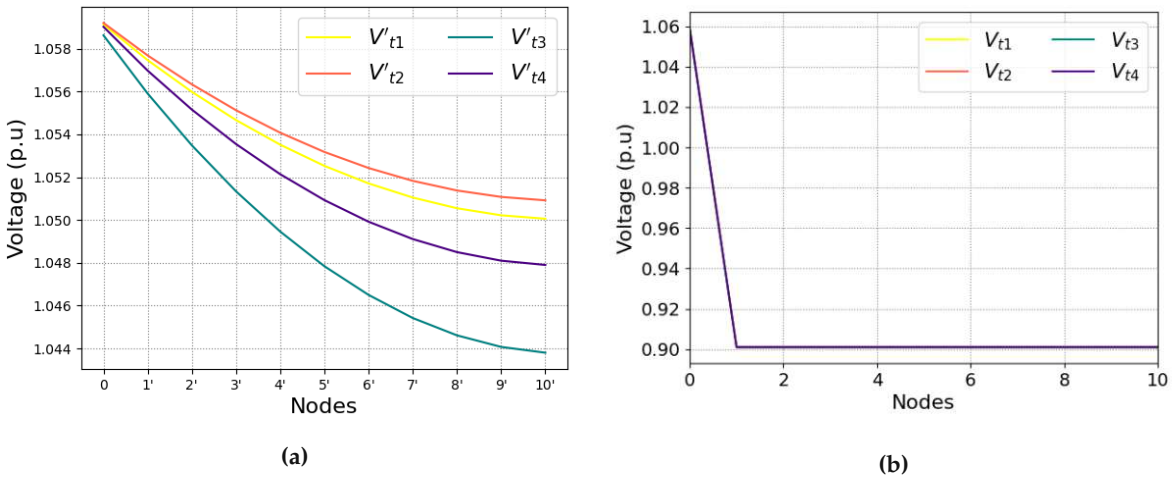

(a) (b)

Fig 6.50. Feeder voltage profile of LV CA grid without PV, with OLTC CVR on (a) *LV* side (b) *CP* side.

are relatively constant, showing that most transformers losses are the no-load (iron) losses. The line losses are also slightly higher than in the case of overhead lines.

While fig. 6.52 depicts the total active power flow and losses of the LV Link-Grid but with cable connection. The left Y-axis is the total active power consumed from the MV Grid-Link in kW, while the right Y-axis is a vertical color bar representing the Losses in kW. The X-axis represents the time-points of the day.

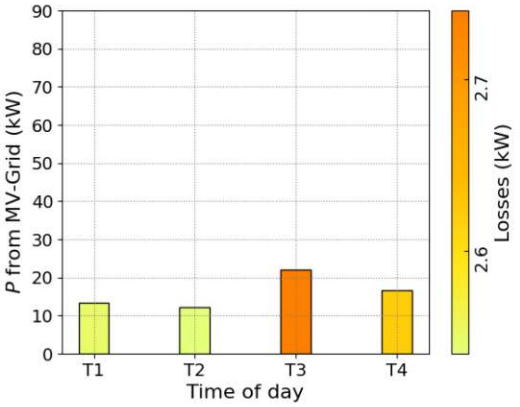

Fig 6.52. Feeder *P* flow and losses of LV CA grid without PV, with OLTC CVR.

At the first and second time-points of the day (*t1* and *t2*), the system incurs the minimum loss of below 2.6 kW (pale yellow), while the third time-point of the day *t3* (dark orange color) incurs the most significant loss which is slightly over 2.7 kW; it also has the highest amount of power flow. In between, slightly under 2.7 kW, comes the loss at the fourth time-point of the day (*t4*) (bright yellow color). The net losses are calculated as in eq. (5.12). To be noted here, that the percentage of losses decreases as the power flow increases, since a considerable part of it is constant.

While fig. 6.53 depicts the net active power P and reactive power Q at each segment, but with cable connection. The Y-axis of the left subfigure is the active power *(P)* from the LV grid in kW, and the Y-axis of the right subfigure is the reactive power *(Q)* consumed from or into the LV grid in kvar. The X-axis is the length of the feeder as segments where power flow is under observation.

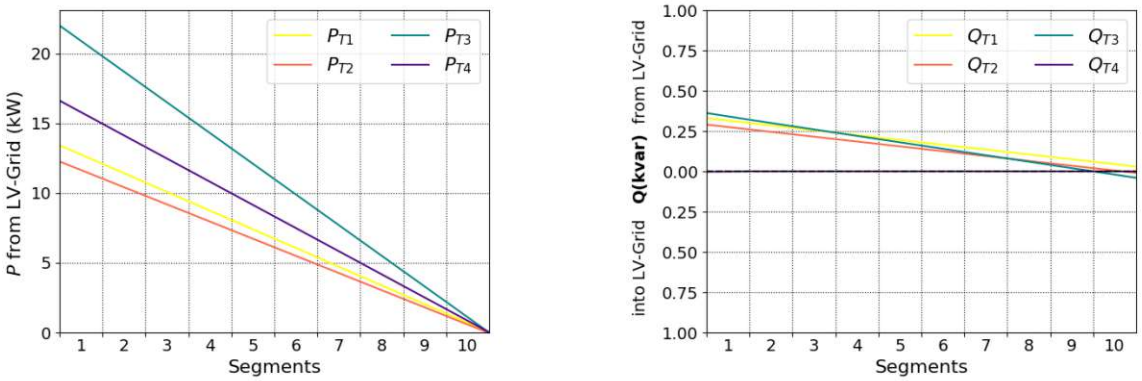

Fig 6.53. Net P (left) and Q (right) at each segment of LV CA grid without PV, with OLTC CVR.

The active power starts above 10 kW at the first and second time-points of the day, yellow and orange lines respectively. At the third time-point of the day, green line, the power starts slightly above twenty kW, and it starts at the fourth time-point of the day, purple line, slightly above fifteen kW.

There is a uniform decrease in P along the feeder's length for all the time-points observed. This is also visible in reactive power *(Q)*, as it tends towards capacitive behavior at the end of the line, a characteristic not seen in the case of overhead lines.

And fig. 6.54 depicts the percentage change of active power for respective customer plants compared to values at $0.9V_{nom}$. The Y-axis is the active power percentage change ΔP, while the X-axis represents the customer plants along the feeder.

As observed from this graph, the customer plants are performing mainly at the optimal CVR efficiency in this case. This is the ideal case, since the percentage change nears 0% along the whole line, meaning there is no difference between the theoretical and obtained results and the full potential of CVR is applied on each and every customer plant that is connected to the feeder.

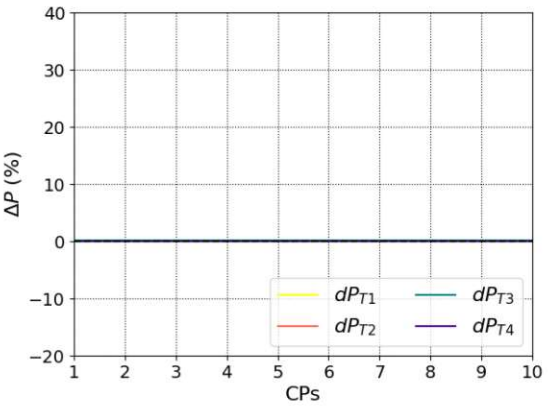

Fig 6.54. Percentage change of active power compared to optimal values of LV CA grid without PV, with OLTC CVR.

6.2.2.2.b. With PV In this simulation case, PV is introduced along with CVR load reduction as illustrated in fig. 4.3b. In comparison to the previous simulation case without PV presence, the resulting graphs only change at the second time-point of the day.

For the voltage profile of this simulation case, fig. 6.55a represents the values on the LV side of the transformer, while fig. 6.55b represents those on the customer plants' side. The

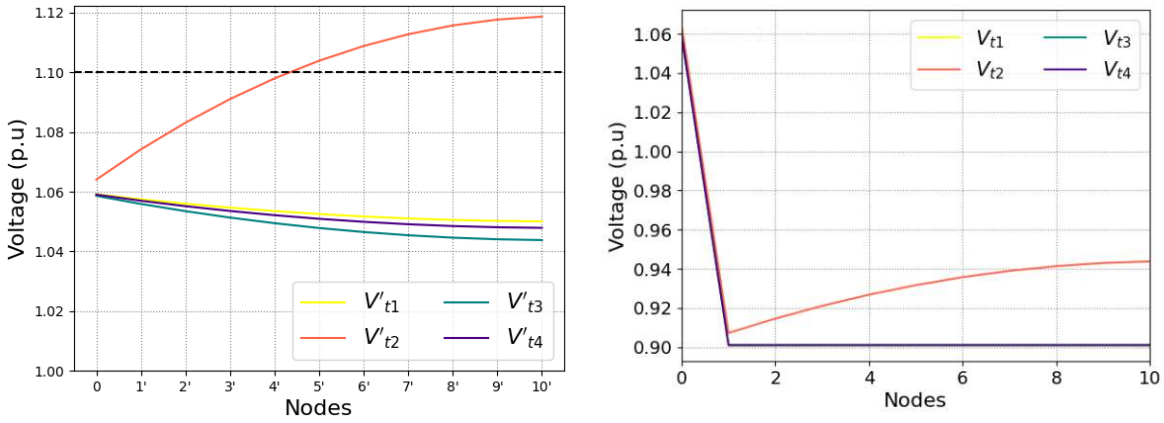

Fig 6.55. Feeder voltage profile of LV CA grid with PV and OLTC CVR on (a) *LV* side (b) *CP* side.

Y-axis is the voltage in per-unit *(pu)* and the X-axis represents the length of the feeder as nodes of customer plants connection, for the left subfigure on the LV side of the OLTCs, and on the customer plants side for the right subfigure.

On the LV side, the upper voltage limit is already reached and exceeded by the fourth node; however, there is no need for a control strategy to keep the voltage within limits because the voltage reaching the customers is within limits in any case, as seen in the right subfigure on the customer plants' side.

And as in the overhead case, the OLTCs can not keep the voltage on the customer plants' side at exactly $0.9V_{nom}$, and the red line V_{t2} increases slightly to reach 0.94 pu at the end of the feeder, meaning that CVR is not optimal at this time-point.

While fig. 6.56 depicts the transformer losses in comparison to the lines losses at the different time-points, after PV installations but with cable lines structure. The Y-axis is the losses obtained in kW, while the X-axis is the time of the day. The summed transformer losses are represented by the green line, but the customer plant transformer losses are represented by the orange line, and the lines losses are represented by the blue line.

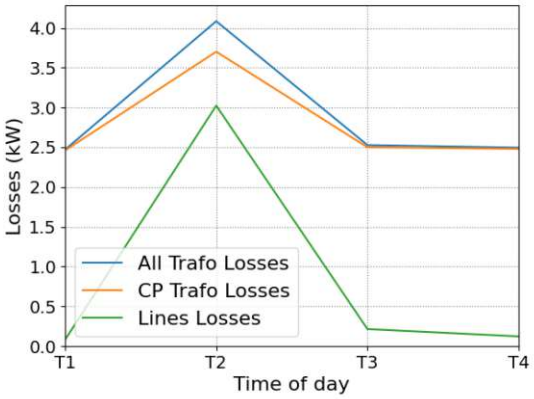

Fig 6.56. Transformers vs. Lines Losses of LV CA grid with PV and OLTC CVR.

It is observed from this graph that the highest line loss is at *t2*; however, it is still exceeded by the transformer losses, due to higher *P* injected back into the grid. The transformers' losses behavior relates to their no-load vs. load losses, as mentioned before.

And fig. 6.57 depicts the total active power flow and losses of the LV Link-Grid, but with cable connection instead. The left Y-axis is the power injected into the MV Grid-Link or consumed from the MV Grid-Link in kW, while the right Y-axis is a vertical color bar representing the Losses in kW. The X-axis represents the times of the day.

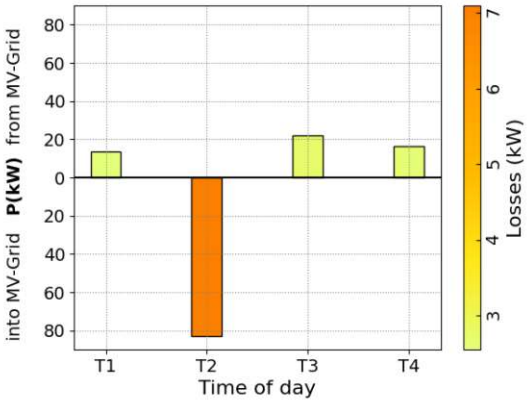

Fig 6.57. Feeder *P* flow and losses of LV CA grid with PV and OLTC CVR.

The highest magnitude of losses (around 7 kW) is incurred at the second time-point of the day *t2* (dark orange color) where the highest amount of power (around 80kW) is injected, while the rest of the time-points exhibit the same behavior as in the case of pure consumers, with relatively small losses (pale yellow).

However, if the losses are viewed as a percentage of the active power flow, they are found to be lowest at the highest flow (*t2*), and highest, at the lowest flow (*t1*).

While fig. 6.58 depicts the total active power passing at each segment of the LV feeder, as in the case of fig. 6.27 but with a cable line structure. The Y-axis of the left subfigure is the active power *(P)* from or into the LV grid in kW, and the Y-axis of the right subfigure is the reactive power *(Q)* in kvar. The X-axis of the two subfigures is the length of the feeder as segments where power flow is under observation.

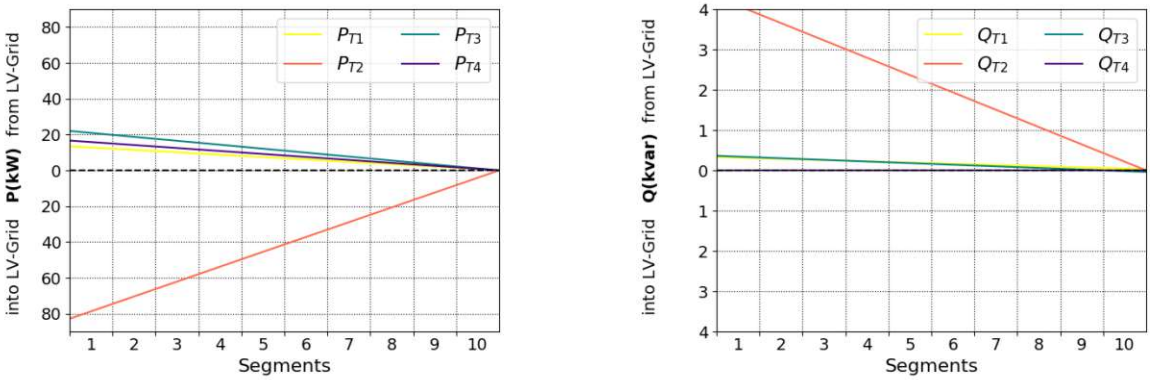

Fig 6.58. Net *P* and *Q* across feeder of LV CA grid with PV and OLTC CVR.

In comparison to the previous simulation case without PV, the only change occurs at *t2* where there is a substantial active power injection and reactive power consumption (red line). The latter diminishes the values occurring at the other time-points. However, in comparison to the same case in overhead lines, the overall reactive power consumption is much lower due to the more capacitive nature of the cable feeder.

While fig. 6.59 depicts the percentage change of active power for respective customer plants compared to values at $0.9V_{nom}$. The Y-axis is the active power percentage change ΔP, while the X-axis represents the customer plants along the feeder *CPs*.

The takeaway from this graph is that the customer plants are performing mainly at the optimal CVR efficiency in this case. There is no difference between the theoretical and obtained results, and the full potential of CVR is applied on each and every customer plant that is connected to the feeder, as the ΔP nears 0%.

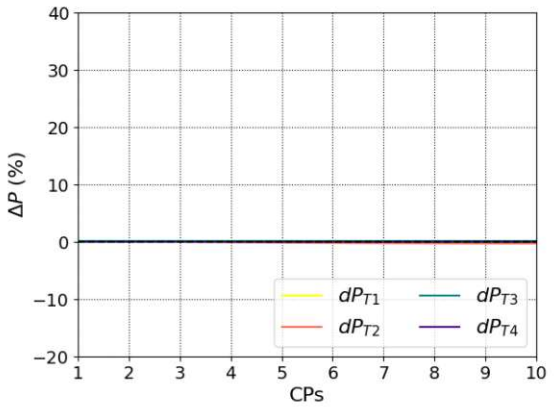

Fig 6.59. Percentage change of active power compared to optimal values of LV CA grid with PV and OLTC CVR.

6.2.2.3. Feeder with controllable coil

As in the case of the overhead connection, the controllable coil at the end of the feeder is added with a control strategy targeting of the optimal voltage $0.9V_{nom}$, but with cable connections.

6.2.2.3.a. Without PV (pure consumer) In this case, no PV production is taken into account and fig. 4.4a depicts the grid under simulation.

Figure 6.60 depicts the voltage profile of this simulation case, pure consumer customer plants in the LV Grid with cable lines. The Y-axis is the voltage in per-unit *(pu)* and the X-axis is the feeder's length starting from the secondary side of the distribution transformer, represented as nodes of customer connection.

It is seen from the graph that the slopes of the four lines representing the time-points are identical with the voltage dropping along the line, since they are controlled by the same control strategy and target value. The values drop non-linearly from the beginning of the feeder at 1.02 pu to reach 0.9 pu.

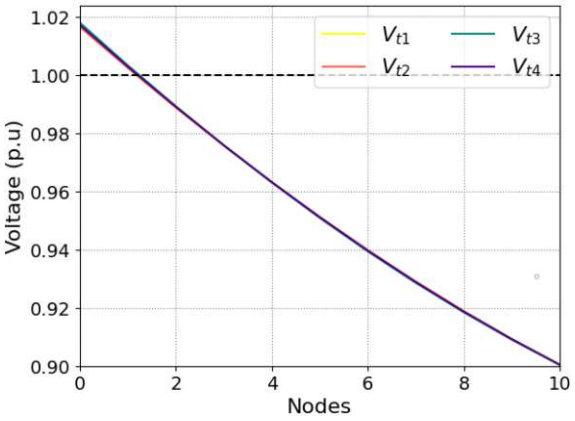

Fig 6.60. Voltage profile of LV CA grid without PV, with controllable coil CVR.

And fig. 6.61 depicts the power flow and losses of the feeder with cable lines. The left Y-axis is the total active power consumed from MV Grid-Link in kW, while the right Y-axis is a vertical color bar representing the Losses in kW. The X-axis represents the time-points of the day.

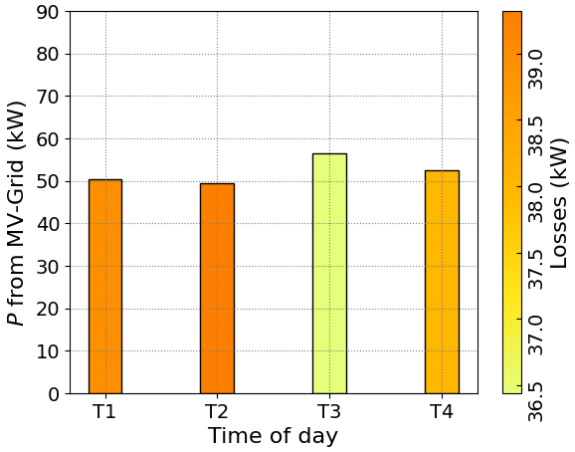

Fig 6.61. Feeder *P* flow and losses of LV CA grid without PV, with controllable coil CVR.

This figure exhibits the highest losses in comparison to all previous simulation cases. At the third time-point of the day *t3*, the system incurs the minimum loss of this case, around 36.5 kW (pale yellow); it also has the highest amount of power flow. While the second time-point of the day *t2* (dark orange color) incurs the most significant loss, which is slightly over 39 kW. In between, around 38 kW, comes the loss at the first and fourth time-point of the day *t1* and (*t4*) (pale orange color).

While fig. 6.62 depicts the net active and reactive power at each segment (1 to 10) with losses included. The Y-axis of the left subfigure is the active power *(P)* from the LV grid in kW, and the Y-axis of the right subfigure is the reactive power *(Q)* in kvar. The X-axis of the two subfigures is the length of the feeder as segments where power flow is under observation.

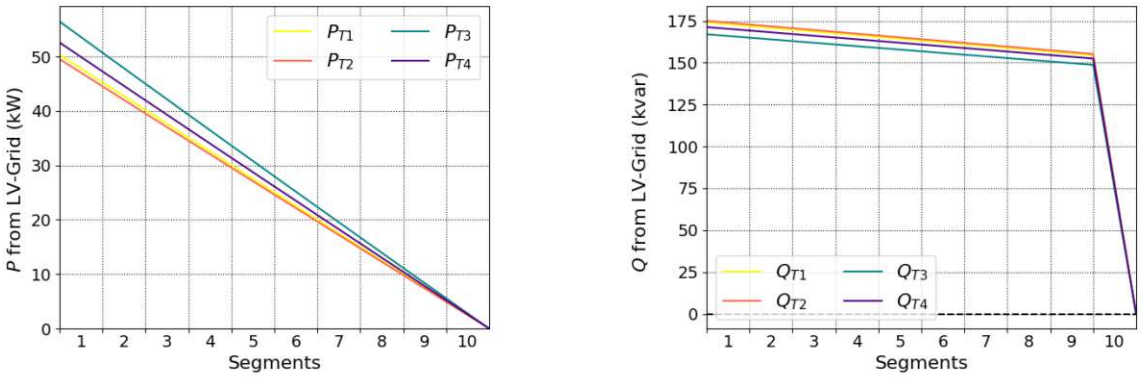

Fig 6.62. Net *P* (left) and *Q* (right) at each segment of LV CA grid without PV, with controllable coil CVR.

Active power *P* decreases uniformly with a similar slope for all the time-points; however, the reactive power consumption shot up compared to the same case in overhead lines.

It starts at about 50 kW at the first and second time-points of the day, yellow and orange lines, respectively. Moreover, at the third time-point of the day, green line, the power starts above 50 kW, and it starts at the fourth time-point of the day, purple line, slightly above 50 kW.

And fig. 6.63 depicts the percentage change of active power for respective customer plants compared to values at $0.9V_{nom}$ for the four time-points of the day, labeled $dP_T1 \ldots dP_T4$, where the Y-axis is the active power percentage change ΔP, and the X-axis represents the customer plants along the feeder *CPs*.

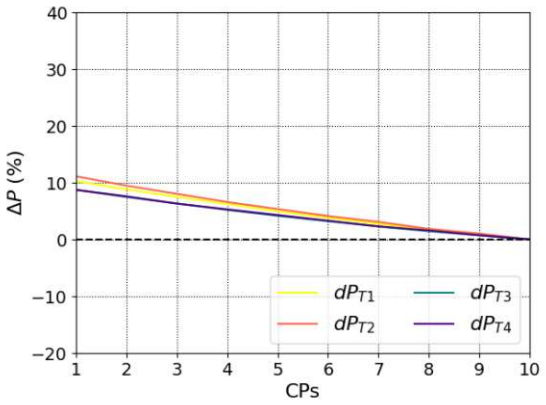

Fig 6.63. Percentage change of active power compared to optimal values of LV CA grid without PV, with controllable coil CVR.

The graph depicts that the maximum potential of CVR is only achieved at the customer plants connected to the last node of the feeder, where the value reaches zero for all time-points. This potential decreases towards the beginning of the feeder, where the $0.9V_{nom}$ was not achieved, and therefore, the percentage increases till it reaches just under 15% in the case of the second time-point of the day (red) and over 10% for the third and fourth time-point, with the first time-point (yellow) in between.

6.2.2.3.b. With PV In this simulation case, a PV production unit is added to each customer plant, with the CVR still implemented through a controlled coil at the end of the distribution feeder. An overview of the grid under study can be found in fig. 4.4b, where PV penetration is considered at 100%.

Figure 6.64 depicts the voltage profile after a PV installation with cable lines. The Y-axis is the voltage in per-unit *(pu)* and the X-axis is the feeder's length starting from the secondary side of the distribution transformer, represented as nodes of customer connection.

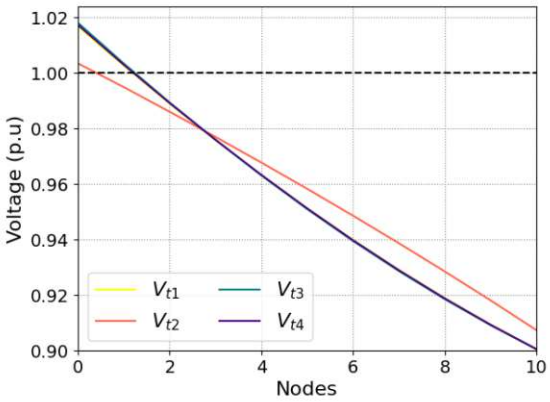

Fig 6.64. Voltage profile of LV CA grid with PV and controllable coil CVR.

It is notable here that the slope at the second time-point of the day *t2* exhibits similar behavior to the overhead simulation case in fig. 6.33, where the slope of V_{t2} (starts at slightly over 1 pu and ends at around 0.91 pu) differs from the other time-points (which are almost identical and start at around 1.02 pu to reach 0.9 pu at the end of feeder), due to power injection that the controllable coil cannot fully bring the voltage to the target voltage of 0.9 pu.

And fig. 6.65 depicts the total active power flow and losses of the LV Link-Grid. The left Y-axis is the power injected into the MV Grid-Link or consumed from the MV Grid-Link in kW, while the right Y-axis is a vertical color bar representing the Losses in kW. The X-axis represents the times of the day.

In comparison to the previous simulation case (with no PV), There is a substantial increase of active power losses at *t2* that dwarfs the other time-points losses, which were already high.

The most significant loss (about 75 kW) is incurred at the second time-point of the day *t2* (dark orange color) where the highest amount of power (around 20kW) is injected, while the other time-points (pale yellow) have the same losses (around 35-40 kW) as in the case of pure consumers.

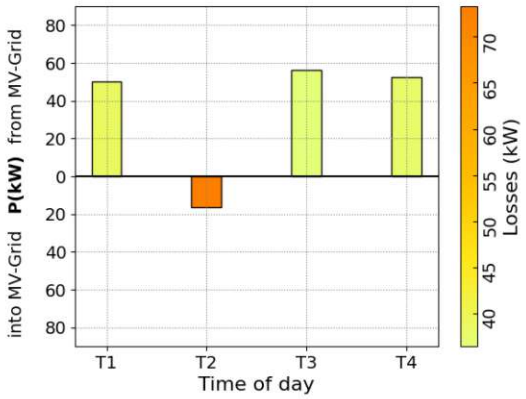

Fig 6.65. Feeder *P* flow and losses of LV CA grid with PV and controllable coil CVR.

While fig. 6.66 (corresponding graph in the case of overhead lines is fig. 6.35) depicts the net active and reactive power at each segment (1 to 10) with losses included after PV installation but with cable lines. The Y-axis of the left subfigure is the active power *(P)* from the LV grid in kW, and the Y-axis of the right subfigure is the reactive power *(Q)* in kvar. The X-axis of the two subfigures is the length of the feeder as segments where power flow is under observation.

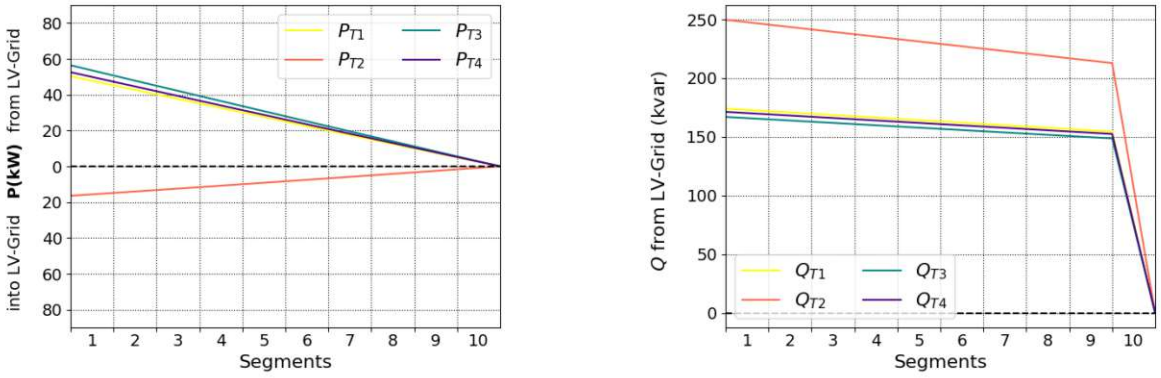

Fig 6.66. Net *P* (left) and *Q* (right) at each segment of LV CA grid with PV and controllable coil CVR.

At the second time-point of the day *t2*, the active power (red line) changes linearly from around 20 kW in the first segment to reach 0 at segment 10. On the other hand, the reactive power consumption also increased significantly in comparison to the other time-points (Q_{t2}

starts at around 250 kvar at beginning of segment 1, while the other time time-points start at around 170 kvar). However, it still has the same distinct behavior as it is slightly consumed along the feeder's length and then most of it is consumed at the end of the line where the controlled coil is found.

And fig. 6.67 depicts the percentage change of active power for respective customer plants after PV installation. The Y-axis is the active power percentage change ΔP, while the X-axis represents the customer plants along the feeder *CPs*. The plotted values indicate the difference in power compared to the estimated theoretical values for each of the time-points.

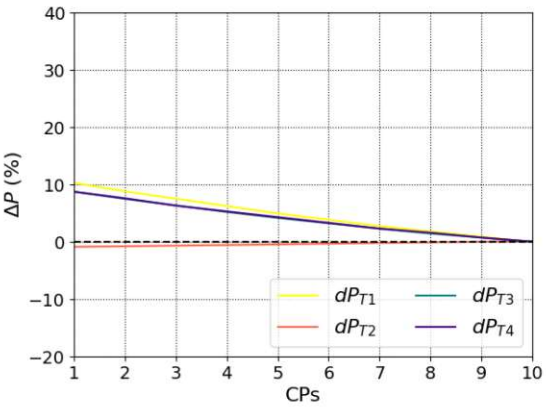

Fig 6.67. Percentage change of active power compared to optimal values of LV CA grid with PV and controllable coil CVR.

At the second time-point of the day *t2* customer plants are operating near the optimal value (as the red line approaches 0% for all customer plants), while the other time-points have the same results as the previous simulation case (without PV), with the furthest line is at the first time-point of the day *t1* (yellow) starting at about 10% for the first customer plant on the feeder and decreasing non-linearly to reach 0% at the last one.

6.2.2.3.c. With PV, targeting upper voltage limit Not surprisingly, the LV cable grid did not differ much from the overhead lines case, with the controllable coil control solution incurring high losses, which puts the previous simulation case out of comparison.

Therefore, this simulation case uses the same CVR technique, to discuss it's potential when targeting to the upper voltage limit at the second time-point of the day *t2*, as discussed in the case of overhead lines. And according to the following graphs, the losses are significantly less than the previous simulation case while successfully maintaining the voltage along the feeder's length within limits.

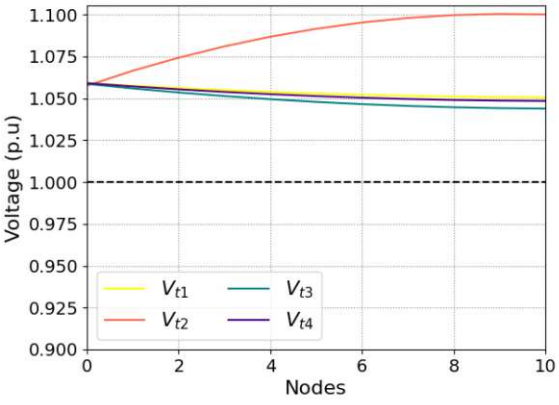

Fig 6.68. Voltage profile of LV CA grid with PV and controllable coil-based CVR targeting upper voltage limit.

Furthermore, fig. 6.68 depicts the voltage profile of the customer plants after a PV installation with cable lines. The Y-axis is the

voltage in per-unit *(pu)* and the X-axis is the feeder's length starting from the secondary side of the distribution transformer, represented as nodes of customer connection.

The voltage at the second time-point of the day *t2* is kept under the upper voltage limit along the feeder's length, while the other time-points remain unchanged from the previous simulation case.

While fig. 6.69 depicts the total active power flow and losses of the LV Link-Grid as obtained after PV installation with cable lines instead. The left Y-axis is the power injected into the MV Grid-Link from the MV Grid-Link in kW, while the right Y-axis is a vertical color bar representing the Losses in kW. The X-axis represents the time-points of the day.

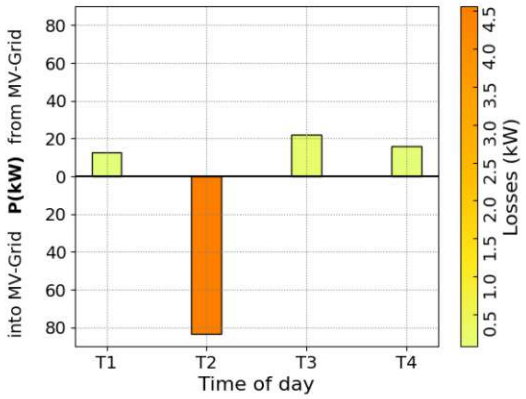

Fig 6.69. Feeder *P* flow and losses of LV CA grid with PV and controllable coil-based CVR targeting upper voltage limit.

A huge improvement is observed here in comparison to the previous simulation case, such that the most significant loss (about 6 kW) is incurred at the second time-point of the day *t2* (dark orange color) where the highest amount of power (around 80kW) is injected, while the rest exhibit the same losses' behavior, around 1 kW, (pale yellow) as in the case of pure consumers (around 20kW). The results are relatively similar to the simulation scenario in the overhead lines grid.

And fig. 6.70 depicts the net active and reactive power at each segment. The Y-axis of the left subfigure is the active power *(P)* from the LV grid in kW, and the Y-axis of the right subfigure is the reactive power *(Q)* in kvar. The X-axis of the two subfigures is the length of the feeder as segments where power flow is under observation.

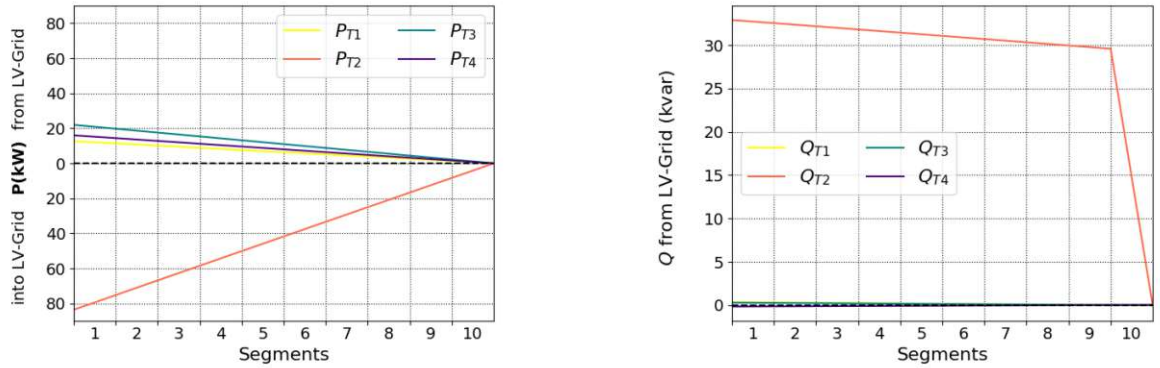

Fig 6.70. Net *P* and *Q* for each segment of LV CA grid with PV and controllable coil-based CVR targeting upper voltage limit.

It is observed from this graph that there is a significant boost to the amount of active power injected into the grid and a significant decrease in the amount of reactive power consumed compared to fig. 6.66 (red line) in comparison to the previous simulation case.

While fig. 6.71 depicts the percentage change of active power for respective customer plants after PV installation. The plotted values indicate the difference in power compared to the estimated theoretical values for each of the time-points. The Y-axis is the active power percentage change ΔP, while the X-axis represents the customer plants along the feeder *CPs*.

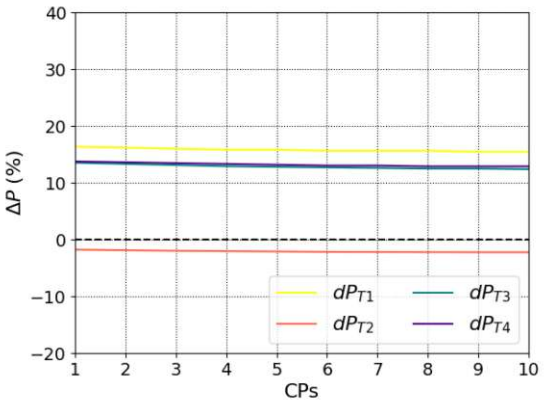

Fig 6.71. Percentage change of active power compared to optimal values of LV CA grid with PV and controllable coil-based CVR targeting upper voltage limit.

The observations from this graph show that the customer plants along the feeder's length at the second time-point of the day *t2* exhibit an almost constant operating point (about -2.5%), close to the optimal value but in the negative axis due to the direction of the power flow (injecting into the grid). Whereas the other time-points show results of around 15% along the line.

6.2.2.4. Comparison of cases in LV grid with cable lines

As a result of comparing all CVR methods applied on this theoretical LV grid with cable lines and typical values of a European grid, there are indeed a few differences than the results of the case of overhead lines, due to the more capacitive nature of cables.

The first technique of using On-load tap changer connections showed better results; however, the generated no-load transformer losses are still a problem as they overshadow the savings. While the second technique of using a controllable coil in a *Q-V* gave even worse results due to the high losses, which removes it out of the comparison altogether, except in the case of using it to keep the voltage within acceptable boundaries in the case of PV injection.

The effects of the employed CVR techniques on power flow and losses (from the perspective of the DTR) are compared and presented in fig. 6.72. In the left subfigure (a), the Y-axis represent the magnitude and direction of the total active power flow in kW, and the X-axis is the time-points of the day. While in the right subfigure (b), the Y-axis is the and the magnitude of the total active power losses (kW) in kW, and the X-axis is the time-points of the day. A summary of the results are also presented in table 6.4, where the exact numbers are presented, for the net active power flow (i.e., power flow after subtracting the losses) and the corresponding losses for all the simulation cases, along with the most important remark on each simulation case.

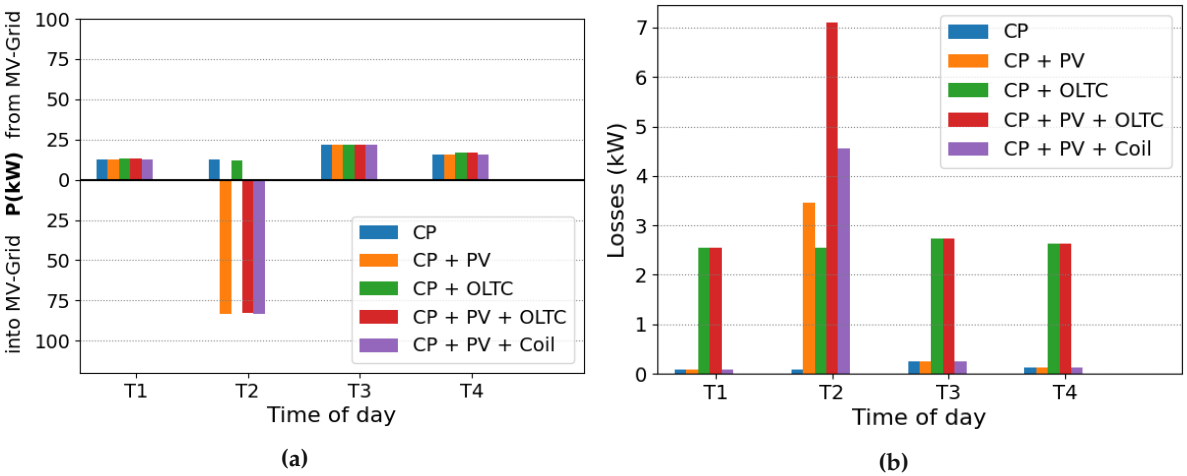

Fig 6.72. Comparison of CVR on cable line LV-grid (a) total power flow, (b) total losses.

The color blue represents the base case of normal customer plants without PV or CVR, the orange is the case of customer plants with PV installation, the green is the case of customer plants with OLTC-based CVR and without PV, the red is the case of customer plants with OLTC-based CVR and PV, and finally the violet is the case of customer plants with PV and a controlled coil-CVR targeting only the upper voltage limit of $1.1V_{nom}$.

At the second time-point of the day *t2*, the power injected into the MV Grid-Link is slightly more than 80 kW in all three simulation cases where PV is considered (i.e., no CVR, CVR with OLTC, CVR with controllable coil targeting the voltage upper-limit). But in the case of using On-load tap changer connections, the power losses are about 8.5% of the provided power (which are slightly lower than the case of overhead lines).

Meanwhile, using the controllable coil targeting $1.1V_{nom}$, about the same amount of power is fed but with slightly fewer losses (about 5.5%), which are also slightly lower than the case of overhead lines.

And the losses of both CVR techniques are considered relatively high compared to the grid setup without CVR (orange column), which demonstrates about 4% of losses.

The CVR of the cable lines LV-grid without using PV, represented in blue column, will consume about 12kW from the MV Grid-Link but with 0.08 kW of losses, meanwhile using the On-load tap changer connections with the same power consumption exhibits, in green column, 2.5kW of losses.

The other 3 time-points of the day do not feed any power into the MV Grid-Link. At the first time-point of the day *t1* the power consumption is around 14 kW in all simulation cases, but the losses are 19% in the case of using On-load tap changer connections with and without PV, in red and green column respectively, which are mostly the same as in the case of using overhead lines.

CVR	PV	Factor	Unit	t1	t2	t3	t4	Remark
No	No	P Flow (MV to LV)	kW	12.66	12.36	21.95	15.98	Slightly lower losses than OH case
		P Losses		0.08	0.08	0.24	0.13	
	Yes	P Flow (MV to LV)		12.66	-82.62	21.95	15.98	Losses~at *t2* lower than OH case
		P Losses		0.08	3.45	0.24	0.13	
OLTC	No	P Flow (MV to LV)		13.43	12.26	22.00	16.62	slightly lower losses than OH Case
		P Losses		2.55	2.54	2.74	2.62	
	Yes	P Flow (MV to LV)		13.43	-82.88	22.00	16.62	More power injected to MV at t2 compared to OH case
		P Losses		2.55	7.1	2.74	2.62	
Coil CVR	Yes	P Flow (MV to LV)		12.66	-83.64	21.95	15.97	Acceptable losses keep V_{t2} under $1.1V_{nom}$
		P Losses		0.08	4.56	0.24	0.13	

Table 6.4. Comparison of CVR on cable lines LV-grid by power flow at distribution transformer.

The power consumption in the third time-point of the day *t3* is about 22kW, but the losses are about 12.5% in the case of using On-load tap changer connections with and without PV, in red and green column respectively, which are about 0.5% lower than the case of using overhead lines.

And at the fourth time-point of the day (*t4*) about 16 kW are consumed but in the case of using On-load tap changer connections with and without PV, in red and green column respectively, with losses of about 16%, which are similar to the case of using overhead lines.

In conclusion, CVR potential is slightly better with the On-load tap changer approach in the cable than the overhead grid; however, the controllable coil solution to achieve $0.9V_{nom}$ scored even worse results than in the overhead system that made it excluded from the comparison, and therefore is only usable as a containment strategy targeting the upper voltage limit in the case of PV injection.

6.3. Medium Voltage Grid-Link

As presented in the previous section which discussed CVR potential in the LV grid case, this section examines the load reduction potential in a theatrical model of an EU MV Grid-Link (graphically depicted in fig. 6.73).

The detailed description of the grid under simulation is found in section 4.3. And the used CVR technique is the most basic one: an open-loop voltage reduction realized at the supply transformer (i.e., TR_{MV}^{HV}) by 2% reduction, while manipulating the following simulation factors:

- Type of feeder: Either overhead or cable, where the type of the feeder applies to the LV grids connected to the MV grid as well.
- PV presences: Either present at all customer plants as well as PV plants on the MV grid, or not.

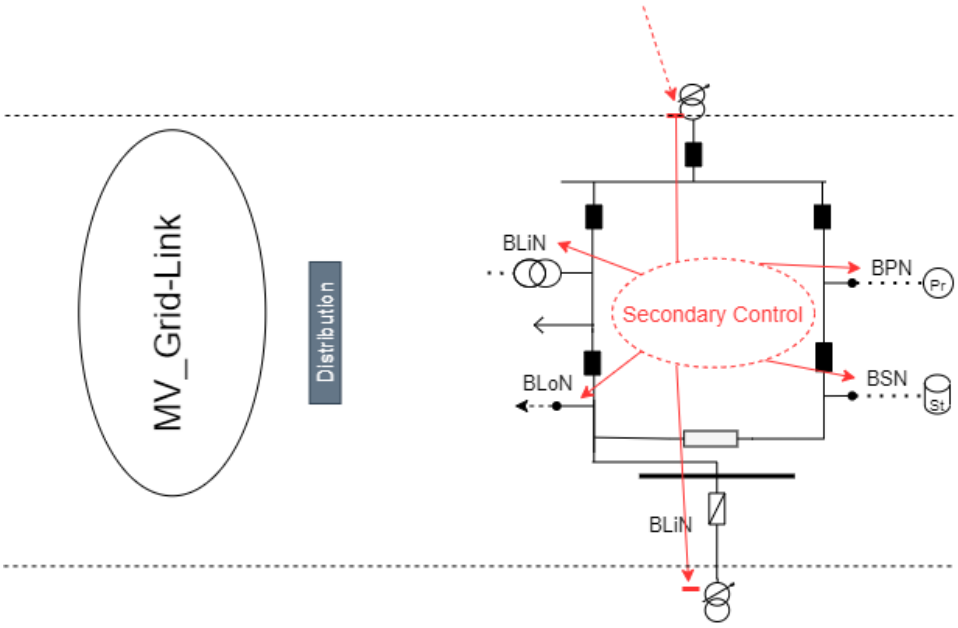

Fig 6.73. MV Grid-Link.

6.3.1. Overhead lines structure

This subsection examines the base case and the chosen CVR method on the basis of an overhead MV structure, and depicts the results for each simulation case with the help of graphs, focusing on the parameters of interest like voltage profile, active power flow as well as losses.

6.3.1.1. Base Case

6.3.1.1.a. Without PV This is the basic simulation case without CVR implementation to be used as a reference for the case without any PV presence. As explained in Chapter 4, fig. 4.5 gives an overview of the grid under simulation, where LV grids are connected to the MV grid through fixed-tap transformers at a 1:1 ratio.

The voltage profile is seen in fig. 6.74, where the voltage drops with distance of the feeder; however, with less drop than the case of LV. This is an intuitive result, intended by design to keep losses as low as possible at all time-points of operation.

The Y-axis is the voltage in pu and the X-axis is the feeder's length starting from the secondary side of the supply transformer, represented as nodes of LV grids connections.

The curves present the voltage for the four different time-points labeled $V_{t1} \dots V_{t4}$, as it covers the distance of the feeder, represented as nodes of connection for the LV grids that are supplied by this MV grid.

The four curves in the plot begin at 1.06pu and drop slightly with distance, losing only about 0.01pu, with the V_{t3} dropping the most due to the customer plants' higher consumption, according to the load model previously presented in section 6.1.

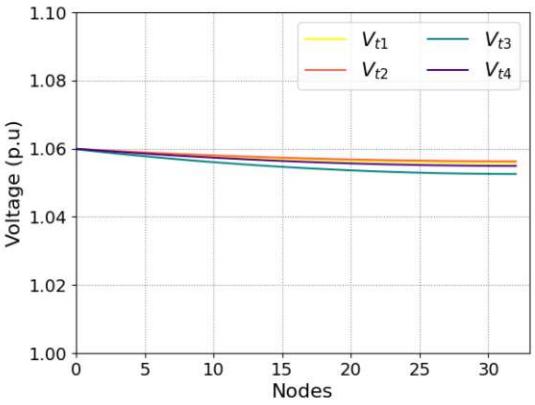

Fig 6.74. Voltage profile of MV overhead grid without PV or CVR.

While fig. 6.75 depicts the total active power consumed from the HV grid and its corresponding losses in kW. The left Y-axis is the total power consumed from HV Grid-Link in kW, while the right Y-axis is a vertical color bar representing the losses in kW. The X-axis is the simulated time-points of the day.

At the first and second time-points of the day (*t1* and *t2*), the system incurs the least losses of around 36 kW (pale yellow) with a total power flow of around 400kW.

The third time-point of the day *t3* (dark orange color) incurs the most significant losses (slightly over 46 kW), and it also has the highest amount of power flow of around 750 kW. And the losses of the fourth time-point of the day (*t4*) (bright yellow color) come slightly under 40 kW, with a total power flow of under 600 kW.

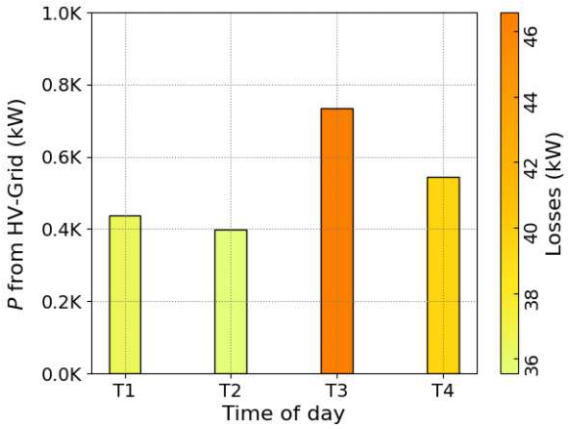

Fig 6.75. Feeder *P* flow and losses of MV overhead grid without PV or CVR.

The results from this graph correspond to the pattern in the case of LV grid, as the losses increase with consumption, although without exponential differences between the time-points.

And fig. 6.76 depicts the net active and reactive power at each segment (1 to 33). The Y-axis on the left subfigure is the active power *P* in kW, and the Y-axis on the right one is the reactive power *Q* in *kvar*. The X-axis for both subfigures is the feeder's length, as represented by feeder segments.

The active power decreases uniformly along the feeder's length, with a similar slope for the four time-points. It starts at about 400 kW at the first and second time-points of the day, yellow and orange lines respectively. At *t3* (green line), the power starts above 600 kW, and it starts at the fourth time-point of the day, purple line, slightly above 400 kW.

It is notable that *t3* is highest in *P* consumption (starting about 700 kW) and *t2* is the lowest (little under 400 kW), corresponding to the same behavior in the LV grids.

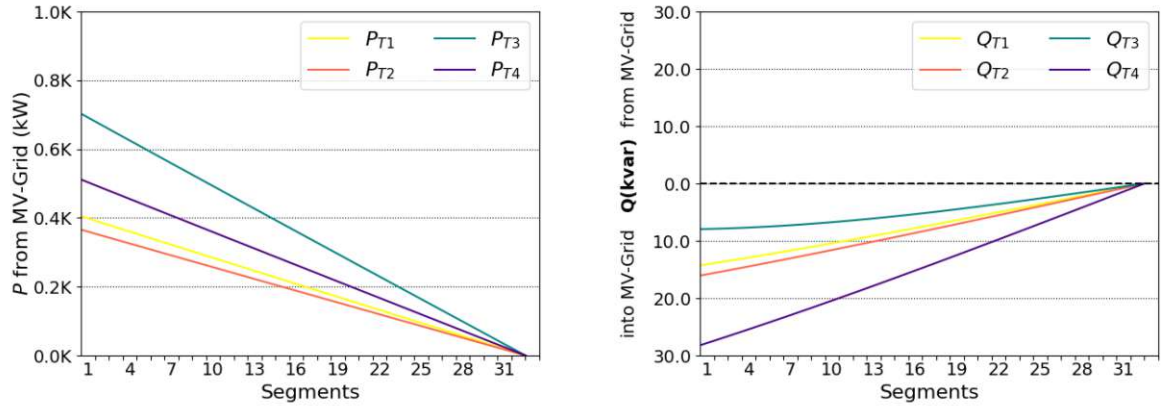

Fig 6.76. Net P (left) and Q (right) at each segment of MV overhead grid without PV or CVR.

Reactive power on the other hand is injected into the grid with a similar slope for the four time-points, but reaching different values at the beginning of the feeder (about 30 kvar in the case of the fourth time-point of the day and less than 10 kvar at the third time-point).

This happens although the overall profile of LV grids consumption is inductive (i.e., consuming reactive power), in part due to the capacitance produced along the MV overhead lines.

Thus, a conclusion can be drawn that the higher inductive power demand there is (i.e., *t3*) the less capacitive behavior at MV feeder is exhibited. The opposite is also true, such that at (*t4*), the amount of reactive power injected into the grid increases since the overall profile of LV grids at this time-point is capacitive.

While fig. 6.77 depicts the type of losses in the grid on the at the four time-points, based on their source (blue bars for line losses and orange for transformer losses) and their voltage level (LV or MV). The Y-axis is the power losses in kW and the X-axis is the network level.

It is noticed that the highest part of losses falls under the MV transformer losses, in orange color, at the four time-points are between 30 and 35 kW. While the line losses for MV grid are not of major value, as they do not exceed 5 kW at the four time-points.

And the transformer losses on the LV level are the least of all types, with the highest value at *t3* of around 1 kW. On the other hand, the line losses on the LV level (dark blue color) at the same time-point is around 10 kW, decreasing to around 5 kW in the other time-points.

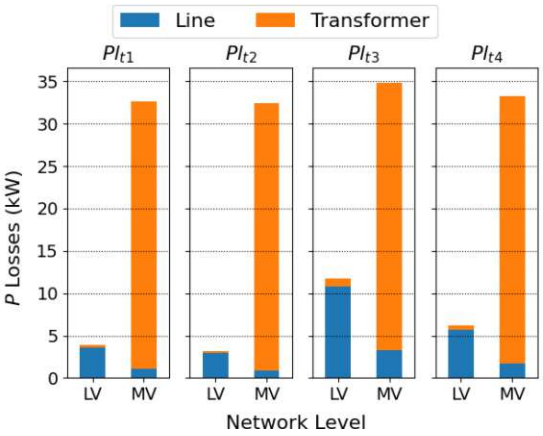

Fig 6.77. Type of losses at each time-point of MV overhead grid without PV or CVR.

The most significant part of losses is due to the main HV/MV transformer at the beginning of the line, and it is roughly stable, suggesting it is mainly due to the no-load losses, and although most line losses happen on the LV level (as expected, considering the previously mentioned grid design parameters), it is still much lower than the total transformer losses.

6.3.1.1.b. With PV PV installations are considered to be present at each customer plant in this simulation case (still without any CVR method applied), as illustrated in fig. 4.6, which gives an overview of the grid under simulation.

The resulting voltage profile is seen in fig. 6.78, where the Y-axis is the voltage in pu and the X-axis is the feeder's length starting from the secondary side of the supply transformer, represented as nodes of LV grids connections.

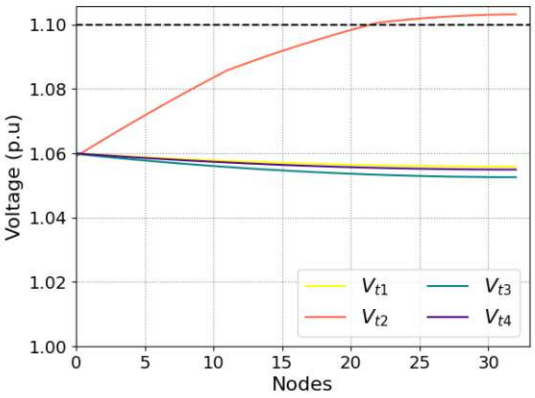

Fig 6.78. Voltage profile of MV overhead grid with PV, without CVR.

In comparison to the previous simulation case (without PV), the only change is seen in V_{t2}. The voltage of all time-points start at 1.06 pu and drops slightly with the MV feeder distance, except at the second time-point of the day, *t2*.

Voltage increases at *t2* to reach more than the upper voltage limit of 1.1 pu (indicated by a dashed line) at the end of the feeder; this is due to PV injected from MV and LV grids. Such impact on the MV grid and the following voltage regulation measures are discussed in details in literature (as in [40]); however, it is not the focus of this discussion.

While fig. 6.79 depicts the sum of active power consumed or produced from the HV grid and its corresponding losses in *kW*. The left Y-axis is the total power consumed or produced from HV Grid-Link in kW, while the right Y-axis is a vertical color bar representing the losses in kW. The X-axis is the simulated time-points of the day.

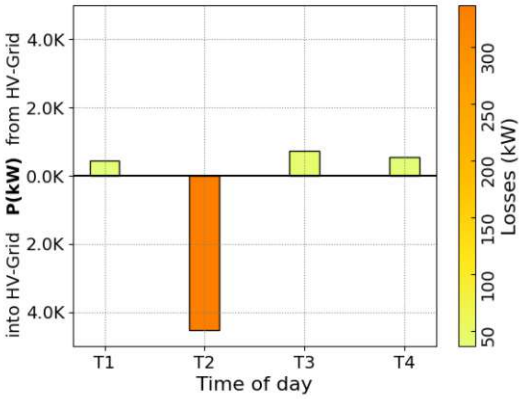

Fig 6.79. Feeder *P* flow and losses of MV overhead grid with PV, without CVR.

The most significant loss, above 300 kW, is incurred at the second time-point of the day *t2* (dark orange color) where the highest amount of power (above 4 MW) is injected, while the other time-points exhibit the same behavior, with a consumption of around 500 kW and losses of around 50 kW.

The losses are calculated according to the eq. (5.13), such that they increase with the total amount of power injected or consumed, thus, the losses at the second time-point of the day *t2* dwarfs the others.

And fig. 6.80 depicts the net active and reactive power at each segment (1 to 33). The Y-axis on the left subfigure is the active power P in kW, and the Y-axis on the right one is the reactive power Q in *kvar*. The X-axis for both subfigures is the feeder's length, as represented by feeder segments.

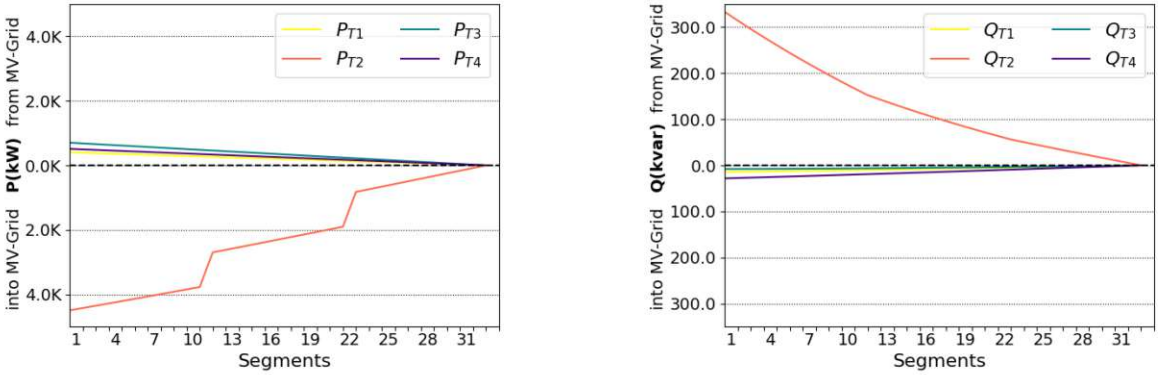

Fig 6.80. Net P (left) and Q (right) at each segment of MV overhead grid with PV, without CVR.

In comparison to the previous simulation case (without PV), the difference noticed in the left subfigure is at the second time-point of the day *t2* (red line), such that it have a linear behavior as the other time-points due to active power injected into the grid, but has 2 notable steps at segment 11 and 22, which are explained by the MV solar power plants connected there.

And as seen in the right subfigure, the reactive power also depicts a different behavior. Not only did it not flip from injecting into the grid to consuming from it, but also moved from an almost linear slope to a parabolic one, starting at the first segment at more than 300 kvar and dropping to 100 kvar in the middle of the feeder, thus, two thirds of the consumed reactive power is in the first half of the feeder. This amount of reactive power dwarfs the other curves of the other time-points (*t1*,*t3*, and *t4*).

While fig. 6.81 depicts the type of losses in the grid on the Y-axis (in kW) at the four time-points, depending on their source (i.e., lines in blue color or transformers in orange) and their voltage level (LV or MV). The Y-axis is the power losses in kW and the X-axis is the network level.

In comparison to the simulation case without PV, the second time-point of the day *t2* incurs high line losses (blue stacked columns) for both the MV and LV, which are slightly under 150 kW, and the same type of losses at the other time-points (not exceeding 10 kW) are not significant in comparison to these values.

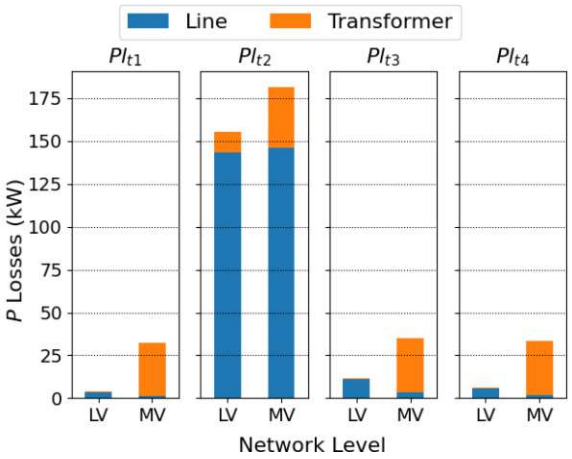

Fig 6.81. Type of losses at each time-point of MV overhead grid with PV, without CVR.

And as for the transformer losses, they stay relatively the same on the MV for all time-points (around 25 kW); however, at *t2* on the LV, they show a significant increase (around 10 kW).

Most notable here is that at *t2*, most of the losses are line losses, both on the MV and LV levels. A jump in MV/LV distribution transformer load losses is also noted compared to the other time-points.

6.3.1.2. Open-loop voltage reduction at supply transformer

This subsection discusses the effects of the simple open-loop CVR technique of reducing the voltage at the secondary-side of the supply transformer TR_{MV}^{HV} by 2% in the case of using overhead lines in both the MV and LV levels.

6.3.1.2.a. Without PV (pure consumer) This is a simulation case with CVR implementation without any PV presence. As detailed in Chapter 4, the illustrative fig. 4.5 gives an overview of the grid under simulation, where LV grids are connected to the MV grid through fixed-tap transformers at a 1:1 ratio.

This grid structure is the same as the base case (where no CVR is applied), since there are no structural changes introduced to apply this method of open-loop voltage reduction at the supply transformer.

The voltage profile of this simulation case is seen in fig. 6.82. The Y-axis is the voltage in per-unit *(pu)* and the X-axis is the feeder's length starting from the secondary side of the supply transformer, represented as nodes of LV grids connections.

The lines present the voltage for the different time-points, labeled $Vt1 \ldots Vt4$, as they cover the distance from the secondary-side of the supply transformer at the beginning of the feeder (node 0) to the last connection point of an LV grid (node 32).

It exhibits an almost identical slope at all time-points for the voltage along the feeder's length, starting at a little under 1.04 pu and only decreasing slightly along the length of the feeder to reach around 1.0375 pu.

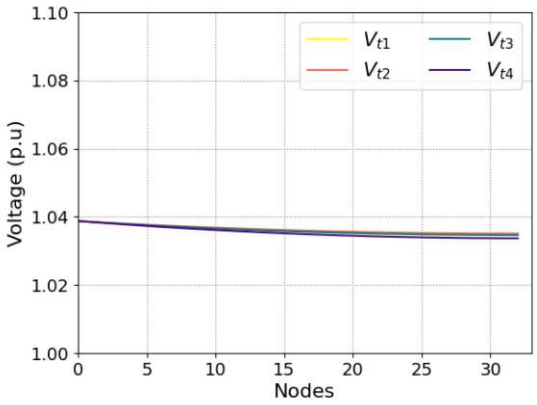

Fig 6.82. Voltage profile of MV overhead grid without PV, with CVR.

While fig. 6.83 depicts the sum of active power consumed from the HV grid and its corresponding losses in kW. The left Y-axis is the total power consumed from the HV grid in kW, while the right is a vertical color bar representing the losses in kW. The X-axis is the simulated time-points of the day.

At the second time-point of the day *t2*, the system incurs the least significant loss of below 36 kW (pale yellow) at a power flow of just under 400 kW, while the forth time-point of the day *t4* (dark orange color) incurs the most significant loss which is above 39 kW as well as the highest amount of power flow, above 500 kW. Lastly, the loss at the first and third time-point of the day *t1* and *t3* (bright yellow color) comes a little under 37kW.

Notably, the losses are considerably lower than the base case, particularly at *t3*.

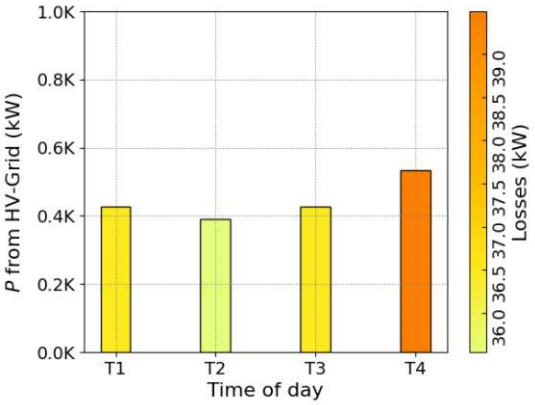

Fig 6.83. Feeder *P* flow and losses of MV overhead grid without PV, with CVR.

While fig. 6.84 depicts the net active and reactive power at each segment. The Y-axis on the left subfigure is the active power P in kW, and on the right side is the reactive power Q in kvar. The X-axis for both subfigures is the feeder's length, as represented by feeder segments.

In the left subfigure, it is seen that the consumed active power decreases linearly along the segments of the feeder, with a similar slope for the four time-points. It starts at the first segment slightly below 400 kW for the first and second time-points of the day, yellow and orange lines, respectively. And at *t3*, green line, it starts at 400 kW, where *t4*,purple line, draws about 500 kW. In comparison to the base case, *t3* is no longer the time-point with the highest *P* consumption, but rather *t4*, since *t3* consumes about 150 kW less than the base case.

And in the right subfigure, it is seen that the reactive power is injected into the grid and exhibits a uniform and a similar slope for all the time-points. The fourth time-point of the day (purple line) exhibits the most *Q* injected, reaching more than 25 kvar, where the other

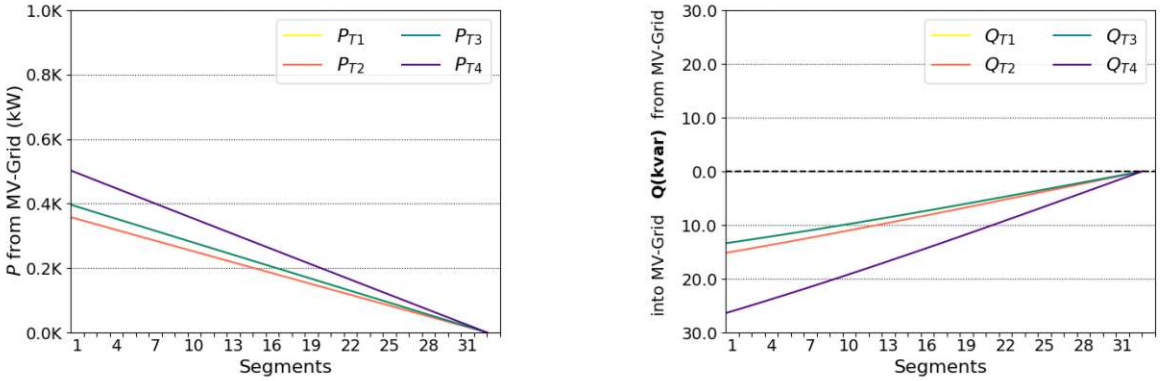

Fig 6.84. Net P (left) and Q (right) at each segment of MV overhead grid without PV, with CVR.

time-points are all under 15 kvar. In comparison to the base case, there's a notable increase in the amount of Q injected at $t3$ of about 50%.

While fig. 6.85 depicts the type of losses in the grid at the four time-points, depending on their source (i.e., lines in blue color or transformers in orange) and their voltage level (LV or MV). The Y-axis is the power losses in kW and the X-axis is the network level.

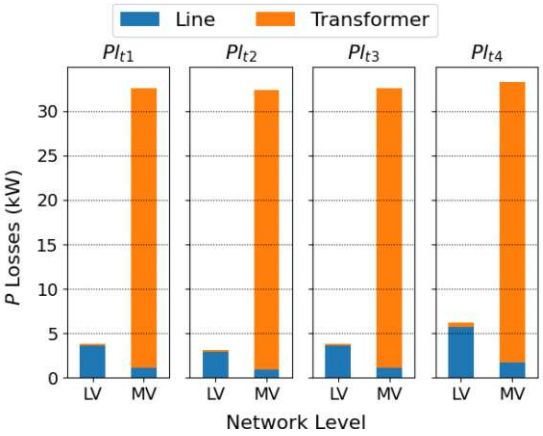

Fig 6.85. Type of losses at each time-point of MV overhead grid without PV, with CVR.

Similar to the base case, the highest losses fall under the MV transformer losses, in orange color, with a similar value for all time-points (due to the no-load losses), around 30 kW. Where the transformer losses on the LV level barely affect the system at any of the four time-points (in all cases under 1 kW). Similarly, the MV line losses (blue color) are also not of major value, as they do not exceed 3 kW at any of the four time-points. LV line losses, on the other hand, are of larger values, with $t4$ incurring the highest loss (slightly over 5 kW).

In comparison to the base case, it is most notable that the LV line losses at $t3$ are significantly reduced, while the MV transformer losses are mostly the same since they are mainly constant losses.

6.3.1.2.b. With PV PV installations are considered to be present at each customer plant in this simulation case (still without any CVR method applied), as illustrated in fig. 4.6, which gives an overview of the grid under simulation.

The resulting voltage profile is seen in fig. 6.86, where the Y-axis of the figure is the voltage in per-unit and the X-axis is the feeder's length as connection nodes.

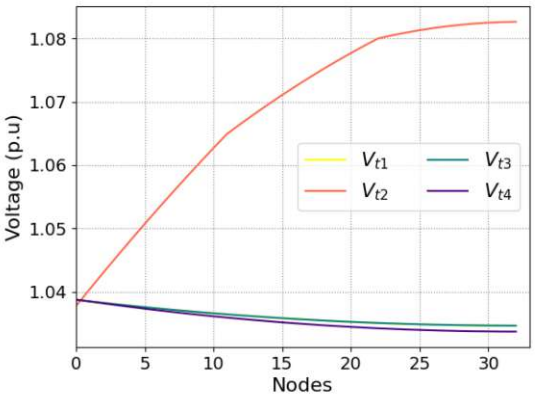

Fig 6.86. Voltage profile of MV overhead grid with PV and CVR.

As seen in the figure, the voltage drops slightly with distance at all time-points of the day except *t2*, However, V_{t2} does not reach the upper voltage limit of $1.1V_{nom}$, and levels off at a little over 1.08 pu at the last feeder segment.

In comparison to the previous simulation case (without PV), the only change is seen in V_{t2}. The voltage of all time-points start at 1.04 pu and drops slightly with the MV feeder distance, except at the second time-point of the day. Voltage increases at *t2*, but does not reach the upper voltage limit of 1.1 pu, but rather a little over 1.08 pu at the last node of feeder (node 32), due to PV injected, both from plants on the MV grid and at the customer plants on the LV grids.

Moreover, fig. 6.87 depicts the sum of active power consumed or produced from the HV grid and its corresponding losses in kW. The left Y-axis is the total power consumed or produced from HV Grid-Link in kW, while the right Y-axis is a vertical color bar representing the losses in kW. The X-axis is the simulated time-points of the day.

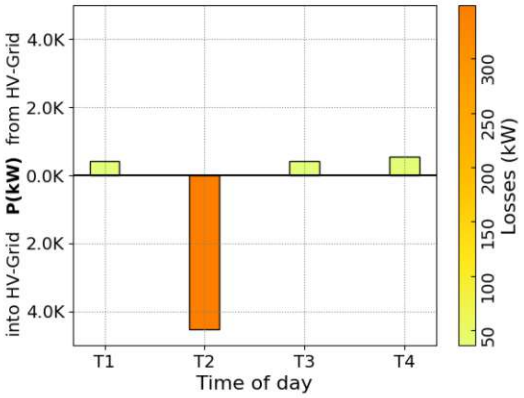

Fig 6.87. Feeder *P* flow and losses of MV overhead grid with PV and CVR.

The most significant loss, above 300 kW, is incurred at the second time-point of the day *t2* (dark orange color) where the highest amount of power is injected (more than 4 MW). These values dwarf the values at the other time-points, where the losses are all under 50 kW.

While fig. 6.88 depicts the net active and reactive power at each segment (1 to 33). With the Y-axis on the left subfigure as the active power *P* in kW and on the right one as the reactive power *Q* in *kvar*. The X-axis for both subfigures is the feeder's length, as represented by feeder segments.

In the left subfigure, it is seen that the active power at *t1*,*t3* and *t4* is the same as the previous simulation case (without PV) and the only difference is seen at the second time-point, where the power flow is reversed, reaching more than 4 MW at the first feeder segment, with notable

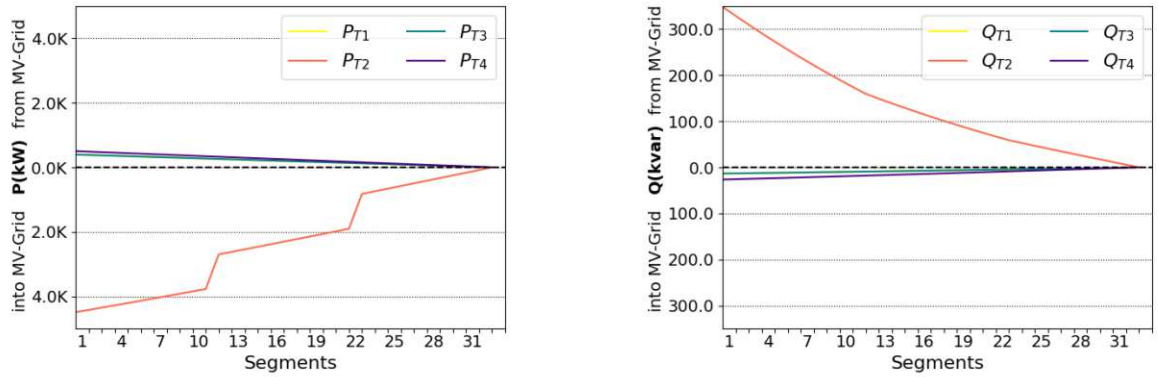

Fig 6.88. Net *P* (left) and *Q* (right) at each segment of MV overhead grid with PV and CVR.

steps at segment 11 and 22 which are explained by the MV solar power plants connected there.

In the right subfigure and in comparison to the case without PV, reactive power at *t2* reversed direction, from slightly capacitive with linear behavior to highly inductive with an almost parabolic behavior. It starts at the first segment at more than 300 kvar and drops to 100 kvar in the middle of the feeder. This means that two thirds of the consumed reactive power is in the first half of the feeder. This amount of reactive power dwarfs the other values at time-points *t1*,*t3*, and *t4*, which stay the same as in the case of without PV.

And fig. 6.89 depicts the type of losses in the grid on the at the four time-points, based on their source (blue colored bars for line losses and orange for transformer losses) and their voltage level (LV or MV). The Y-axis is the power losses in kW and the X-axis is the network level.

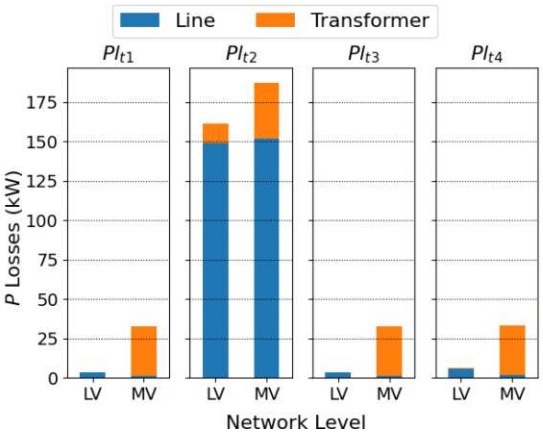

Fig 6.89. Type of losses at each time-point of MV overhead grid with PV and CVR.

As seen in the figure and in comparison to the previous simulation case (without PV), the second time-point of the day *t2* incurs high line losses (blue stacked columns) for both the MV and LV, each around 150 kW. The same type of losses at the other time-points are not significant in comparison to these values, as they do not exceed 10 kW.

And in comparison to the base case, the line losses here are higher at slightly higher at *t2*, but lower at *t3*, where there is no significant difference at *t1* and *t4*.

As for the transformer losses, they stay mostly constant on the MV level for all time-points (around 25 kW). However, there are no significant values on the LV level, except at *t2*, where a multifold increase is seen, as it reaches more than 10 kW.

6.3.1.3. Comparison of cases in MV grid with overhead lines

Comparing the CVR method applied here to the base case, it is clear that the decrease in voltage is effective in consuming less power from the supplying HV grid, keeping in mind that the utilized voltage drop is minimal at only 0.02 pu and presents no threat to the traditional grid management efforts.

The effects of the employed CVR techniques on power flow and losses (from the perspective of the supply transformer) are presented in fig. 6.90, comparing the results of all simulation cases. In the left subfigure (a), the Y-axis represent the magnitude and direction of the total active power flow in kW, and the X-axis is the time-points of the day. While in the right subfigure (b), the Y-axis is the and the magnitude of the total active power losses in kW, and the X-axis is also the time-points of the day.

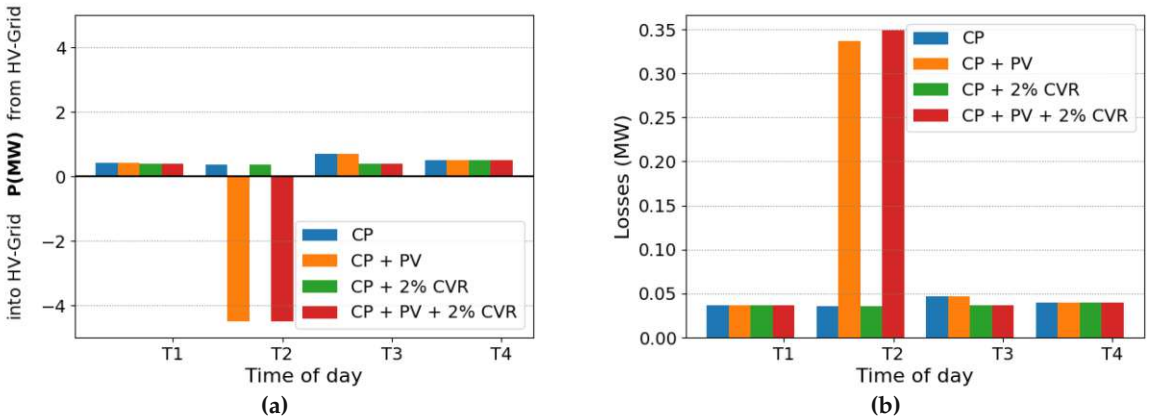

Fig 6.90. Comparison of CVR on overhead lines MV Grid-Link (a) total power flow, (b) total losses.

The color blue represents the base case of normal customer plants without PV or CVR, orange is the case of customer plants with PV installation, the green is the case of customer plants with the 2% CVR but without PV, and finally the red is the case of customer plants with 2% CVR and PV.

At the second time-point of the day *t2*, the power injected into the HV grid is slightly more than 4 MW in both simulation cases using PV, with CVR (red) and without (orange); however, a slight decrease is observed in the case with CVR, and both cases have similar amount of losses ; power losses are 336.79 kW and 348.86 kW (about 7.5% and 7.8% of the net active power) without CVR and with applying it, respectively. The other 3 time-points of the day do not feed any power into the HV grid, and thus do not show any difference in the case of using PV.

As for the case without PV, applying CVR (green column) results in a considerably lower active power consumption at *t3* (396 kW) in comparison to the base case (blue column) (703 kW), with lower losses as well (36 and 46 kW respectively). That's an impressive decrease

in total power consumption, but the difference is not so significant at the other time-points, with roughly the same amount of losses, but with an overall decrease in power consumption. These differences arise from the different load values and composition, that originate from the load model.

At the first time-point of the day *t1*, the power consumption in the base case is around 404 kW and the losses are 36 kW. Interestingly, CVR brings the power consumption down to 396 kW, but the losses stay mostly the same but when applying 2% CVR the power consumption dropped to 396 kW. That corresponds to about 2% decrease in active power. A similar result is found for *t4*, as power consumption decreased through CVR from 511 to 502 kW.

CVR	PV	Factor	Unit	t1	t2	t3	t4	Remark
No	No	Net *P* (*HV* to *MV*)	kW	404.85	365.88	703.06	511.64	Normal behavior
		P Losses		36.47	35.55	46.58	39.45	
	Yes	Net *P* (*HV* to *MV*)		404.85	-4497.35	703.06	511.64	Losses increase at *t2* with increased injected power
		P Losses		36.465	336.79	46.58	39.45	
Yes	No	Net *P* (*HV* to *MV*)		396.76	358.07	396.76	502.95	Losses are roughly the same, but less power is consumed
		P Losses		36.47	35.55	36.47	39.49	
	Yes	Net *P* (*HV* to *MV*)		396.76	-4493.27	396.76	502.95	Losses increased slightly at *t2*
		P Losses		36.47	348.86	36.467	39.49	

Table 6.5. Comparison of CVR on overhead lines MV Grid-Link by power flow at supply transformer.

CVR savings are visible in both total active power consumed and losses, which are most significant at *t3*. However, CVR faces a slight decrease in performance in the case of PV due to the high production at *t2*. A summary of these results is found in table 6.5, where the exact numbers are presented, for the net active power flow (i.e., power flow after subtracting the losses) and the corresponding losses for all the simulation cases, along with the most important remark on each simulation case.

In conclusion, this simple CVR method on the MV level is worth pursuing, especially as the consumption of customer plants on the feeder increases, with minimum structural changes, costs, staff training and engineering effort.

6.3.2. Cable lines structure

In this subsection, the base case and the chosen CVR method are presented and compared on the basis of a cable lines MV structure. The results of each simulation case are depicted with the help of graphs, with focus on the relevant parameters, i.e., voltage profile, active power flow as well as losses.

6.3.2.1. Base Case

6.3.2.1.a. Without PV This is the basic simulation case, where CVR is not implemented, which is meant to be used as a reference point for the case of no PV distributed generation

present on the grid, both on the LV and the MV level. As explained in details in Chapter 4, fig. 4.5 gives an overview of the grid under simulation, where LV grids are connected to the MV grid through fixed-tap transformers at a 1:1 ratio. This shows no difference from the overhead case, since there are no structural alterations in the grid, except for the type of the feeders.

The respective voltage profile is seen in Figure 6.91 of a pure consumer case. The curves present the voltage for different time-points, labeled $V_{t1} \dots V_{t4}$ as it covers the distance from the first node at the beginning of the feeder to the last one. The Y-axis is the voltage in per-unit *(pu)* and the X-axis is the feeder's length starting from the secondary side of the supply transformer, represented as nodes of LV grids connections.

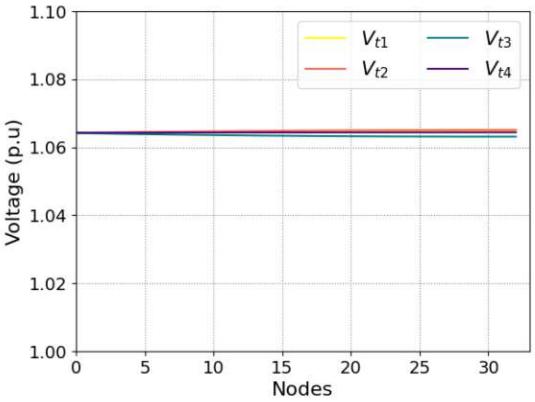

Fig 6.91. Voltage profile of MV cable grid without PV or CVR.

In comparison to the same case with overhead lines, it is noticeable that the voltage of all time-points starts at a higher value with a difference of about 0.05pu, but remains relatively constant with distance, with a lower voltage drop as it moves further along the feeder's length or even with a slight increase. This fact would translate into a higher potential for CVR gains, due to the possible voltage drop.

While fig. 6.92 depicts the sum of active power consumed from the HV grid and its corresponding losses in kW. The left Y-axis is the total power consumed from HV Grid-Link in kW, while the right Y-axis is a vertical color bar representing the losses in kW. The X-axis is the simulated time-points of the day.

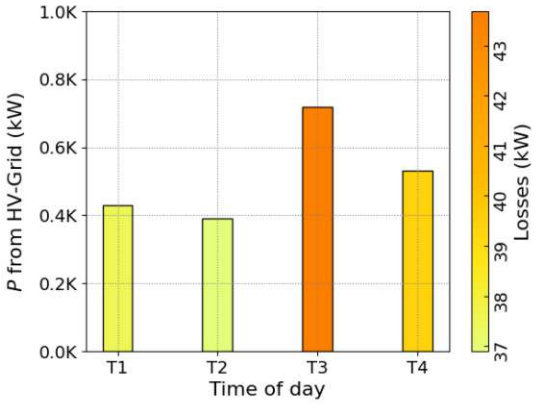

Fig 6.92. Feeder *P* flow and losses of MV cable grid without PV or CVR.

At the first and second time-points of the day (*t1*, *t2*), the system incurs the least losses, just under 37 kW (pale yellow) with a total power flow of around 400kW; while *t3* (dark orange color) incurs the most significant losses (slightly over 43 kW), and it also has the highest power flow of around 730 kW, and finally the losses of *t4* (bright yellow color) come around 40 kW with a total power flow slightly under 550 kW.

In comparison to the values of the same case but with overhead lines, there's a slight decrease in the net active power which is sourced from the HV grid, for all time-points.

However, such a pattern is not found in the losses, as the losses at *t4* stay roughly the same, and decrease slightly at *t3*, but actually increase for *t1* and *t2*. This is due to the nature of load and its ZIP composition at each time-point.

While fig. 6.93 depicts the net active and reactive power at each segment (1 to 33) behaving linearly. The Y-axis on the left subfigure as the active power *P* in kW and on the right one as the reactive power *Q* in *kvar*. The X-axis for both subfigures is the feeder's length, as represented by feeder segments.

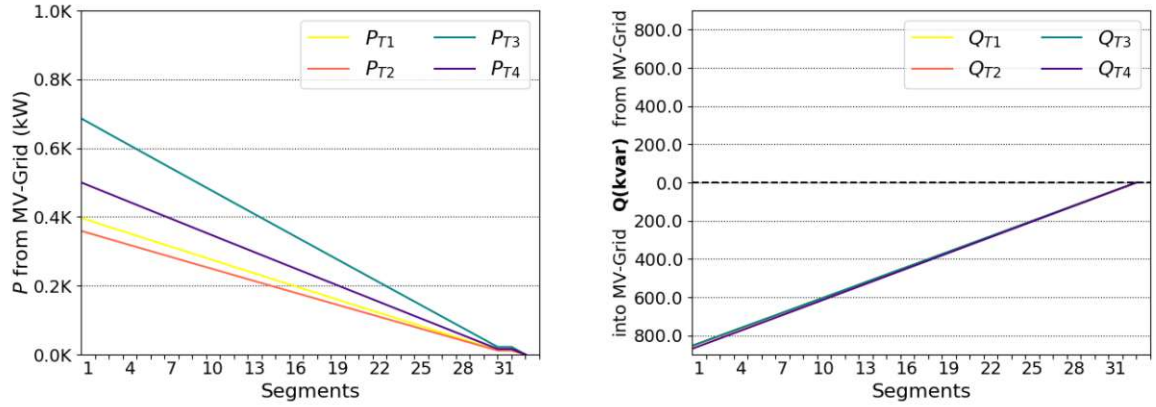

Fig 6.93. Net *P* (left) and *Q* (right) at each segment of MV cable grid without PV or CVR.

In the left subfigure, the active power starts slightly below 400 kW for *t2* and at 400 kW for *t1*, yellow and orange lines respectively. At the third time-point of the day, green line, the power starts above 600 kW, and at the fourth time-point, purple line, it is around 500 kW. The active power passing at each segment decreases uniformly, with a similar slope for the four time-points.

And in the right subfigure, the reactive power is not consumed but rather injected into the grid (capacitive behavior) at a much higher value than the case of overhead lines. The values for the four time-points are almost identical, with a similar slope, starting at 0 at the last feeder segment, and reaching more than 800 kvar at the first segment (as opposed to 10 - 30 kvar in the overhead case); the more-capacitive nature of the cable lines accounts for this difference.

While fig. 6.94 depicts the type of losses in the grid, based on their source (blue colored

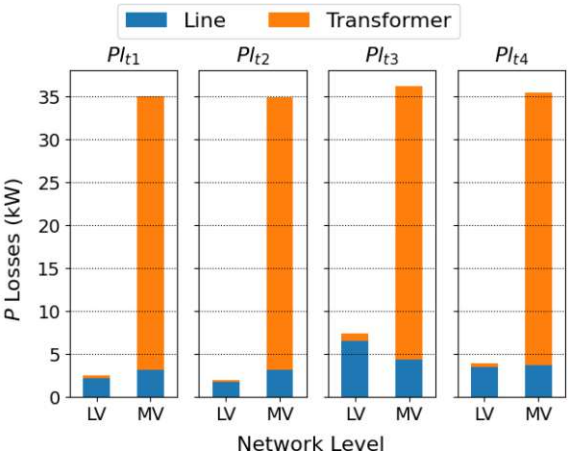

Fig 6.94. Type of losses at each time-point of MV cable grid without PV or CVR.

bars for line losses and orange for transformer losses) and their voltage level (LV or MV). The Y-axis is the power losses in kW and the X-axis is the network level.

The MV transformer losses, in orange color, constitute the major losses, as they are roughly at 35 kW at all time-points, slightly higher than its values in the case of overhead lines. While the LV transformer losses are the least significant, with the highest value being about 1 kW at time-point three, *t3*.

As for the LV line losses (blue color), the most significant value is slightly above 6 kW at the third time-point of the day *t3*, and the least is roughly 2 kW at *t2*. In comparison to the overhead case, LV Line losses are reduced by some 40%.

And as for the MV line losses, they range around 3-5 kW at the four time-points, with slightly higher values than the overhead case. Note that the overall line losses are still much lower than transformer losses.

6.3.2.1.b. With PV In this simulation case, PV installations are considered to be present at all customer plants on the LV level, as well as 2 MV PV plants, as illustrated in fig. 4.6, which gives an overview of the grid under simulation.

The resulting voltage profile is seen in fig. 6.95, where the Y-axis is the voltage in per-unit *(pu)*, and the X-axis is the feeder's length as connection nodes.

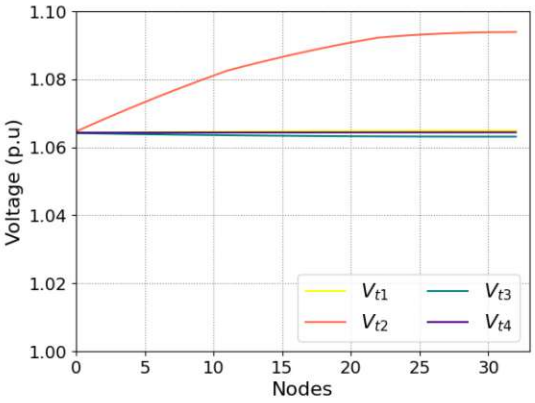

Fig 6.95. Voltage profile of MV cable grid with PV, without CVR.

In comparison to the overhead simulation case without CVR implementation and with PV installations, it is observed that all time-points have a slightly higher voltage starting point at node 0 (secondary side of the supply transformer TR_{MV}^{HV}), where they begin at around 1.065 pu as opposed to 1.06 pu.

And in comparison to the previous simulation case (no PV), the time-points *t1*,*t3* and *t4* behave the same way as they drop slightly with distance. But at the second time-point of the day, *t2* (red line), the line increases non-linearly, due to PV injected from MV and LV grids. However, it does not exceed the upper voltage limit $1.1V_{nom}$ as in the case of the overhead lines, but only up to about 1.094 pu.

Moreover, fig. 6.96 depicts the sum of active power consumed or produced from the HV grid and its corresponding losses in *kW*. The left Y-axis is the total power consumed or produced from the HV Grid-Link in kW, while the right Y-axis is a vertical color bar representing the losses in kW. The X-axis is the simulated time-points of the day.

The most significant loss, about 225 kW, is incurred at the second time-point of the day *t2* (orange color) where the highest amount of power flows (above 4 MW), while the rest exhibit the same losses' behavior, below 50 kW (pale yellow), as in the case of pure consumers (around 500 kW).

As noticed, the losses increase with the power flow, such that the losses at the second time-point of the day *t2* dwarfs the others; however, they are still less than that of the case of overhead lines (above 300 kW). The losses are calculated according to section 5.13.

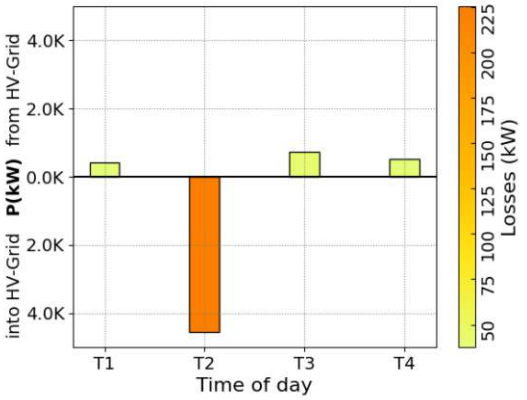

Fig 6.96. Feeder *P* flow and losses of MV cable grid with PV, without CVR.

While fig. 6.97 depicts the net active and reactive power at each segment (1 to 33). The Y-axis on the left subfigure is the active power P in kW, and the Y-axis on the right one is the reactive power Q in kvar. The X-axis for both subfigures is the feeder's length, represented by feeder segments.

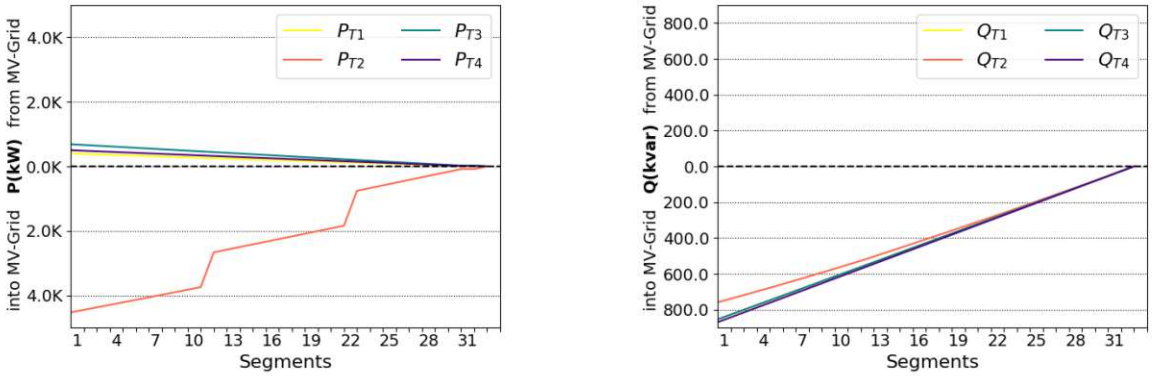

Fig 6.97. Net *P* (left) and *Q* (right) at each segment of MV cable grid with PV, without CVR.

In comparison to the previous simulation case without PV, the net active power in the left subfigure, at *t2* (red line) behaves differently due to the power injected into the grid, such that it is in the opposite side of the X-axis and no longer linear along the feeder, but has 2 notable steps; due to the presence of the MV PV power plants.

And as seen in the right subfigure with the reactive power, the Q_{T2} is slightly less capacitive than the case of without PV. The other time-points have the same values as the previous case without PV.

Furthermore, fig. 6.98 depicts the type of losses in the grid based on their source (blue colored bars for line losses and orange for transformer losses) and their voltage level (LV or MV). The Y-axis is the power losses in kW and the X-axis is the network level.

As seen in the figure and in comparison to the previous simulation case (without PV), the second time-point of the day *t2* incurs high line losses (blue stacked columns) for both the MV and LV, both are above 90 kW, and the same type of losses at the other time-points are not significant in comparison as they do not exceed 10 kW,

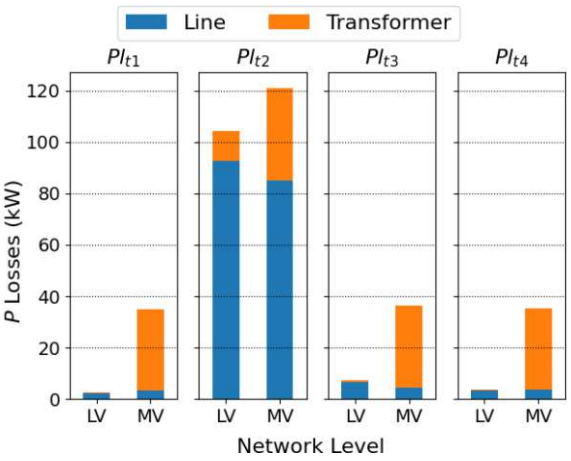

Fig 6.98. Type of losses at each time-point of MV cable grid with PV, without CVR.

As for the transformer losses (orange stacked columns), they stay relatively the same on the MV for all time-points (around 35 kW) as they are mostly constant losses; however, the LV transformer losses at *t2* show a significant increase (around 12 kW), a value that dwarfs the values at the other time-points. Most notable here is that at *t2*, most of the losses are line losses, both on the MV and LV levels. A jump in MV/LV distribution transformer load losses is also noted compared to the other time-points.

6.3.2.2. Open-loop voltage reduction at supply transformer

This subsection discusses the effects of the simple open-loop CVR technique of reducing the voltage at the secondary-side of the supply transformer by just 2% in the case of using cable lines structure in both the MV and LV levels.

6.3.2.2.a. Without PV (pure consumer) This simulation case considers the mentioned CVR technique without any PV presence in the grid. Chapter 4 detailed the grid under simulation, as it was illustrated in fig. 4.5, where LV grids are connected to the MV grid through fixed-tap transformers at a 1:1 ratio. This grid structure is the same as the base case (where no CVR is applied), since there are no structural changes introduced.

The voltage profile seen in fig. 6.99 exhibits an almost identical slope to the base case for

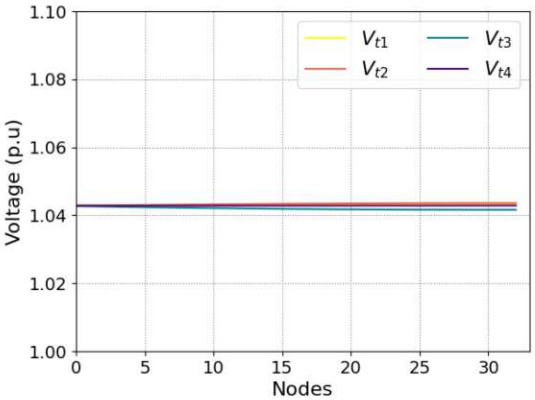

Fig 6.99. Voltage profile of MV cable grid without PV, with CVR.

all time-points; however, with a lowered voltage start by 2%. The Y-axis is the voltage in per-unit *(pu)* and the X-axis is the feeder's length as nodes of connection.

As seen in the figure, the voltage at all time-points remains relatively constant with distance, with a lower voltage drop as it moves further along the feeder's length or even with a slight increase as compared to the overhead lines case.

While fig. 6.100 depicts the sum of active power consumed from the HV grid and its corresponding losses in kW. The left Y-axis is the total power consumed from HV Grid-Link in kW, while the right Y-axis is a vertical color bar representing the losses in kW. The X-axis is the simulated time-points of the day.

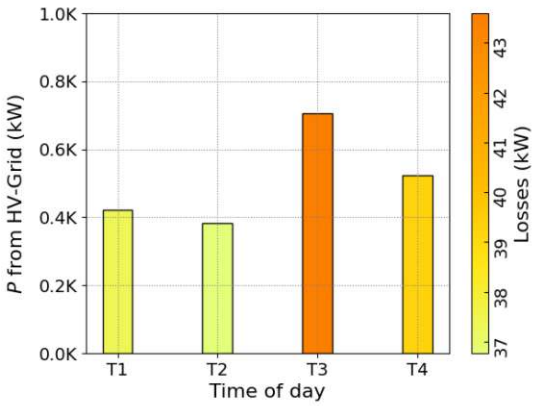

Fig 6.100. Feeder *P* flow and losses of MV cable grid without PV, with CVR.

At the second time-point of the day (*t2*), the system incurs the minimum loss of about 37 kW (pale yellow), while the third time-point of the day *t3* (dark orange color) incurs the most significant loss which is above 43 kW; it also has the highest amount of power flow of about 700 kW. The first and fourth time-point of the day (*t1* and *t4*) (pale and bright yellow color respectively) incur loss value in between the above values. In comparison to the base case (without CVR or PV), there is no significant difference observed.

While fig. 6.101 depicts the net active and reactive power at each segment (1 to 33) behaving linearly. The Y-axis of the left subfigure is the active power *(P)* from the LV grid in kW, and that of the right subfigure is the reactive power *(Q)* in kvar. The X-axis for both subfigures is the feeder's length, as represented by feeder segments.

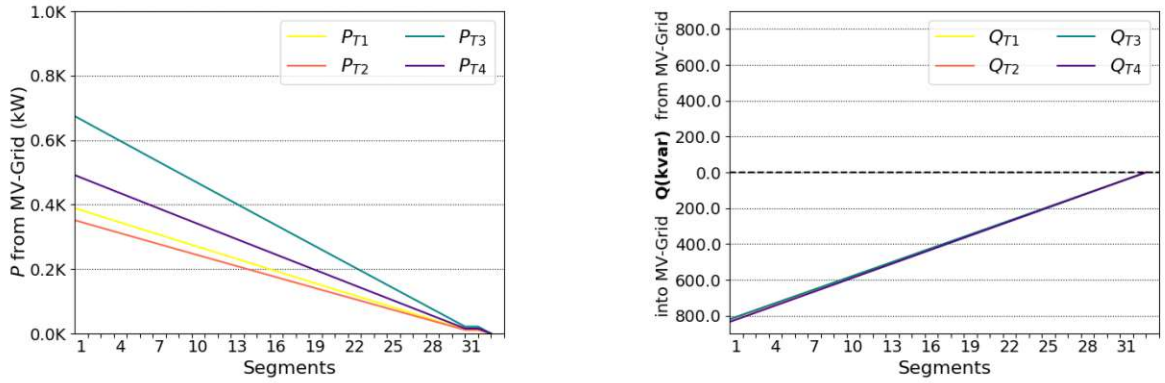

Fig 6.101. Net *P* (left) and *Q* (right) at each segment of MV cable grid without PV, with CVR.

The active power starts slightly below 400 kW at the first and second time-points of the day, yellow and orange lines, respectively. At the third time-point of the day, green line, the power starts above 600 kW, and at the fourth time-point, purple line, at around five hundred kW. There is no significant change from the base case to be seen.

While fig. 6.102 depicts the type of losses in the grid on the at the four time-points, based on their source (blue colored bars for line losses and orange for transformer losses) and their voltage level (LV or MV). The Y-axis is the power losses in kW and the X-axis is the network level.

The MV transformer losses (orange stacked columns) at the four time-points are mostly no-load losses with values constant around 35 kW; while the LV transformer losses are non-significant at all time-points, except at the third time-point of the day *t3* which is about 1 kW.

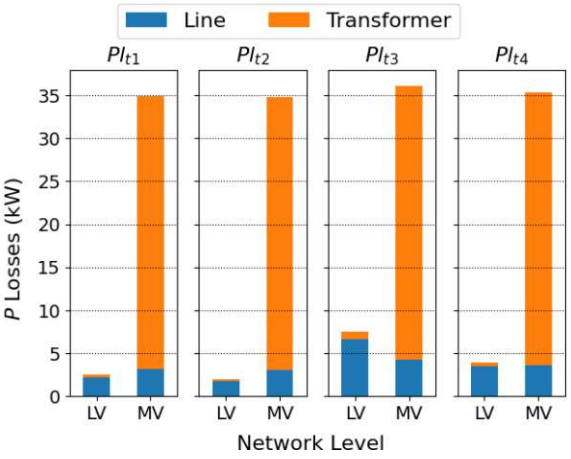

Fig 6.102. Type of losses at each time-point of MV cable grid without PV, with CVR.

The most significant line losses are at *t3* LV level (blue), a little over 5 kW. The line losses for MV level do not exceed 5 kW at the four time-points. It is observed that there is no significant change in results from the base case.

6.3.2.2.b. With PV In this simulation case, the mentioned CVR technique is applied, and PV installations are considered to be present at all customer plants on the LV level, as well as 2 MV PV plants, as illustrated in fig. 4.6, which gives an overview of the grid under simulation.

The resulting voltage profile of this simulation case is seen in fig. 6.103 , where the Y-axis is the voltage in per-unit *(pu)*, and the X-axis is the feeder's length as connection nodes. As seen in the figure, the voltage at all time-points starts at 1.045 pu and drops slightly with distance at *t1*, *t2* and *t3* (identical to the behavior at the previous simulation case where no PV was installed), but at the second time-point of the day (*t2*), where it increases non-linearly to reach 1.073 pu at the last node of the feeder.

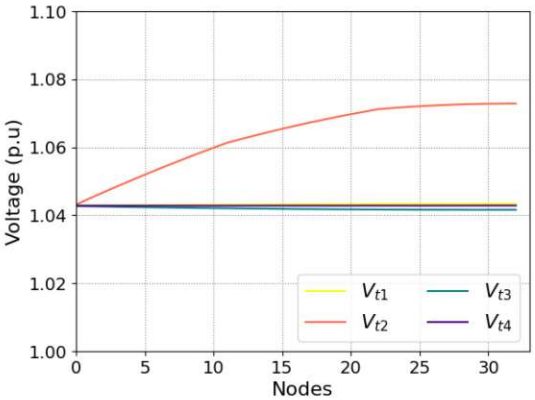

Fig 6.103. Voltage profile of MV cable grid with PV and CVR.

Furthermore, fig. 6.104 depicts the sum of active power consumed or produced from the HV grid and its corresponding losses in kW. The left Y-axis is the total power consumed from HV Grid-Link in kW, while the right Y-axis is a vertical color bar representing the losses in kW. The X-axis is the simulated time-points of the day.

There is no significant difference between this case and the base case with PV. The most significant loss, above 225 kW, is incurred at the second time-point of the day *t2* (dark orange color) where the highest amount of power (around 4 MW) is injected, while the rest exhibit the same losses' behavior below 50 kW, (pale yellow). The losses at the second time-point of the day t2 dwarfs the others; however, it is still less than that of the case of overhead lines with PV installed and CVR applied, where it almost reaches 350 kW.

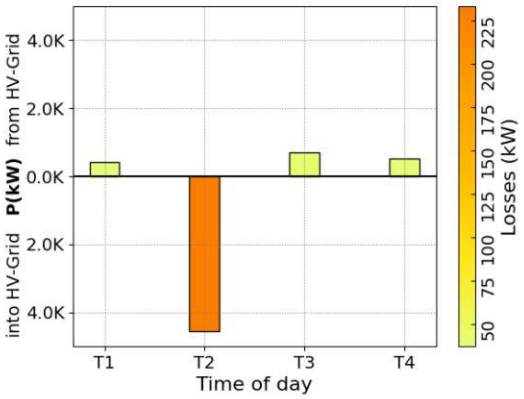

Fig 6.104. Feeder *P* flow and losses of MV cable grid with PV and CVR.

While fig. 6.105 depicts the net active and reactive power at each segment (1 to 33). The Y-axis on the left subfigure as the active power *P* in kW and on the right one as the reactive power *Q* in *kvar*. The X-axis for both subfigures is the feeder's length, as represented by feeder segments.

Similar to the overhead lines case, the net active power (red line) injected into the grid is no longer linear along the feeder but has 2 notable steps (because of MV PV plants). With reactive power, it is noticed that at the second time-point of the day t2, there is less capacitive behavior than the case without PV.

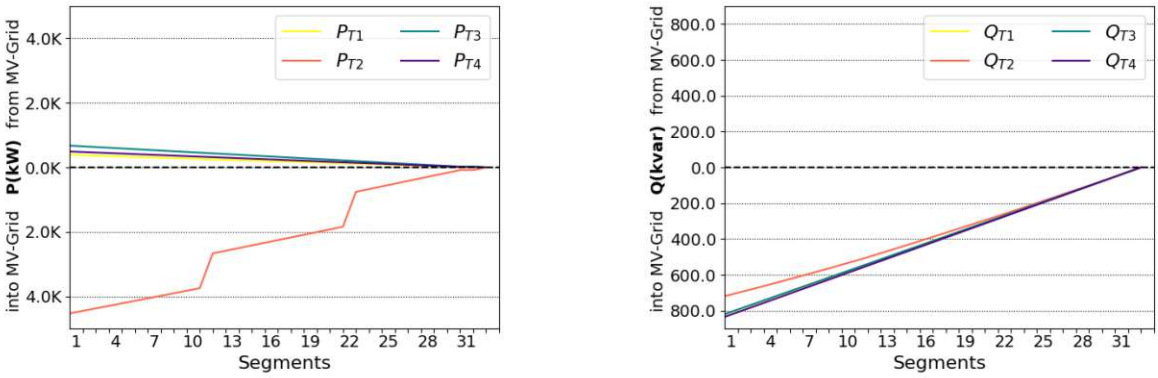

Fig 6.105. Net *P* (left) and *Q* (right) at each segment of MV cable grid with PV and CVR.

While fig. 6.106 depicts the type of losses in the grid on the Y-axis (in kW) at the four time-points, whether they are from the line or transformers, and whether they are on the LV or MV level.

Transformer losses for the MV level are relatively same in all time-points, less than 40kW. For the LV level, the most significant transformer loss is incurred at time-point two (dark orange color), and is less than 20kW. At the rest of the time-points, transformer losses are below 5 kW.

Line losses for both MV and LV do not exceed 10 kW at all the time-points except for ($t2$). The second time-point has the most significant line losses (blue color) for both MV and LV; around 90 kW Here again, there is no significant change from the base case to be seen.

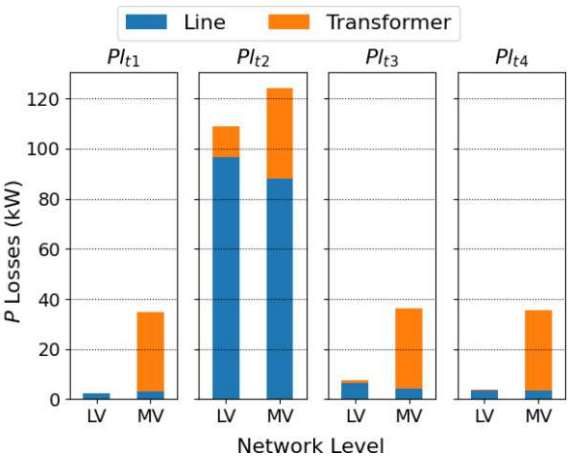

Fig 6.106. Type of losses at each time-point of MV cable grid with PV and CVR.

6.3.2.3. Comparison of cases in MV grid with cable lines

After going through the results of applied CVR method on this theoretical MV grid with cable lines structure and typical values of a European grid, this subsection provides an overview and comparison of the simulation cases, as there are noticeable differences than the case of overhead lines.

The effects of CVR employed techniques on power flow and losses (from the perspective of the supply transformer) are compared and presented in fig. 6.107. In the left subfigure (a), the Y-axis represent the magnitude and direction of the total active power flow in kW, and the X-axis is the time-points of the day. While in the right subfigure (b), the Y-axis is the and the magnitude of the total active power losses (kW) in kW, and the X-axis is also the time-points of the day.

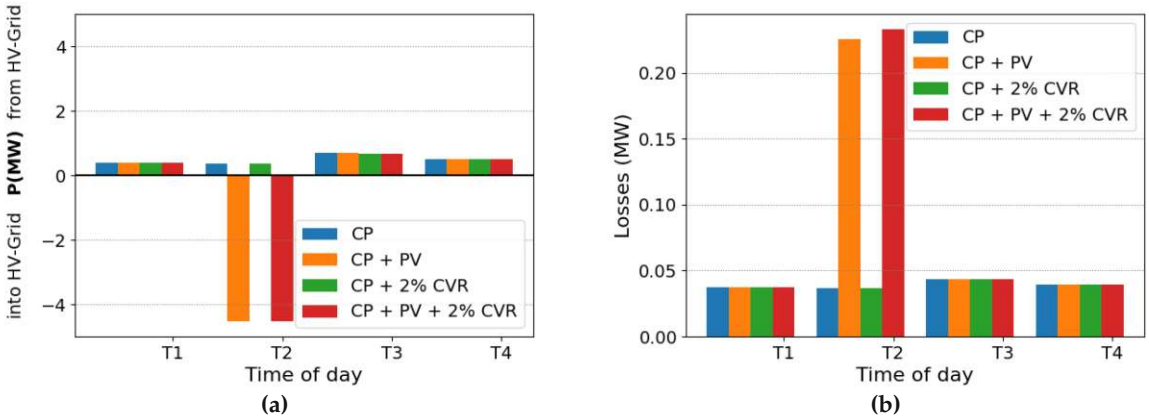

Fig 6.107. Comparison of CVR on cable line MV Grid-Link (a) total power flow, (b) total losses.

The color blue represents the base case of normal customer plants without PV or CVR,

the orange is the case of customer plants with PV installation, the green is the case of pure consumer customer plants with 2% voltage reduction at the secondary side of the supply transformer, and finally the red is the case of customer plants with distributed generation (PV) with 2% voltage reduction at the secondary side of the supply transformer.

It is observed that in the case of PV presence and at the second time-point of the day (*t2*), the power injected into the HV grid is slightly more than 4 MW in the two cases, with applying 2% CVR (red color) and without applying 2% CVR (orange color). However, the power losses are 225.37 kW and 233.1 kW (about 4.9 and 5.1% of the provided power) in the cases without and with CVR, respectively. These losses are indeed lower than the corresponding simulation case using overhead lines at *t2*, which were presented previously. These losses are about six-fold the values at the same time-point of the cases without PV.

Furthermore, and in the case of applying CVR without PV (shown in green column), the system at *t2* consumes around 2.2% less power than the base case (shown in blue column). These savings are slightly higher than the case of overhead lines, with roughly the same losses (about 36 kW) in both cases, which are almost the same as in the overhead simulation case.

The other 3 time-points of the day do not feed any power into the HV grid. At the first time-point of the day *t1*, the power consumption in the cases with CVR is 389 kW, which is roughly 2.2% less than the case without CVR, which is around 397 kW. These levels of consumption are less than the case of overhead lines, even though they have slightly higher losses, with a difference of about 1 kW.

The power consumption at the third time-point of the day *t3* in the cases without CVR is about 687 kW (slightly lower than using of overhead lines), and 675 with CVR. That's roughly 2% savings, but not as effective as the results of the same case in overhead lines, although the losses are about 43.5 kW, which are slightly lower than the case of overhead lines. These differences arise from different load ZIP composition when combined with the reactance/capacitance characteristics of the feeder.

CVR	PV	Factor	Unit	t1	t2	t3	t4	Remark
No	No	Net *P* (*HV* to *MV*)	kW	397.34	359.58	686.65	500.5	Base case
		P Losses		37.53	36.9	43.68	39.43	
	Yes	Net *P* (*HV* to *MV*)		397.34	-4530.5	686.65	500.5	Losses at *t2* are lower than OH case
		P Losses		37.53	225.37	43.68	39.43	
Yes	No	Net *P* (*HV* to *MV*)		389.2	351.73	674.72	491.76	less power is consumed than the OH case
		P Losses		37.4	36.77	43.59	39.3	
	Yes	Net *P* (*HV* to *MV*)		389.2	-4530.6	674.72	491.76	Less losses at *t2* than the OH case
		P Losses		37.4	233.1	43.59	39.3	

Table 6.6. Comparison of CVR on cable line MV Grid-Link by power flow at supply transformer.

And at the fourth time-point of the day, around 512 kW are consumed in the cases without CVR, and 503 with CVR, achieving the same saving percentage of 2%. The losses are about 39.5 kW also in all cases (almost the same as in using of overhead lines).

A summary of these results is found in table 6.6, where the exact numbers are presented, for the net active power flow (i.e., power flow after subtracting the losses) and the corresponding losses for all the simulation cases, along with the most important remark on each simulation case.

In conclusion, CVR proves to be effective with the MV theoretical grid with typical European values and cable structure. The savings correspond to the ones mentioned in the established literature of similar CVR techniques, where 1% CVR can achieve up to 1% in active power savings, which can be of huge economical benefit to the distribution system operators in a large scale, specially with the simple and cheap method of application. In comparison to the results in the overhead case, there's a decrease in overall power consumption, except in particular cases (i.e., at the third time-point of the day with CVR). And in the case of distributed generation (PV), there are lower losses than the case of overhead lines.

7. Conclusion

Building on the booming research efforts to accommodate new technologies in the EU grid as per a holistic view of smart grids (LINK-Solution), this thesis seeks to establish the viability of applying Conservation Voltage Reduction (CVR) in the European distribution grids, motivated by its success in helping utility grids in the USA to realize high power and energy savings at a low implementation cost with little technical overhead required.

The thesis also present a survey of the existing literature on the topic, starting with CVR definition, ZIP principal and how the European grids differ from those in the United States. Moreover, it puts forward a select group of existing projects that proved the viability of the solution, particularly in the United States, where the practice was first mainstreamed. The theoretical background of the strategic LINK-Solution is presented, which is developed at the Technical University of Vienna (TUW), and constitutes the building block for how the thesis viewed CVR across the grid.

And since the effects of CVR are not directly measurable, the topic of quantifying its results is discussed, along with the factors and the ongoing efforts to standardize the process. Furthermore, the thesis present different methodologies that can be used to quantify CVR effects, each with its advantages and disadvantages. The thesis picks one of these (the simulation-based methodology) to be the basis for its CVR study.

The thesis moves on to present the techniques typically used for CVR application; open-loop methods which are highly convenient and cost-effective, but limit the depth of voltage reduction, and closed-loop techniques that achieve optimal voltage reduction and a greater energy-saving effect, but at a higher cost of sophistication. Both are used in different simulation contexts in the thesis, in order to test established and experimental CVR with the European grid specifications.

The thesis also presents the load models used in simulations, that have been developed, also at TUW, to be time-variant, in order to counter the disadvantages of the traditional models and to accommodate for the changing behavior of customer plants. The thesis also discuses further technical barriers that faced the author and the subsequent technical choices in data handling.

Moreover, a deep insight into the simulation cases and their parameters at each voltage level under investigation is presented, as well as the modelling methods behind the simulation. The simulated theoretical grids with their diagrammatic illustrations show how CVR is applied through the voltage chain with cable lines or overhead feeders. The simulation scenarios take into account the presence of PV power plants as distributed generation throughout the grid (either at customer plants on the LV level such that they are not purely consumers anymore, or directly connected plants to the grid on the MV level).

The experimental CVR techniques applied on the LV level are based on closed-loop control strategies. The first technique is connecting customer plants to the LV grid not directly, but rather through OLTCs, and the second one is using a controllable coil at the end of the feeder to bring down the voltage through consumption of reactive power.

However, on the other hand, the technique applied on the MV grids is a simple and inexpensive open-loop one, realizing CVR by an 2% voltage drop at the secondary side of the supply transformer.

The thesis comes to findings that the simple open-loop CVR on the MV level remains dominant and more economical than the sophisticated experimental techniques. It can indeed increase overall system efficiency in a typical European grid, with minimum structural changes, costs, staff training and engineering effort. However, the results differ depending on the type of the feeder, the level of instantaneous power flow and the corresponding ZIP coefficients at the time-point, as well as the presence of distributed generation.

Such that, with an MV grid of overhead lines, an average of 2% power saving occurs with a 2% voltage drop. The only recorded inefficiency in this case is in the presence of PV injecting power into the grid in the middle of the day. And with an MV grid of cable lines, the same average is achieved, with slightly better results than the overhead case in most cases.

On the other hand, the thesis did not find such promising results with the techniques used on the LV level, even though they would provide a tailored consumption efficiency profile for each application case. The OLTC CVR method suffered most notably from increased no-load losses (with the cable grid performing slightly better than the overhead one), while the controllable coil method only proved helpful in the case of using it as a Volt/Var control system to keep the voltage of the feeder within acceptable boundaries in the case of PV injection. Moreover, these 2 techniques require a high initial investment in labor and capital is required.

Finally, and according to the reviewed literature and the findings of this thesis, it is safe to say that CVR holds a lot of potential for the future of the European grids.

The author hopes that this thesis will be a stepping stone towards further research and analysis of CVR according to the LINK-Solution, particularly in developing power-electronics solutions to connect customer plants with the LV grids, seeking to achieve the best optimization possible for each case, while stepping over the no-load losses problem of the OLTCs. Another research direction could be to seek new ways of integrating distributed renewable generation with CVR in a holistic view, that serves the undergoing evolution of the electricity grid.

As grids grow ever more complex, their complexity can only be tackled by foreseeing the evolution and adapting to needs of the market, and this can only be done through further research of such topics as CVR and DG, and accepting them as the new reality of communities transcending grids centralized around fossil-fired power plants.

A. Appendix

Type	A [mm^2]	I_{th}[A]	R' [$\frac{\Omega}{km}$]	X'_L [$\frac{\Omega}{km}$]	C' [$\frac{\mu F}{km}$]	R'/X'_L
C-AL	25	100	1.2000	0.0890	0.550	13.48
	50	145	0.6410	0.0850	0.720	7.54
	95	215	0.3200	0.0820	0.950	3.90
	150	**275**	**0.2060**	**0.0800**	**1.040**	**2.58**
	240	360	0.1250	0.0800	1.200	1.56
C-CU	16	100	1.1500	0.0890	0.500	12.92
	25	130	0.7270	0.0880	0.550	8.26
	35	155	0.5240	0.0850	0.630	6.16
OL-AL	50	210	0.6152	0.3764	0.000	1.63
	150	**320**	**0.3264**	**0.3557**	**0.000**	**0.92**

Table A.1. Typical and used LV cable and overhead specifications

Type	A [mm^2]	I_{th}[A]	R' [$\frac{\Omega}{km}$]	X'_L [$\frac{\Omega}{km}$]	C' [$\frac{\mu F}{km}$]	R'/X'_L
OH-AL	240	0.35	0.358	0.376	0.0096	0.95
CA-AL	240	0.419	0.206	0.1222	0.254	1.69

Table A.2. Used MV cable and overhead lines specifications.

Transformer	S [kVA]	V_p [kV]	V_s [kV]	v_{sc} [%]	v_r [%]	Vector Group
LV-CP	10	0.4	0.4	4	2.5	DYN11
MV-LV	160	20	0.4	4.04	1	YZN5
HV-LV	18500	110	20	10.12	0.45	YNYN6

Table A.3. Transformers specifications used in simulation at each voltage level.

Time point	ZIP-coefficients					
	$C^Z_{P,t}$	$C^I_{P,t}$	$C^P_{P,t}$	$C^Z_{Q,t}$	$C^I_{Q,t}$	$C^P_{Q,t}$
t1	0.516397538	-0.07230807981	0.5559105418	1.048431681	-0.5783105487	0.5298788677
t2	0.5534362781	-0.08026182914	0.526825551	1.137853709	-0.6033501539	0.4654964448
t3	0.4137082428	-0.008458703467	0.5947504607	-0.5667300224	1.860898801	-0.2941687788
t4	0.3791550011	0.06161631978	0.5592286791	3.895275978	-3.258945535	0.3636695574
Time point	**Nominal peak load**					
	$P^{lumped}_{nom,t} / P^{peak}$			$Q^{lumped}_{nom,t} / P^{peak}$		
t1	0.436718			0.09670790861		
t2	0.3934245			0.09081613616		
t3	0.762449			0.04789621917		
t4	0.554983			-0.04170629632		

Table A.4. Relevant ZIP coefficients as adapted from[35]

Presence of PV	Factor	Unit	t1	t2	t3	t4	Remark
No	$P_{0.9V_n}$	kW	0.397	0.355	0.703	0.512	Reference Value
	$\Delta\%P_{V_n}$	%	10	10.76	8.43	8.48	Consumption inc.
	$\Delta\%P_{1.1V_n}$	%	21.13	22.74	17.76	17.79	with Voltage
	$Q_{0.9V_n}$	kvar	0.083	0.077	0.044	-0.024	Reference Value
	$\Delta\%Q_{V_n}$	%	16.46	18.46	8.51	70.71	Consumption inc. with
	$\Delta\%Q_{1.1V_n}$	%	35.37	39.62	15.79	154.72	voltage specially at t4
Yes (only the changed Values)	$P_{0.9V_n}$	kW	-	-2.14	-	-	Reference Value
	$\Delta\%P_{V_n}$	%	-	-1.79	-	-	Power injection
	$\Delta\%P_{1.1V_n}$	%	-	-3.78	-	-	dec. with higher voltage

Table A.5. Summary of *CP* load reduction results.

List of Equations

List of Figures

List of Tables

Bibliography

[1] L. L. Jansen, N. Andreadou, I. Papaioannou, and A. Marinopoulos. *Smart grid lab research in Europe and beyond*. Dec. 2019. URL: onlinelibrary.wiley.com/doi/abs/10.1002/er.4818.

[2] R. U. Rob Ardis. *CVR is here to stay*. URL: www.tdworld.com/grid-innovations/smart-grid/article/20965787/cvr-is-here-to-stay.

[3] F. Stern and N. DeDominicis. *Conservation Voltage Reduction: What Are The Savings?* 2013. URL: www.iepec.org/conf-docs/conf-by-year/2013-Chicago/104.pdf.

[4] S. Lefebvre, G. Gaba, A. Ba, D. Asber, A. Ricard, C. Perreault, and D. Chartrand. "Measuring the efficiency of voltage reduction at Hydro-Québec distribution". In: *2008 IEEE Power and Energy Society General Meeting - Conversion and Delivery of Electrical Energy in the 21st Century*. 2008, pp. 1–7. DOI: 10.1109/PES.2008.4596511.

[5] A. Regalado. *Rage Against the Smart Meter*. Feb. 2020. URL: www.technologyreview.com/2012/04/26/186333/rage-against-the-smart-meter/.

[6] R. Preiss and V. Warnock. "Impact of voltage reduction on energy and demand". In: *IEEE Transactions on Power Apparatus and Systems* PAS-97.6 (1978), pp. 1–36. DOI: 10.1109/tpas.1978.354752.

[7] B. R.W. *Utility Distribution System Efficiency Initiative (DEI)*. URL: neea.org/resources/vutility-distribution-system-efficiency-initiative-dei-phase-i-final-market-progress-and-evaluation-report.

[8] K. P. Schneider, J. C. Fuller, F. K. Tuffner, and R. Singh. "Evaluation of Conservation Voltage Reduction (CVR) on a National Level". In: (Sept. 2010). DOI: 10.2172/990131.

[9] F. Stern and N. DeDominicis. "Conservation Voltage Reduction: What Are the Savings?" In: 2013.

[10] W. Ellens, A. Berry, and A. West. In: *POWERCON 2012: 2012 IEEE International Conference on Power System Technology: Auckland, New Zealand, 30 October - 2 November 2012*. IEEE, 2012, pp. 1–6.

[11] E. Diskin, T. Fallon, G. O'mahony, and C. Power. In: *CIRED 2012 Workshop: Integration of Renewables into the Distribution Grid*, pp. 1–4.

[12] A. Ilo, W. Schaffer, T. Rieder, and I. Dzafic. "Dynamic optimization of distribution networks. Closed loop operation results; Dynamische Optimierung der Verteilnetze. Closed loop Betriebsergebnisse". In: (2012).

[13] T. L. Wilson. "Measurement and verification of distribution voltage optimization results for the IEEE power energy society". In: *IEEE PES General Meeting*. 2010, pp. 1–9. DOI: 10.1109/PES.2010.5589762.

[14] T. Wilson. *AdaptiVolt™ Vs LDC CVR*. Dec. 2010.
URL: www.scribd.com/document/82176951/AdaptiVolt-vs-LDC-CVR.

[15] *Standardizing Conservation Voltage Reduction Verification – Paving the Way to Ensure Efficiency*. Oct. 2020. URL: www.tdworld.com/test-and-measurement/article/21145733/standardizing-conservation-voltage-reduction-verification-paving-the-way-to-ensure-efficiency.

[16] A. Ilo. "Effects of the Reactive Power Injection on the Grid—The Rise of the Volt/var Interaction Chain". In: *Smart Grid and Renewable Energy* 07.07 (2016), pp. 217–232.
DOI: 10.4236/sgre.2016.77017.

[17] J. Milanovic, J. Matevosyan, A. Gaikwad, A. Borghetti, S. Djokic, Z. Dong, Andrew, Halley, L. Korunovic, S. Martinez Villanueva, J. Ma, P. Pourbeik, F. Resende, S. Sterpu, F. Villella, K. Yamashita, O. Auer, K. Karoui, D. Kosterev, and Y. Xu. *Modelling and Aggregation of Loads in Flexible Power Networks*. Feb. 2014.

[18] A. Ilo.
""Link"—The smart grid paradigm for a secure decentralized operation architecture".
In: *Electric Power Systems Research* 131 (2016), pp. 116–125. ISSN: 0378-7796.
DOI: doi.org/10.1016/j.epsr.2015.10.001.
URL: www.sciencedirect.com/science/article/pii/S0378779615002904.

[19] A. ILO. *Design of the Smart Grid Architecture According to Fractal Principles and the Basics of Corresponding Market Structure*. Oct. 2019.
URL: www.mdpi.com/1996-1073/12/21/4153/htm.

[20] A. Ilo. *LINK-Paradigm, Albana Ilo/powersyslink*. 2019. URL: www.powersys-link.com/.

[21] Z. Wang and J. Wang.
"Review on Implementation and Assessment of Conservation Voltage Reduction".
In: *IEEE Transactions on Power Systems* 29.3 (2014), pp. 1306–1315.
DOI: 10.1109/tpwrs.2013.2288518.

[22] J. J. Grainger and S. W. D. Jr. *Power system analysis*. McGraw-Hill, 1994.

[23] R. Fletcher and A. Saeed.
"Integrating engineering and economic analysis for conservation voltage reduction".
In: *IEEE Power Engineering Society Summer Meeting*, vol. 2. 2002, 725–730 vol.2.
DOI: 10.1109/PESS.2002.1043401.

[24] M. J. Krok and S. Genc. "A coordinated optimization approach to Volt/VAr control for large power distribution networks".
In: *Proceedings of the 2011 American Control Conference*. 2011, pp. 1145–1150.
DOI: 10.1109/ACC.2011.5991606.

[25] K. Fagen and C. Bernier. "Efficiencies in Distribution Design and Operating Practices Mid-Study Analysis (February 2007)". In: *2007 IEEE Rural Electric Power Conference*. 2007, B6-B6–14. DOI: 10.1109/REPCON.2007.369554.

[26] R. W. Uluski. "VVC in the Smart Grid era". In: *IEEE PES General Meeting*. 2010, pp. 1–7. DOI: 10.1109/PES.2010.5589850.

[27] *Inland Power and Light*. URL: www.inlandpower.com/.

[28] T. Wilson and D. Bell.
"Energy conservation and demand control using distribution automation technologies".
In: *Rural Electric Power Conference, 2004*. 2004, pp. C4–1.
DOI: 10.1109/REPCON.2004.1307059.

[29] K. Fagen.
"Distribution Efficiency voltage optimization supports lowest cost new resource".
In: *IEEE PES General Meeting*. 2010, pp. 1–6. DOI: 10.1109/PES.2010.5590142.

[30] R. Singh, F. Tuffner, J. Fuller, and K. Schneider.
"Effects of distributed energy resources on conservation voltage reduction (CVR)".
In: *2011 IEEE Power and Energy Society General Meeting*. 2011, pp. 1–7.
DOI: 10.1109/PES.2011.6039702.

[31] H.-G. Yeh, D. F. Gayme, and S. H. Low.
"Adaptive VAR Control for Distribution Circuits With Photovoltaic Generators".
In: *IEEE Transactions on Power Systems* 27.3 (2012), pp. 1656–1663.
DOI: 10.1109/TPWRS.2012.2183151.

[32] J. Carrasco, L. Franquelo, J. Bialasiewicz, E. Galvan, R. PortilloGuisado, M. Prats, J. Leon, and N. Moreno-Alfonso. "Power-Electronic Systems for the Grid Integration of Renewable Energy Sources: A Survey".
In: *IEEE Transactions on Industrial Electronics* 53.4 (2006), pp. 1002–1016.
DOI: 10.1109/TIE.2006.878356.

[33] M. Farivar, C. R. Clarke, S. H. Low, and K. M. Chandy.
"Inverter VAR control for distribution systems with renewables".
In: *2011 IEEE International Conference on Smart Grid Communications (SmartGridComm)*. 2011, pp. 457–462. DOI: 10.1109/SmartGridComm.2011.6102366.

[34] D. Schultis and A. Ilo. "Adaption of the Current Load Model to Consider Residential Customers Having Turned to LED Lighting".
In: *2019 IEEE PES Asia-Pacific Power and Energy Engineering Conference (APPEEC)*. 2019, pp. 1–5.

[35] D. Schultis. *Daily load profiles and ZIP models of current and new residential customers*. June 2019. URL:
www.narcis.nl/dataset/RecordID/oai:easy.dans.knaw.nl:easy-dataset:129336.

[36] A. Ilo. "The Energy Supply Chain Net".
In: *Energy and Power Engineering* 05 (Jan. 2013), pp. 384–390.
DOI: 10.4236/epe.2013.55040.

[37] R. J. Smith and R. C. Dorf.
Circuits, devices and systems: a first course in electrical engineering. Wiley-India, 2011.

[38] C. Concordia and S. Ihara. "Load Representation in Power System Stability Studies". In: *IEEE Transactions on Power Apparatus and Systems* PAS-101.4 (1982), pp. 969–977. DOI: 10.1109/TPAS.1982.317163.

[39] D. Fitzpatrick. *Analog design and simulation using OrCAD Capture and PSpice*. Newnes, 2018.

[40] C. Farkas, A. Tóth, and I. Orlay. "Voltage Control Methods in the MV Grid with a Large Share of PV". In: *International Journal of Emerging Electric Power Systems* 20.4 (2019), p. 20190057. DOI: doi:10.1515/ijeeps-2019-0057. URL: https://doi.org/10.1515/ijeeps-2019-0057.